Doctoral Thesis

Design of Redundant Drive Wire Mechanism with Velocity Constraint Modules to Reduce the Number of Actuators for Producing Fast and Precise Motions

March 2017

LE Nhat Tam

Doctoral Thesis Reviewed
by Ritsumeikan University

Design of Redundant Drive Wire Mechanism with Velocity Constraint Modules to Reduce the Number of Actuators for Producing Fast and Precise Motions

(アクチュエータ数を低減する速度高速モジュールを有する高速・高精度動作生成のための冗長駆動ワイヤ機構の設計)

March 2017
2017 年 03 月

LE Nhat Tam
ル　ナット　タム

Principal referee: Professor NAGAI Kiyoshi
主査: 永井清教授

Abstract

This thesis proposes the design of redundant drive wire mechanism (RDWM: Redundant Drive Wire Mechanism) for producing fast and precise motions. The RDWM is configured with double actuator modules (DAMs: Double Actuator Modules) with two actuators for providing high acceleration global and high precise local motions. In the thesis, the method to configure RDWM using DAMs, the method to reduce the required number of actuators by introducing velocity constraint module (VCM: Velocity Constraint Module) and the experiment of RDWM prototype will be discussed.

First, a method to configure RDWM using DAM, a method to judge whether or not a RDWM candidate can produce the resultant force needed to achieve required motions will be shown. In the case of RDWM with DAMs is used for producing multi-directional motions, the size of the wire matrix would become large as the number of actuators increases. This takes time for judgment of the candidates. Therefore, it is necessary to introduce a simpler method for judging RDWM candidates. This problem can be done by converting the wire matrix of the candidate to new form then making the judgment using the essential part of the new form wire matrix related to the global motion.

Second, by introducing VCM as the solution to reduce the required number of actuators, a method to judge whether or not the candidates of RDWM with VCM can produce resultant force needed to achieve required motions is shown. This judgment method has three steps: (1) Static force analysis to check whether the resultant force for producing required motion can be produced in the whole motion space. (2) Kinematic analysis to find the active constraint space where the top plate can generate velocity. (3) Static force analysis to check whether the resultant force for producing required motion can be produced in the active constraint space. This study also clarifies the role of VCM in reducing the required number of actuators while keeping the orientation of the top plate. In addition, because only the essential part of the new form wire matrix is used in the judgment, the procedure will be simpler.

Third, based on the above two methods, numerical examples are shown where the method to configure RDWM candidates and the method to reduce the required number of actuators are applied. From the results of the numerical examples, the effectiveness of the proposed method is verified and the role of VCM is confirmed.

Finally, the experimental results of the 1D RDWM prototype are shown. Based on the results, the ability to produce global motion and local motion of RDWM is confirmed.

Abstract in Japanese

本論文は、高速・高精度な動作を生成するための冗長駆動ワイヤ機構（RDWM: Redundant Drive Wire Mechanism）の設計について述べたものである。この RDWM は、二つのアクチュエータをもつダブルアクチュエータモジュール（DAM: Double Actuator Modules）により構成され、トッププレートの高速な広域動作とトッププレート上の精密な局所動作の組み合わせにより、高速・高精度な動作を生成するものである。本論文では、DAM を用いた RDWM の構成方法、速度拘束モジュール（VCM: Velocity constraint module）の導入によるアクチュエータ数の削減方法、および RDWM の試作機による動作実験について議論される。

本論文では第一に、DAM を用いた RDWM の構成方法として、RDWM の候補が、必要動作生成のための駆動力を発生できるかを判定する方法が示される。この際、多自由度動作を生成する RDWM の候補においては、アクチュエータ数の増加に伴ってワイヤ行列のサイズが大きくなり、妥当性の判定が複雑になる。このため、より簡単な判定方法を明らかにすることが課題となる。そしてこの課題は、RDWM の候補のワイヤ行列を新しい形態に変換し、そのワイヤ行列の広域動作対応成分を用いて妥当性を判定することにより解決される。

第二に、VCM の導入によるアクチュエータ数の削減方法として、VCM を導入した RDWM の候補が、必要動作生成のための駆動力を発生できるかを判定する方法が示される。この判定方法は、次の三つの手順：(1) 全空間を対象として、必要動作生成のための駆動力を発生できるかを判定する静力学解析、(2) トッププレートが速度を生成できる能動拘束空間を見い出す運動学解析、および、(3) その能動拘束空間を対象として、必要動作生成のための駆動力を発生できるかを判定する静力学解析、により構成される。この議論では、トッププレートの姿勢を固定しながら必要アクチュエータ数を削減するという VCM の役割も明らかとなる。また、この判定方法では、ワイヤ行列の新しい形態における広域動作対応成分のみが使用されるため、前述の判定方法と同様に、その判定方法は簡単化されている。

第三に、前述の二つの手法に基づき、RDWM の候補の判定方法、およびアクチュエータ数の削減方法を適用した数値例が示される。この数値例の結果により、提案手法の有効性が検証され、また、VCM の役割が確認される。

最後に、1 自由度の RDWM の試作機を用いた実験結果が示される。この実験結果により、広域動作と局所動作を生成する RDWM の運動生成機能が確認される。

Acknowledgments

I would like to show my deep gratitude to Japanese government for giving me a chance for challenging myself with this Doctoral Program. I cannot write this PhD thesis without the MEXT scholarship to attend this program.

I would like to show my deep gratitude to my supervisor - Prof. Kiyoshi Nagai for his supervision and instruction during my doctoral research.

I would like to give my thanks to Assistant Professor Hiroki Dobashi, Prof. Tsuneo Yoshikawa, Prof. Yoshikatsu Hayashi and Prof. Koji Ito for the fruitful discussions during the research seminars. I also would like to thank Mrs. Satomi Nagasawa for helping me in many paper works related to my research and all the members in Nagai-Dobashi Robotics lab for their helps during the time I was there. I would like to thank Mr. Hiroyuki Sugimoto and the other staffs at the Workshop Center for helping me to fabricate the experimental parts in my research.

I would like to express my thanks to Prof. Sadao Kawamura, Prof. Shinichi Hirai, Prof. Ryuta Ozawa and the other lecturers in the department of Robotics for giving their valuable opinions on my research during the annual poster sections and many other occasions.

I would like to give my thanks to the staffs in the Office of the Robotics department, the Administrative Office of the Graduate School of Science & Engineering and the International Center at BKC for their supports during my PhD research in Ritsumeikan University.

I would like to thank the Vietnamese community in Shiga Prefecture for sharing me with some beautiful as well as difficult times when living far away from the home country.

For spending their time on examining this PhD thesis, I would like to thank the Screening Committee members: Prof. Sadao Kawamura, Prof. Satoshi Ueno and Prof. Kiyoshi Nagai for reviewing and giving their valuable comments on the thesis.

Finally, I would like to show my deepest gratitude to my beloved parents and family members, who are always besides and encouraging me whenever and wherever.

Table of Contents

Abstract i

Abstract in Japanese ii

Acknowledgments iii

Table of Contents iv

List of Figures viii

List of Tables x

1 Introduction 1

1.1 Related Works 1

1.2 Background of the Research 4

1.3 Objective of this Thesis 4

1.4 Organization of this Thesis 5

2 Basic Concept and Problem Statement 7

2.1 Basic Concept of RDWM 7

2.1.1 Pick and Place Motion in Industrial Application 7

2.1.2 Using DAMs for Producing High Acceleration and High Precise Motions 7

2.1.3 Using VCMs for Reducing Number of Actuators and Keeping the Orientation of the Top Plate 10

2.1.4 Wire Outlet Module for Reducing Friction and Changing Wire Direction 10

2.2 Problem Statement 11

3 How to Configure RDWM with DAMs 13

3.1 Wire Matrix and Problem Statement 13

3.1.1 The Derivation of the Normal Expression of Wire Matrix 13

3.1.2 Problem Statement 14

3.2 The Conversion of Wire Matrix to the New Expression 14

3.2.1 Procedure to Derive the Wire Matrix in Normal Form 14
3.2.2 Conversion of the Wire Matrix to New Form 16
3.3 New Judgment Method for Checking A RDWM Candidate 17
3.4 Discussion and Conclusion 20

4 How to Keep the Orientation of the Top Plate and Reduce the Number of Actuators 21
4.1 Problem Statement 21
4.1.1 Basic Structure of RDWM 21
4.1.2 Basic Concept of RDWM with VCM 22
4.1.3 Technical Problems to be Solved 25
4.2 Proposal of the Judgment Procedure to Find RDWM Configuration That Can Produce Desired Velocity 25
4.2.1 Outline of the Procedure 26
4.2.2 Details of Step 1: Checking the Necessary Condition for Holding the Vector Closure 27
4.2.3 Details of Step 2: Find the Producible Velocity Space by Kinematical Analysis (KA) 27
4.2.4 Details of Step 3: Check the Vector Closure Condition within the Producible Velocity Space by Static Force Analysis (SFA) 31
4.3 Discussion and Conclusion 35

5 Numerical Examples 36
5.1 Introduction 36
5.2 Proper Configuration of the 1D Wire Mechanism with One VCM 36
5.3 Proper Configuration of the Planar RDWM with Fixed Orientation Around the Z-axis while Maintaining Translational Motion in the X and Y Directions 40
5.3.1 First configuration: The Mechanism Does Not Satisfy the 1^{st} Point of Step 1 40
5.3.2 Second configuration: The Mechanism does not satisfy the 2^{nd} point of Step 1 44
5.3.3 Third configuration: planar RDWM with four DAMs 47
5.3.4 Fourth configuration: planar RDWM with two DAMs and one DAM with a VCM 50
5.3.5 Fifth configuration: improper planar RDWM with two DAMs and one DAM with a VCM 54

5.4 Proper Configuration of 3D RDWM with Fixed Orientations Around X-, Y-, and Z-axes while Maintaining Translational Motions in the X, Y and Z Directions 57
5.4.1 First configuration: 3D RDWM with seven DAMs 57
5.4.2 Second configuration: 3D RDWM with four sets of DAMs with VCMs . 62
5.5 Discussion and Conclusion 67

6 Experiment of the 1D RDWM 69
6.1 Objective of the Experiment 69
6.2 Experiment Set Up 69
6.2.1 Configuration of the 1D RDWM 69
6.2.2 Kinematics relation 69
6.2.3 Specification of the control system 73
6.2.4 Control Diagram of the 1D RDWM 73
6.2.5 Controlling of Motor-Drum Unit Using Speed Control Driver and a Control Method Based on I-PD Control 75
6.3 Result and Discussion 75

7 Conclusion 79
7.1 Conclusion 79
7.2 Future works: 80

Appendix A List of notations and symbols 82

Appendix B Derivation of the Normal Form and New Form Wire Matrix for RDWM based on DAMs with and without VCM 84
B.1 Normal Form of Wire Matrix of RDWM contains DAMs with and without VCMs 84
B.2 New Form of Wire Matrix of RDWM contains DAMs with VCMs 85

Appendix C Normal Form and New Form Wire Matrix of Each Mechanism 86
C.1 Proper Configuration of the Planar RDWM with Fixed Orientation Around the Z-axis while Maintaining Translational Motion in the X and Y Directions 86
C.1.1 First configuration: The Mechanism Does Not Satisfy the 1^{st} Point of Step 1 86
C.1.2 Second configuration: The Mechanism does not satisfy the 2^{nd} point of Step 1 87
C.1.3 Third configuration: planar RDWM with four DAMs 88
C.1.4 Fourth configuration: planar RDWM with two DAMs and one DAM with a VCM 89

C.1.5 Fifth configuration: improper planar RDWM with two DAMs and one DAM with a VCM 89
C.2 Proper Configuration of 3D RDWM with Fixed Orientations Around X-, Y-, and Z-axes while Maintaining Translational Motions in the X, Y and Z Directions 90
C.2.1 First configuration: 3D RDWM with seven DAMs 90
C.2.2 Second configuration: 3D RDWM with four sets of DAMs with VCMs . 92

Appendix D Conversion from face form to span form **94**

Bibliography **95**

List of Figures

2.1 Pick and Place motion. 7
2.2 Double actuators module. 8
2.3 1D RDWM. 9
2.4 An image of the target wire mechanism. 9
2.5 Concept of RDWM with VCM. 10
2.6 wire outlet system. 11

3.1 The set of force and moment equivalent to a set of wire tensions applied to a DAM. 15
3.2 Wire vectors on the top plate with DAMs and the simple expression. 18
3.3 Moment on the top plate. 19

4.1 Velocity Constraint Modules. 22
4.2 Basic concept of RDWM with VCM. 23
4.3 A planar RDWM with a VCM. 24

5.1 1D wire mechanism with one VCM. 37
5.2 The mechanism does not satisfy the 1^{st} point of the step 1. 40
5.3 The mechanism does not satisfy the 2^{nd} point of the step 1. 43
5.4 A planar RDWM using DAMs. 46
5.5 A planar RDWM with a VCM. 51
5.6 Improper planar RDWM configuration with two DAMs and one VCM. 55
5.7 A 3D RDWM using DAMs. 58
5.8 3D RDWM with four VCMs. 63

6.1 Overview of the 1D RDWM experimental prototype. 70
6.2 1D RDWM experimental prototype frame. 71
6.3 Top plate. 72
6.4 DAM and Servo-Amp cabinet. 72
6.5 Electronic interface diagram. 73
6.6 1D RDWM control system. 74

6.7 Motor-drum unit control system. 75
6.8 Control Diagram in Matlab. 76
6.9 Finger rotations. 77
6.10 Top plate motion. 77
6.11 Motor rotations. 78

D.1 Conversion from face form to span form. 94

List of Tables

6.1 Mechanical parameters. 70
6.2 Specification of the control system 73
6.3 Experiment conditions 75

A.1 List of notations and symbols 82

Chapter 1

Introduction

1.1. Related Works

Wire driven mechanism has a variety of applications from its initial appearance with the simple pulley system. There are the investigations on its application for moving heavy parts to ships in the seaports [1] or for ship maintenance in the factory [2] where the platform is suspended and can move around the ship so that the workers stand on the platform can do their works. Its applications are then extended to the information broadcasting or entertainment; for instance Skycam [3] for live broadcast of sport events and radio telescope [4, 5]. There are also investigations of the application on human machine interaction; such as surgery systems, rehabilitation systems [6–8]. With the emergence of biomimetics trend, robot hands with the tendon driven concepts [9] with different approaches [10, 11] were studied and attained some attractive results. Wire driven mechanism was also be used in ankle foot [12] which can be applied in prosthetic leg for human or for the humanoid robots. Behind the results on the applications that are easily to be observed, there are a lot of technical issues and problems that are required to be solved. During its first appearance until now, there are numerous of studies with the purpose to solve those technical aspects. Presented below is a review on the related studies to my research in the field of wire driven mechanism.

The structure of wire mechanisms are often employed to configure fast mechanisms. Wire mechanisms reduce the inertia of the top plate, enabling large acceleration motions. For example, the wire driven method called "FALCON" was configured in a high-speed manipulator [13], with a peak acceleration of 43 G. In this method, the redundant drive concept was applied in a parallel mechanism to produce a large resultant force. The "NINJA" mechanism [14] was rendered light-weight by arranging the motors on a base. Its top plate with six degrees of freedom (DOF) was driven by four sub-arms with a parallel link structure. The design parameters of the mechanism were optimized while reducing the inertia of the top plate. In experiments, the encoders computed that "NINJA" can accelerate to $\geq$ 100 G. The mechanisms of "DELTA" [15] and "HEXA" [16] were based on similar concepts. Later, Nagai et al. [17] introduced a high-speed parallel mechanism for electronic part mounters, known as

"the constrained differential drive mechanism" (CDDM). They analyzed a typical four-DOF pick-and-place motion and divided the trajectory into two regions, A and B. In region A, high-precise motions were produced, whereas high-acceleration motions were produced in region B. Thereafter, they integrated CDDM and the virtual force redundancy (VFR) concept into a high-speed parallel mechanism. Experimentally, this mechanism accelerate to $\geq$ 20 G. Recently, a mechanism known as "the capturing robot" was introduced, which achieved accelerations of 100 G [18] by utilizing the spring energy in the pre-shaping dynamics of the link fingers. However, high-acceleration motions were limited to one direction when moving to grasp an object.

Accompanying with high acceleration motion of robot, high precise motion was also required in most of the mechanisms [19–21]. By the time, the requirement of the accuracy motion is much more strict. Generally in mechanical engineering, vibration affect a lot in the precise motion, therefore many investigations on the vibration and methods to reduce or suppress the vibration were conducted [22, 23]. Especially in field of wire driven mechanism, because wire has elasticity or wire stiffness, researches on the affect of wire elasticity on the operation of the mechanism were studied [24–26]. Then the study on the method to suppress vibration on wire driven mechanism was investigated [27].

The configurations of mechanisms with separated parts for global and local motions have also been studied. Osumi and colleagues [28, 29] installed a manipulator on the top plate. In this mechanism, the top plate produced the global motion, whereas the changing pose of the manipulator produced the local motion. Lampariello et al. [30] introduced their robot named "KUKA," which produces similar motions by two manipulators installed on a platform. However, installing the actuators or manipulators on the top plate impacts a very high inertia to the top plate, reducing the capability for high-acceleration global motions.

To judge whether wire tension can constrain the top plate and whether the conventional wire mechanism can generate an omnidirectional resultant force, Cong Pham et al. [31, 32] adopted the force closure condition [33] in the workspace analysis. They proposed an algorithm that determines the optimal workspace with the optimal tension factor value, thereby simplifying the analysis. Related to workspace analysis, because workspace is a very important characteristic of wire driven mechanism, there are lots of investigations on it [34–37]. Wire interference is one of the topics related to workspace analysis; there is study in the collision between wires and also between wires with the top plate or with the environment [38]; there is also study on the permitting of collision between wires [39].

On the other hand, ways of changing the position and orientation of the top plate have also been studied. Because a large translational motion is required while only a small rotational motion is needed, the standard method is to maintain the translational motion while fixing the

orientation of the top plate and installing an arm on it. Contour crafting construction system for automated construction of civil structure has been getting the interests of some researchers [40, 41]. A new method known as "contour crafting cartesian cable robot" (C^4) has been proposed [42, 43], wherein the cables are mounted in pairs, and the two cables in each pair are controlled to have the same length. A parallelogram is then formed by each pair of cables, the corresponding crossbar and end-effector edge. By maintaining this parallelism, the orientation of the top plate remains fixed and only translational motion is possible. The research [42] presented the kinematics and statics of the proposed method while the research [43] presented the dynamics and developed a controller of the system. Though the working principle is not mechanical, it heavily depends on the controller. Realizing this idea, the research introduced the design method of a cable-driven robot with translational motion focusing on the tension condition in the cables then showed a prototype of the system [44]. Using a similar approach, the designers of "Beta Bot" developed a mechanism with six cables and a spine in the middle of the end effector [45]. The six cables were grouped into three pairs, and the two wires in each pair were connected to one side of the end-effector. The other ends of the two wires were then wound onto two pulleys driven by the same actuator. The two wires, together with the line which connected the two contact points on the pulleys and the end-effector edge, formed a parallelogram. The three parallelograms ensured that the end-effector would only perform three translational motions, with no change in orientation. The design of "Beta Bot" halved the number of actuators presented in [42]. In contrast to the idea of maintaining the parallelism of wires to fix the orientation of the top plate as the above researches, the authors in [46] developed a power assist device to help elderly patients and patients with disabilities in moving, without using the parallelism of wires while fixing the orientation of the supporting element. The device contained the upper part and the lower part. The upper part could produce the translational motion in the horizontal only using a set A including three wires strung at the same length and a set B including two wires strung at the same length. The lower part contained three pairs of wires, two wires in a pair were reeled in and out to have the same length by the three corresponding actuators put on the upper part. By using these three pairs of wires, the lower part could move with three degrees of freedom in the vertical plane for the motions of standing up and sitting down of the user. The lower part could also perform a rotation motion around the vertical axis w.r.t the upper part using a connecting part between the upper part and the lower part to help the user in changing the moving direction. Another approach changed the orientation of the end-effector and installed arms on the top plate [28–30]. The orientation of the end effector could be changed by changing the position of the arm. However, the placement of the actuators on the top plate gave the mechanism high inertia. One way to reduce the inertia of the top plate is to introduce a parallel module such as "DELTA" [15] or "HEXA" [16]

into the the top plate of wire mechanism.

1.2. Background of the Research

Following the above investigation on the trending research topics in wire driven mechanism, we began seeking a mechanism that yields high-acceleration motion, a mechanism that generates both global and local motions with the reduction number of actuators, and a method for judging the configurations of this wire driven mechanism. The frame of the research on this wire driven mechanism has been presented in the patent [47]. Then, the redundant drive wire mechanism (RDWM) with double actuator modules (DAMs) for realizing fast and precise motion has been already proposed [48]. The DAM is a pair of actuators that control the length or tension of a single wire, generating a large translational force that greatly accelerates the top plate. Because the actuators are positioned outside of the top plate, the top plate develops low inertia and achieves high-acceleration motions. In addition, precise-local motions are generated on the top plate to perform tasks. When constructing an RDWM, it is necessary to judge whether the mechanism can produce the resultant force in all directions. Since the number of actuators in an RDWM is large, especially in the 3D case, the size of the wire matrix also becomes large: at least eight in the planar case and 14 in the 3D case. This creates difficulties in judging the configuration of the mechanism using the conventional method. In our approach [49], the wire matrix is based on the structure of the DAM, and only the essential component is used to judge the configuration of the RDWM.

To reduce the number of actuators, previously a velocity constraint module (VCM) was introduced into RDWM [50]. The VCM applies the same velocities to different points of the top plate, then constrains the orientation around a certain axis. This constraint is irrelevant to the RDWM because the orientation of the end effector can be adjusted by a local mechanism. The literature has confirmed the strong performance of VCM in the planar case, but the 3D case requires further investigation. Moreover, methodologies for judging the RDWM candidates remain insufficiently studied.

Therefore, [51, 52] investigated the reduction in the number of actuators by introducing VCMs to RDWM in the 3D case, not merely in the planar case. [51] then discussed the judgment procedure, which assessed whether RDWM candidate configurations generate the desired motion space.

1.3. Objective of this Thesis

This thesis proposes a method to develop an RDWM for producing high acceleration motion and high precise motion while reducing the number of actuators. It aims to propose a simple method for checking RDWM candidates containing many wires whether the orientation of

the top plate can be maintained with the reduction number of actuators. The experiments presented in the thesis also verify the concept of producing global motion and local motions by using DAMs.

As the beginning stage of the research on RDWM, this thesis is proceeded under the assumption that wires are lines without masses, they contain no slack and possess ideal stiffness without wire elasticity. In addition, the idle pulleys are considered points with zero radii and there is no friction between wire and idle pulley. Later, those parameters of wire and idle pulley will be strictly treated so that the mechanism can produce high acceleration and high precise motions.

1.4. Organization of this Thesis

The organization of this thesis contains: the configuration of RDWM based on DAMs, the introduction of VCM into RDWM to keep the orientation of the top plate while reducing the number of actuators, the numerical examples on finding appropriate RDWM configurations and the experiment of the 1D RDWM prototype.

In this beginning chapter, the related works to wire driven mechanism are introduced. Then, the background on RDWM research, the objective and organization of the thesis are discussed.

In chapter 2, the basic concept of RDWM based on the industrial requirement is introduced. After that, the problems to be solved will be discussed.

In chapter 3, an explanation on how to configure RDWM is discussed and a simple procedure for checking RDWM is proposed to check RDWM candidates. First, a method for deriving the wire matrix of an RDWM based on DAMs in normal expression is presented. Second, a new method for judging candidate RDWMs is introduced, including a new form of wire matrix. The proposed judgment of candidates uses the essential component of the new form which has the size equal to only a quarter of the size of the wire matrix; hence, it makes finding and checking candidate RDWMs easier and simpler.

In chapter 4, the method to keep the orientation of the top plate and reduce the number of actuators are discussed. First, the basic structure and basic concept of RDWM using DAMs with and without VCMs is introduced, then the technical problems of introducing VCMs into RDWM are discussed. Second, the procedure with three steps for judging candidate RDWMs using DAMs with and without VCMs is proposed. The essential component of the new form of wire matrix is used in the judgment procedure makes it simpler and easier.

In chapter 5, the theories discussed in chapter 3 and 4 will be applied to find proper configuration of RDWM that can produce the producible velocity space. The analysis of the numerical examples of RDWM in 1D, 2D and 3D cases verifies the validity of the proposed methods in judging RDWM candidates. These examples also confirm the role of the VCMs in reducing the

number of actuators while keeping the orientation of the top plate.

In chapter 6, an experiment of the 1D RDWM prototype is presented. The experimental result verifies the basic concept of RDWM in producing global motion and local motions by using DAMs.

Chapter 7 summarizes the attained findings, gives suggestions for future works.

Chapter 2

Basic Concept and Problem Statement

2.1. Basic Concept of RDWM

2.1.1 Pick and Place Motion in Industrial Application

Figure 2.1 shows that fast motion and high precise motion are not simultaneously required. The pick-and-place motion can therefore be divided into two separate stages. In this figure, the top plate can move an object from point P_1 to P_4 following the trajectory P_1-P_2-P_3-P_4. For time reduction, all the motions in region B should be kept short. In contrast, all the motions in region A must be precise.

2.1.2 Using DAMs for Producing High Acceleration and High Precise Motions

The concept of RDWM uses DAMs to produce high acceleration and high precise motions. The DAM contains two actuators that move the top plate and rotate the local pulley, as shown in figure 2.2. Actually, there is a research introduces about DAMs [9], however the research focuses on the rotational motions to control their tendon-driven robotic hand without any utilization of the translational motion for producing fast motion. In this proposed DAM, when the two actuators rotate in the same direction, the translational motion is produced as global motion. Then, when the two actuators rotate in different directions, local motion will be produced by the rotation of the local pulley, this is utilized to perform precise motion. In

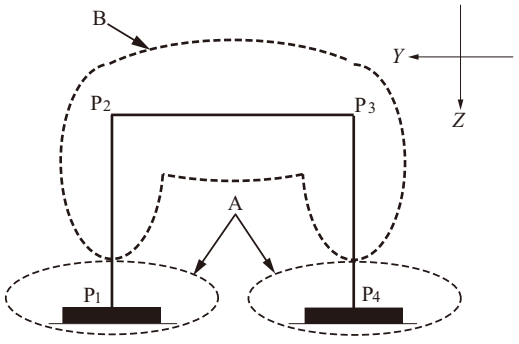

Figure. 2.1: Pick and Place motion.

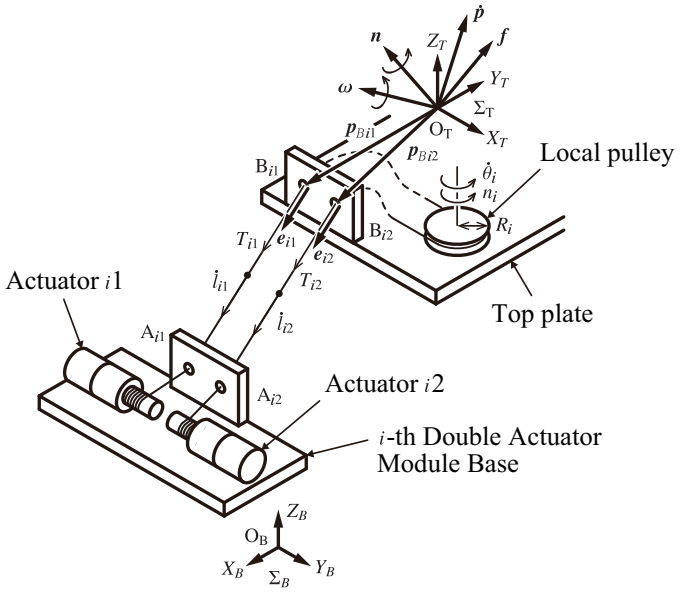

Figure. 2.2: Double actuators module.

this schematic figure, the points $\boldsymbol{A}_{i1}$, $\boldsymbol{A}_{i2}$, $\boldsymbol{B}_{i1}$, $\boldsymbol{B}_{i2}$ are shown as holes for making the figure to be simple; however, in the real mechanism, some small pulley systems need to be introduced into the DAM and into the top plate such that those points are the tangential points between wires and the outlet pulleys. An example of the pulley system to reduce the affect of friction is shown in figure 2.6. This system allows the wire to change its direction in response to the posture of the top plate and therefore it helps to reduce the affect of friction.

The wire mechanism has the ability to move an object in a wide range of motions using translational motion. To change the orientation of an object, only a small range of motion is required. Translational motions are used to realize global fast motion only when the orientation can be fixed. Local motions are then used to change the orientation of the manipulator and realize precise motions. Figure 2.3 shows the structure of the simple 1D RDWM. It has the basic features of RDWM: produce global motion with high acceleration to approach the target and local motions with high precise motions for performing tasks. The high acceleration motion can be produced by utilizing of DAMs then high precise motion can be attained by using high gear ratio of $\mathrm{n}_g = \frac{\mathrm{Z}_2}{\mathrm{Z}_1}$ between local pulley and finger.

A more complicated configuration of RDWM in 3D case is shown in figure 2.4. In this mechanism, the top plate is controlled by fourteen wires in seven DAMs. It can move through a large working space with fast motion and can also undertake specific tasks with highly precise motion using the three fingers on the top plate. The three fingers can perform grasping tasks using a common DOF, and can hold the object using two DOFs for each finger.

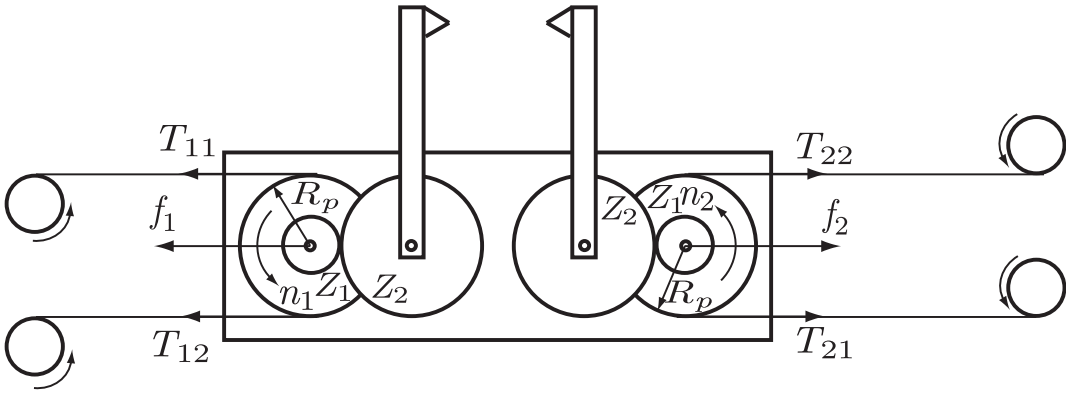

Figure. 2.3: 1D RDWM.

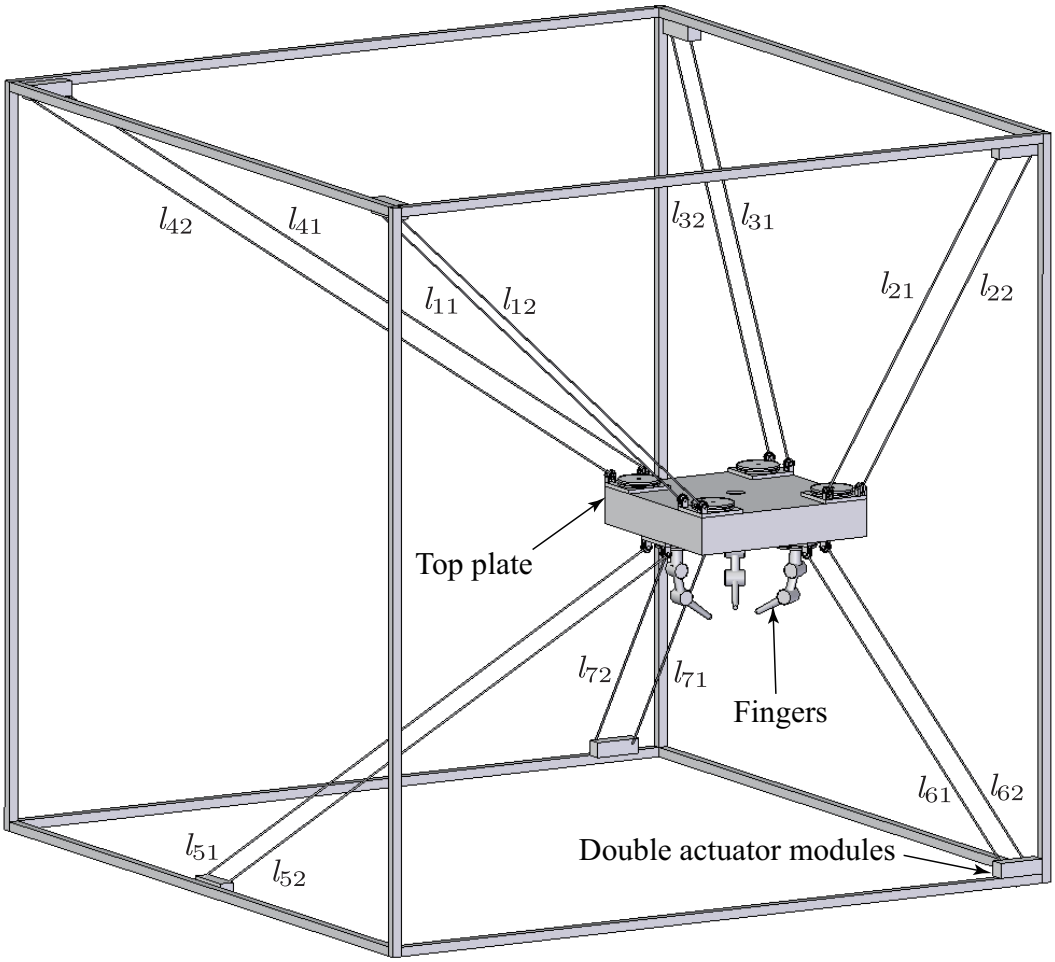

Figure. 2.4: An image of the target wire mechanism.

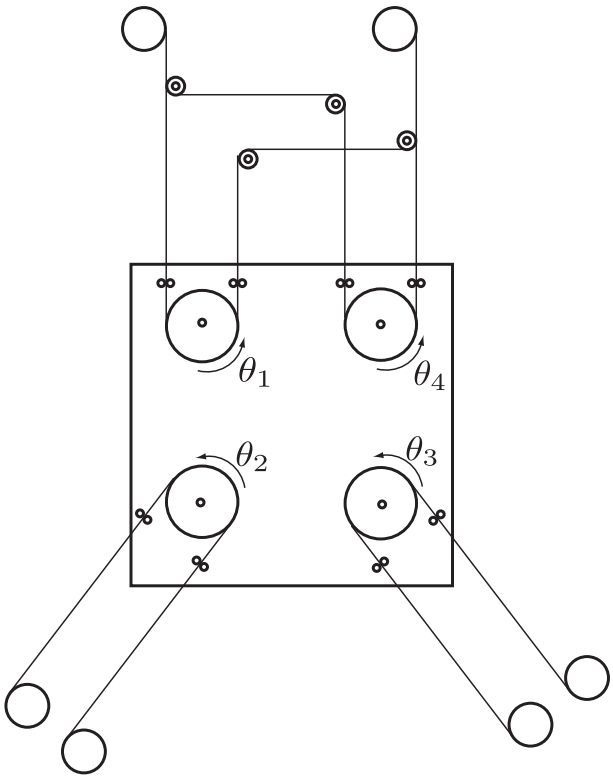

Figure. 2.5: Concept of RDWM with VCM.

2.1.3 Using VCMs for Reducing Number of Actuators and Keeping the Orientation of the Top Plate

When RDWM is extended to the 2D or 3D cases, the required number of actuators becomes large. The VCM can be used to reduce the number of actuators in the wire mechanism. As a consequence of using this module, the orientation of the top plate becomes fixed. An illustration of a wire mechanism using the VCM is shown in figure 2.5. The required number of actuators in this case is $\{(n-1)+1\} \times 2 = 6$ (where $n = 3$ is the number of DOFs in the 2D case). It requires only six units, reduced two units compared with the case where four DAMs, i.e. eight actuators, are used for producing high acceleration motion. In the same way, the required number of actuators is only eight in the 3D case. It reduces six units, compared with the case where seven DAMs, i.e. fourteen actuators are used. The mechanism shown in figure 2.5 can not only achieve high translational acceleration in any direction but can also create local motion by the rotation of pulleys θ_1, θ_2, θ_3, and θ_4. Through these local motions, the robot can change the orientation of the end-effector, as required when performing certain tasks.

2.1.4 Wire Outlet Module for Reducing Friction and Changing Wire Direction

When the top plate is moving in the 3D space, the wires can take any direction. A module that can allow the wire to change its directions in response to the posture of the top plate is therefore needed for the operation of RDWM. Figure 2.6 shows a design of this kind of module. Using this structure, the output part that directs the wire to the actuator unit can produce the

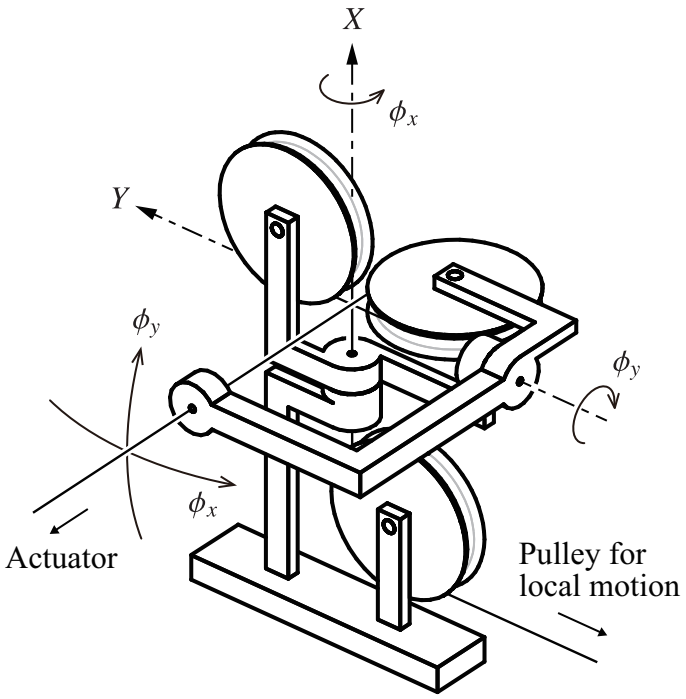

Figure. 2.6: wire outlet system.

ϕ_x, ϕ_y rotations, changing the wire direction in response to the position of the top plate. As the result of using this module, wire can easily be wound onto or out of the DAM and move into or out of the top plate smoothly with small affect of friction.

2.2. Problem Statement

This thesis is interested in the problems arising when introducing DAMs or VCMs into the configuration of wire driven mechanism (RDWM). Because using DAMs will double the number of wires, this takes time for finding suitable candidates of RDWM. Therefore the first problem arising from using DAMs is to look for a simple method for finding suitable RDWM configurations.

The second problem, because of using DAMs, the number of actuators is doubled to the number of actuator in typical wire driven mechanism with uni-wire. Therefore, this thesis studied a mechanism which helps to reduce the required number of actuators called velocity constraint module(VCM).

The third problem is a common one of wire driven mechanism. In general wire driven mechanism or in RDWM using DAMs that moves in 3D space, wire are arranged in spatial space, the orientation of the top plate is very easy to be changed even with small difference in motor sides when it moves to new position. Then, the robot cannot perform precise tasks after unexpected change in the orientation. In fact, with the current development of control

engineering, the top plate orientation can be detected by some kinds of sensor and the changing in orientation can be compensated in the control algorithm; however, this will increase the production cost and burden to the control system. Therefore, it had better to mechanically fix the orientation of the top plate and the precise tasks can be performed by some local motions on the top plate. The VCM introduced for reducing the required number of actuators has valuable characteristic to apply the same velocity to different points of the top plate. Therefore it can be applied to maintain the orientation of the top plate.

The final problem comes from using VCM in RDWM to keep the orientation of the top plate. It's necessary to build up a judgment procedure for checking whether the RDWM candidates can produce desired producible velocity space.

The next chapters of this thesis discuss methods to deal with the above problems.

Chapter 3

How to Configure RDWM with DAMs

3.1. Wire Matrix and Problem Statement

3.1.1 The Derivation of the Normal Expression of Wire Matrix

In the i-th DAM shown in figure 2.2, ${}^{B}\dot{\boldsymbol{p}}_{Bij}$ is the velocity of the wire end points on the top plate w.r.t the base coordinate, ${}^{B}\dot{\boldsymbol{p}}_{T}$ is the velocity of the center of the top plate w.r.t the base coordinate, ${}^{B}\boldsymbol{\omega}$ is the angular velocity of the top plate, and ${}^{B}\boldsymbol{p}_{Bij}$ is the position of the wire end points on the top plate w.r.t the base coordinate. The following relationships can then be obtained:

$$ {}^{B}\dot{\boldsymbol{p}}_{Bij} = {}^{B}\dot{\boldsymbol{p}}_{T} + {}^{B}\boldsymbol{\omega} \times {}^{B}\boldsymbol{p}_{Bij}, \tag{3.1} $$

i=1,..., N_D; j=1, 2.

The operator $\times$ in Eq. (3.1) represents the cross product of two vectors ${}^{B}\boldsymbol{\omega}$ and ${}^{B}\boldsymbol{p}_{Bij}$. The wire velocities are given by

$$ \begin{cases} \dot{l}_{i1} = {}^{B}\boldsymbol{e}_{i1}^{\mathrm{T}}\,{}^{B}\dot{\boldsymbol{p}}_{Bi1} + R_i\dot{\theta}_i, \\ \dot{l}_{i2} = {}^{B}\boldsymbol{e}_{i2}^{\mathrm{T}}\,{}^{B}\dot{\boldsymbol{p}}_{Bi2} - R_i\dot{\theta}_i, \end{cases} \tag{3.2} $$

where $\dot{l}_{i1}$, $\dot{l}_{i2}$ are the wire velocities, ${}^{B}\boldsymbol{e}_{i1}$, ${}^{B}\boldsymbol{e}_{i2}$ are the wire vectors with unit length, R_i is the radius of the pulley, and $\dot{\theta}_i$ is the angular velocity of the pulley.

Substituting Eq. (3.1) into Eq. (3.2) and applying the scalar triple product gives

$$ \begin{bmatrix} \dot{l}_{i1} \\ \dot{l}_{i2} \end{bmatrix} = \begin{bmatrix} {}^{B}\boldsymbol{e}_{i1}^{\mathrm{T}} & ({}^{B}\boldsymbol{p}_{Bi1} \times {}^{B}\boldsymbol{e}_{i1})^{\mathrm{T}} & R_i \\ {}^{B}\boldsymbol{e}_{i2}^{\mathrm{T}} & ({}^{B}\boldsymbol{p}_{Bi2} \times {}^{B}\boldsymbol{e}_{i2})^{\mathrm{T}} & -R_i \end{bmatrix} \begin{bmatrix} {}^{B}\dot{\boldsymbol{p}}_{T} \\ {}^{B}\boldsymbol{\omega} \\ \dot{\theta}_i \end{bmatrix}. \tag{3.3} $$

Applying duality, the resultant force caused by T_{i1} and T_{i2} are:

$$ \begin{bmatrix} {}^{B}\boldsymbol{f}_i \\ {}^{B}\boldsymbol{n}_i \\ n_i \end{bmatrix} = \begin{bmatrix} {}^{B}\boldsymbol{e}_{i1} & {}^{B}\boldsymbol{e}_{i2} \\ {}^{B}\boldsymbol{p}_{Bi1} \times {}^{B}\boldsymbol{e}_{i1} & {}^{B}\boldsymbol{p}_{Bi2} \times {}^{B}\boldsymbol{e}_{i2} \\ R_i & -R_i \end{bmatrix} \begin{bmatrix} T_{i1} \\ T_{i2} \end{bmatrix}. \tag{3.4} $$

When the wire mechanism containing N_D DAMs is considered in the n directional space, the relationship between the resultant force vector and the wire tension vector is given by

$$ \boldsymbol{F} = \boldsymbol{W}\boldsymbol{T}, \tag{3.5} $$

where: $\boldsymbol{T} = \begin{bmatrix} T_{11} & T_{12} & T_{21} & T_{22} & \dots & T_{N_D1} & T_{N_D2} \end{bmatrix}^{\mathrm{T}}_{2N_D\times 1}$ is the wire tension vector, $\boldsymbol{F}$ (= $\begin{bmatrix} f_x & f_y & f_z & n_x & n_y & n_z & n_1 & \dots & n_{N_D} \end{bmatrix}^{\mathrm{T}}_{(n+N_D)\times 1}$ in the case of $n = 6$) is the resultant force vector, $\boldsymbol{W}$ is the wire matrix defined as

$$\boldsymbol{W} = \begin{bmatrix} \boldsymbol{W}_G \\ \boldsymbol{W}_L \end{bmatrix}_{(n+N_D)\times 2N_D}. \tag{3.6}$$

Here, the size of the wire matrix $\boldsymbol{W}$ is $(n+N_D)\times 2N_D$, where $(n+N_D)$ is the number of rows and includes n DOFs in the global motion space and N_D DOFs in the local motion space. The number of columns is $2N_D$, which is two times the number of DOFs in the local motion space. The matrix $\boldsymbol{W}$, which contains the matrix $\boldsymbol{W}_G$ contributing to the resultant force exerted on the top plate, and the matrix $\boldsymbol{W}_L$ contributing to the local moments of the local pulleys. The two matrices are as follows:

$$\boldsymbol{W}_G = \begin{bmatrix} {}^B\boldsymbol{e}_{11} & {}^B\boldsymbol{e}_{12} & {}^B\boldsymbol{e}_{21} & {}^B\boldsymbol{e}_{22} \\ {}^B\boldsymbol{p}_{B11}\times {}^B\boldsymbol{e}_{11} & {}^B\boldsymbol{p}_{B12}\times {}^B\boldsymbol{e}_{12} & {}^B\boldsymbol{p}_{B21}\times {}^B\boldsymbol{e}_{21} & {}^B\boldsymbol{p}_{B22}\times {}^B\boldsymbol{e}_{22} \\ \dots & {}^B\boldsymbol{e}_{N_D1} & {}^B\boldsymbol{e}_{N_D2} & \\ \dots & {}^B\boldsymbol{p}_{BN_D1}\times {}^B\boldsymbol{e}_{N_D1} & {}^B\boldsymbol{p}_{BN_D2}\times {}^B\boldsymbol{e}_{N_D2} & \end{bmatrix}_{n\times 2N_D}, \tag{3.7}$$

$$\boldsymbol{W}_L = \begin{bmatrix} R_1 & -R_1 & 0 & 0 & \dots & 0 & 0 \\ 0 & 0 & R_2 & -R_2 & \dots & 0 & 0 \\ \vdots & \vdots & \vdots & \vdots & \vdots & \vdots & \vdots \\ 0 & 0 & 0 & 0 & \dots & R_{N_D} & -R_{N_D} \end{bmatrix}_{N_D\times 2N_D}. \tag{3.8}$$

3.1.2 Problem Statement

The matrix $\boldsymbol{W}$ with size $(n+N_D)\times 2N_D$ becomes very large when developing wire mechanisms using a large number of DAMs to move in a multi-directional space. This is inconvenient, making it difficult to judge whether the wire mechanism has a proper configuration using standard approaches. A method for dealing with large wire matrices is therefore necessary for developing a multi-directional RDWM.

3.2. The Conversion of Wire Matrix to the New Expression

The proposed method consists of two procedures. The procedure for converting the wire matrix by considering the sums and differences of the sets of two wire tensions of the DAMs is described first. The procedure for judging a candidate mechanism using the components of the wire matrix that relate the resultant forces and the combination of the sums of the sets of two wire tensions of the DAMs is presented in the following section.

3.2.1 Procedure to Derive the Wire Matrix in Normal Form

Defining ${}^T\boldsymbol{p}_{TCi}$, $\boldsymbol{R}_i$, ${}^T\boldsymbol{p}_{TDi}$ and ${}^T\boldsymbol{p}_{Bij}$

Figure 3.1 shows the relations between the parameters of a DAM. Here, ${}^T\boldsymbol{p}_{TCi}$ is the position vector of the center point $\boldsymbol{C}_i$ of $\boldsymbol{B}_{i1}\boldsymbol{B}_{i2}$ w.r.t the top plate's center $\boldsymbol{O}_T$; ${}^T\boldsymbol{p}_{Bi1}$ and ${}^T\boldsymbol{p}_{Bi2}$ are the

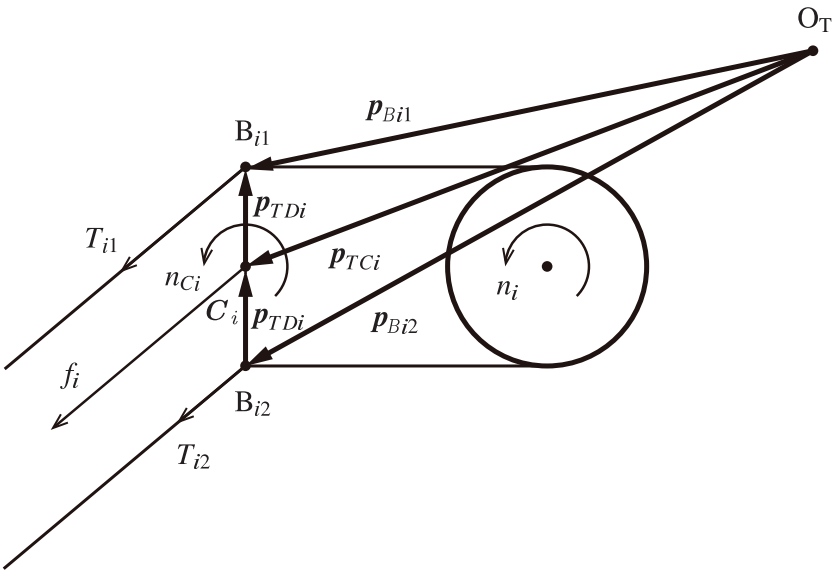

Figure. 3.1: The set of force and moment equivalent to a set of wire tensions applied to a DAM.

position vectors of $\boldsymbol{B}_{i1}$ and $\boldsymbol{B}_{i2}$ w.r.t $\boldsymbol{O}_T$; ${}^T\boldsymbol{p}_{TDi}$ is the position vector of $\boldsymbol{B}_{i1}$ w.r.t $\boldsymbol{C}_i$, and it has the norm equal to the pulley radius R_i. As shown in the figure, the three vectors ${}^T\boldsymbol{p}_{Bi1}$, ${}^T\boldsymbol{p}_{TCi}$ and ${}^T\boldsymbol{p}_{TDi}$ create a triangle; the three vectors ${}^T\boldsymbol{p}_{Bi2}$, ${}^T\boldsymbol{p}_{TCi}$ and ${}^T\boldsymbol{p}_{TDi}$ also create a triangle; therefore the below relations can be derived:

$$\begin{cases} {}^T\boldsymbol{p}_{Bi1} = {}^T\boldsymbol{p}_{TCi} + {}^T\boldsymbol{p}_{TDi}, \\ {}^T\boldsymbol{p}_{Bi2} = {}^T\boldsymbol{P}_{TCi} - {}^T\boldsymbol{p}_{TDi}. \end{cases} \tag{3.9}$$

Set of Position ${}^B\boldsymbol{p}_T$ and Orientation ${}^B\boldsymbol{R}_T$ of the Top Plate

The initial position ${}^B\boldsymbol{p}_T$ and orientation ${}^B\boldsymbol{R}_T$ of the top plate can have an arbitrary value inside the working space of the top plate.

Position of Wire End Points on the Top Plate

This is given by the following equation:

$${}^B\boldsymbol{p}_{Bij} = {}^B\boldsymbol{p}_T + {}^B\boldsymbol{R}_T{}^{\mathrm{T}}\boldsymbol{p}_{Bij}, \tag{3.10}$$

where ${}^B\boldsymbol{R}_T$ is the rotational matrix from the base coordinate to the top coordinate.

Position of Wire End Points on the Frame

The positions of the wire end points on the frame ${}^B\boldsymbol{p}_{Aij}$ need to be chosen so that the wire vectors span the motion direction of the top plate.

Calculating the Wire Vectors ${}^B\boldsymbol{e}_{ij}$

The wire vectors can be derived from the following equation:

$${}^B\boldsymbol{e}_{ij} = \frac{{}^B\boldsymbol{p}_{Aij} - {}^B\boldsymbol{p}_{Bij}}{\|{}^B\boldsymbol{p}_{Aij} - {}^B\boldsymbol{p}_{Bij}\|}\ . \tag{3.11}$$

Here, ${}^B\boldsymbol{p}_{Aij} = \left[{}^Bx_{Aij} \;\; {}^By_{Aij} \;\; {}^Bz_{Aij}\right]^{\mathrm{T}}$ are the positions of the wire end points on the frame w.r.t the base coordinate and ${}^B\boldsymbol{p}_{Bij} = \left[{}^Bx_{Bij} \;\; {}^By_{Bij} \;\; {}^Bz_{Bij}\right]^{\mathrm{T}}$ represents the positions of the wire end points on the top plate w.r.t the base coordinate. The symbol $\|.\|$ in Eq. (3.11) represents the Euclidean norm of a vector.

Checking if the Two Wires in a DAM Are in Parallel

Because the top plate can change its orientation when the system is operating, there will have cases where the two wires in a DAM are twisted and contacted with each other, which make bad affect to the operation of RDWM. This chapter assumes that the change of the orientation of the top plate is small enough and the set of two wires of DAM can be treated to be parallel. The method to fix the orientation of the top plate to ensure this assumption will be discussed in the next chapter.

Derivation of the Wire Matrix in Normal Form

The derivation of the wire matrix in normal form is shown in Eqs. (3.6), (3.7), and (3.8).

3.2.2 Conversion of the Wire Matrix to New Form

With the structure of DAM shown in figure 3.1, the two wires in each DAM are in parallel so the two wire vectors ${}^B\boldsymbol{e}_{i1}$, ${}^B\boldsymbol{e}_{i2}$ can be represented as one vector ${}^B\boldsymbol{e}_i$ with the same direction at the center point $\boldsymbol{C}_i$. Then ${}^B\boldsymbol{e}_i$ can be derived as follows:

$$ {}^B\boldsymbol{e}_i = {}^B\boldsymbol{e}_{ij}. \tag{3.12}$$

The vectors ${}^B\boldsymbol{p}_{TCi}$ and ${}^B\boldsymbol{p}_{TDi}$ are derived from the position of points $\boldsymbol{B}_{ij}$ as follows:

$$\begin{cases} {}^B\boldsymbol{p}_{TCi} = ({}^B\boldsymbol{p}_{Bi1} + {}^B\boldsymbol{p}_{Bi2})/2, \\ {}^B\boldsymbol{p}_{TDi} = ({}^B\boldsymbol{p}_{Bi1} - {}^B\boldsymbol{p}_{Bi2})/2. \end{cases} \tag{3.13}$$

Then Eq. (4.1) becomes

$$\begin{bmatrix} {}^B\boldsymbol{f}_i \\ {}^B\boldsymbol{n}_i \\ n_i \end{bmatrix} = \begin{bmatrix} {}^B\boldsymbol{e}_{\mathrm{i}} & \boldsymbol{0} \\ {}^B\boldsymbol{p}_{TC\mathrm{i}} \times {}^B\boldsymbol{e}_i & {}^B\boldsymbol{p}_{TDi} \times {}^B\boldsymbol{e}_i \\ 0 & R_i \end{bmatrix} \begin{bmatrix} T_{i1} + T_{i2} \\ T_{i1} - T_{i2} \end{bmatrix}. \tag{3.14}$$

The expressions in Eqs. (3.5) and (3.6) can be converted into a new expression as

$$\boldsymbol{F} = \boldsymbol{W}^{'}\boldsymbol{T}^{'}. \tag{3.15}$$

Here, $\boldsymbol{T}^{'} = \begin{bmatrix} \boldsymbol{T_S} & \boldsymbol{T_D} \end{bmatrix}^{\mathrm{T}}_{2N\times 1}$ is the new expression of the wire tension vector;
$\boldsymbol{T_S} = \begin{bmatrix} (T_{11} + T_{12}) & \ldots & (T_{N_D1} + T_{N_D2}) \end{bmatrix}^{\mathrm{T}}_{N_D\times 1}$ is the vector of the sums of the sets of two wire tensions of the DAMs and $\boldsymbol{T_D} = \begin{bmatrix} (T_{11} - T_{12}) & \ldots & (T_{N_D1} - T_{N_D2}) \end{bmatrix}^{\mathrm{T}}_{N_D\times 1}$ is the vector of the differences of the sets of two wire tensions of the DAMs. The new expression of wire matrix $\boldsymbol{W}^{'}$ is given by

$$\boldsymbol{W}^{'} = \begin{bmatrix} \boldsymbol{W}^{'}_G & \boldsymbol{W}_C \\ \boldsymbol{O} & \boldsymbol{W}^{'}_L \end{bmatrix}_{(n+N_D)\times 2N_D}. \tag{3.16}$$

Inside the matrix $\boldsymbol{W}^{'}$ the matrix $\boldsymbol{W}_L^{'}$ contributes to producing local moments of pulleys on the top plate while the set of matrices $\boldsymbol{W}_G^{'}$ and $\boldsymbol{W}_C$ contributes to producing the resultant force and resultant moment on the top plate. The contents of $\boldsymbol{W}_G^{'}$, $\boldsymbol{W}_L^{'}$, and $\boldsymbol{W}_C$ are shown below:

$$\boldsymbol{W}_G^{'} = \begin{bmatrix} {}^B\boldsymbol{e}_1 & {}^B\boldsymbol{e}_2 & \dots & {}^B\boldsymbol{e}_{N_D} \\ {}^B\boldsymbol{p}_{TC1} \times {}^B\boldsymbol{e}_1 & {}^B\boldsymbol{p}_{TC2} \times {}^B\boldsymbol{e}_2 & \dots & {}^B\boldsymbol{p}_{TCN_D} \times {}^B\boldsymbol{e}_{N_D} \end{bmatrix}_{n \times N_D}, \tag{3.17}$$

$$\boldsymbol{W}_L^{'} = \begin{bmatrix} R_1 & 0 & \dots & 0 \\ 0 & R_2 & \dots & 0 \\ \vdots & \vdots & \vdots & \vdots \\ 0 & 0 & \dots & R_{N_D} \end{bmatrix}_{N_D \times N_D}, \tag{3.18}$$

$$\boldsymbol{W}_C = \begin{bmatrix} \boldsymbol{O} & & & \\ \boldsymbol{p}_{TD1} \times {}^B\boldsymbol{e}_1 & \boldsymbol{p}_{TD2} \times {}^B\boldsymbol{e}_2 & \dots & \boldsymbol{p}_{TDN_D} \times {}^B\boldsymbol{e}_{N_D} \end{bmatrix}_{n \times N_D}. \tag{3.19}$$

$$\boldsymbol{O} = [\boldsymbol{0}]_{N_D \times N_D}. \tag{3.20}$$

The converted matrix $\boldsymbol{W}^{'}$ describes the geometrical meaning of the sums and differences of the sets of two wire tensions of the DAMs. In figure 3.1, the set of wire tensions $[T_{i1},\ T_{i2}]$ is equivalent to the set of force and moment $[f_i,\ n_{Ci}]$ derived from the sum $(T_{i1} + T_{i2})$ and difference $(T_{i1} - T_{i2})$. The component ${}^B\boldsymbol{p}_{TCi} \times {}^B\boldsymbol{e}_i$, which produces the moment at the center of the top plate comes from the sum $(T_{i1} + T_{i2})$ while the component ${}^B\boldsymbol{p}_{TDi} \times {}^B\boldsymbol{e}_i$ produces the moment at the center of $\mathrm{B}_{i1}\mathrm{B}_{i2}$ from the difference $(T_{i1} - T_{i2})$.

3.3. New Judgment Method for Checking A RDWM Candidate

The procedure for judging whether a candidate RDWM can produce the resultant forces for achieving the required motions is discussed in this section. Figure 3.2(a) shows the wire vectors on the top plate with four sets of DAMs. When two wires in the DAM are in parallel, the two wire vectors ${}^B\boldsymbol{e}_{i1}$ and ${}^B\boldsymbol{e}_{i2}$ can be expressed as a common vector in the center of $\mathrm{B}_{i1}\mathrm{B}_{i2}$ labeled ${}^B\boldsymbol{e}_i$ as shown in figure 3.2(b).

In order to check the ability for producing force in any direction, it is not necessary to evaluate the whole matrix $\boldsymbol{W}$. Instead, matrix $\boldsymbol{W}$ is converted into matrix $\boldsymbol{W}^{'}$.Although the two matrices are of the same size, this matrix is already divided into small components by Eq. (3.16), and only the matrix $\boldsymbol{W}_G^{'}$ relating to the global motion needs to be checked for vector closure condition. Note that neither of the matrix $\boldsymbol{W}$ nor the matrix $\boldsymbol{W}^{'}$ is necessary to be derived from now. What we need to do is to derive ${}^B\boldsymbol{e}_i$ and ${}^B\boldsymbol{p}_{TCi}$ then substitute them to Eq. (3.17) to get matrix $\boldsymbol{W}_G^{'}$ for the process of judgment of a candidate. Matrix $\boldsymbol{W}_G^{'}$ has size $n \times N$ with rows equal to the number of DOF n of the motion space and columns equal to the

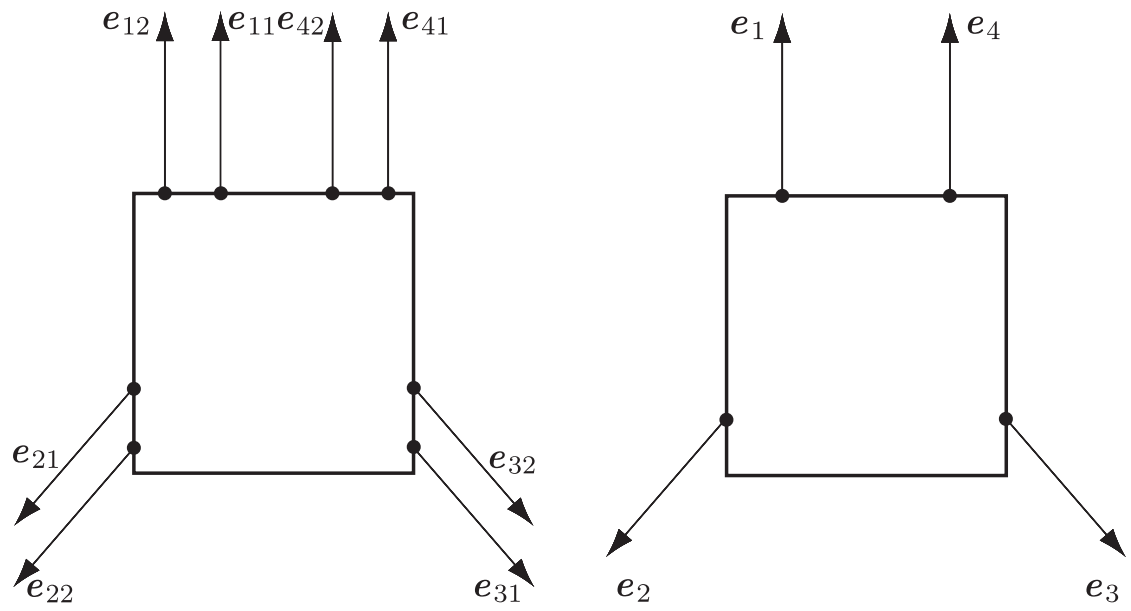

(a) Wire vectors on the top plate with DAMs. (b) The simple expression of wire vectors.

Figure. 3.2: Wire vectors on the top plate with DAMs and the simple expression.

number of DAMs N. This is a quarter of the size of the matrix $\boldsymbol{W}$, making the judgment much more convenient.

From the statics relationship between wire tensions and the resultant force in Eq. (3.5), the new expression of statics relations is given by Eq. (3.15). The resultant force and moment on the top plate are given by

$$\begin{bmatrix} f_x \\ f_y \\ f_z \\ n_x \\ n_y \\ n_z \end{bmatrix} = \begin{bmatrix} \boldsymbol{W}'_{Gf} \\ \boldsymbol{W}'_{Gm} \end{bmatrix} \boldsymbol{T_S} + \begin{bmatrix} \boldsymbol{O} \\ \boldsymbol{W}_{Cnz} \end{bmatrix} \boldsymbol{T_D}, \tag{3.21}$$

where:

$$\boldsymbol{W}'_{Gf} = \begin{bmatrix} {}^B\boldsymbol{e}_1 & {}^B\boldsymbol{e}_2 & \dots & {}^B\boldsymbol{e}_{N_D} \end{bmatrix}_{n_f \times N_D} \tag{3.22}$$

is the part of matrix $\boldsymbol{W}'_G$ in Eq. (3.17) which is related to the resultant force on the top plate;

$$\boldsymbol{W}'_{Gm} = \begin{bmatrix} {}^B\boldsymbol{p}_{TC1} \times {}^B\boldsymbol{e}_1 & {}^B\boldsymbol{p}_{TC2} \times {}^B\boldsymbol{e}_2 & \dots & {}^B\boldsymbol{p}_{TCN_D} \times {}^B\boldsymbol{e}_{N_D} \end{bmatrix}_{n_m \times N_D} \tag{3.23}$$

is the part of matrix $\boldsymbol{W}'_G$ which is related to the resultant moment on the top plate;

$$\boldsymbol{O} = [\boldsymbol{0}]_{n_f \times N_D} \tag{3.24}$$

is an $n_f \times N_D$ zero matrix;

$$\boldsymbol{W}_{Cnz} = \begin{bmatrix} \boldsymbol{p}_{TD1} \times {}^B\boldsymbol{e}_1 & \boldsymbol{p}_{TD2} \times {}^B\boldsymbol{e}_2 & \dots & \boldsymbol{p}_{TDN_D} \times {}^B\boldsymbol{e}_{N_D} \end{bmatrix}_{n_m \times N_D} \tag{3.25}$$

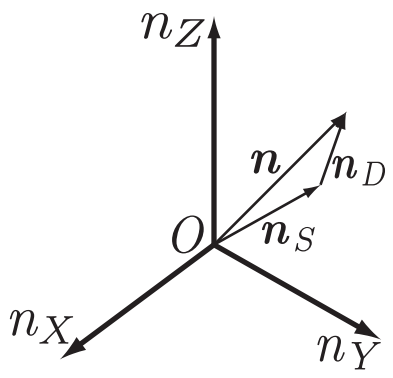

Figure. 3.3: Moment on the top plate.

is the non-zero part of matrix $\boldsymbol{W}_C$ in Eq. (3.19). Here, $n_f + n_m = n$, where n_f is the number of DOFs under the resultant force, n_m is the number of DOFs under the resultant moment and n is the total number of DOFs of the whole motion space.

From Eq. (3.21), the resultant moment can be derived as

$$\boldsymbol{n} = \boldsymbol{n_S} + \boldsymbol{n_D}. \tag{3.26}$$

Here, $\boldsymbol{n} = [n_x \;\; n_y \;\; n_z]^{\mathrm{T}}$ is the resultant moment on the top plate, $\boldsymbol{n_S} = \boldsymbol{W}'_{Gm}\boldsymbol{T_S}$ is the moment from the sum of the sets of two wire tensions of the DAMs, and $\boldsymbol{n_D} = \boldsymbol{W}_{Cnz}\boldsymbol{T_D}$ is the moment from the difference of the sets of two wire tensions of the DAMs. Matrix $\boldsymbol{W}'_{Gm}$ is the part of matrix $\boldsymbol{W}'_G$ related to the resultant moment while matrix $\boldsymbol{W}_{Cnz}$ is the non-zero part of matrix $\boldsymbol{W}_C$.

Figure 3.3 shows the vector form of Eq. (3.26). Theoretically, because $\boldsymbol{n_S}$ always has a positive value and $\boldsymbol{n_D}$ has much smaller value than $\boldsymbol{n_S}$, $\boldsymbol{n}$ always has a positive value and can be produced in any direction. To check the ability for producing force in any direction, the moment $\boldsymbol{n_S}$ will be used; however, to produce global motion, the resultant moment $\boldsymbol{n}$ needs to be in any direction.

To check whether a conventional wire mechanism can produce force in any direction, the force closure condition is used for workspace analysis [31, 32]. On the other hand, the vector closure condition is discussed in [13, 55] as a simpler way to evaluate the ability to produce force in any direction of conventional wire mechanism. For developing RDWM, the modified vector closure condition is expressed as follows:

In an n-dimension space, an RDWM with N_D DAMs ($N_D \geq$ n+1) is said to satisfy the vector closure condition if the wire matrix of global motion $\boldsymbol{W}'_G$ satisfies the following two conditions:

C1) rank($\boldsymbol{W}'_G$) = n.

C2) *There exists a vector $\boldsymbol{T_S} > \boldsymbol{0}$ that satisfies $\boldsymbol{W}'_G\boldsymbol{T_S} = \boldsymbol{0}$.*

Any wire mechanism wherein matrix $\boldsymbol{W}'_G$ satisfies the two conditions C1), C2) will satisfy

the vector closure condition and the resultant force can be produced in any direction in the motion space.

3.4. Discussion and Conclusion

This chapter discussed the new judgment method for RDWM candidates using DAMs. Because the normal form of wire matrix has large size, which is very inconvenient when developing wire mechanism to move in a multi-direction space, it is converted to the new form. Then only the essential component of the new form which is just a quarter of the size of the normal form is needed for the judgment. This is very important as will be described in the next chapter, the essential component will be used in the proposed judgment procedure of RDWM to make it simpler and easier. Then, the numerical examples in chapter 5 will make clear and verify the proposed method of using the essential component of the new form of wire matrix.

Chapter 4

How to Keep the Orientation of the Top Plate and Reduce the Number of Actuators

4.1. Problem Statement

4.1.1 Basic Structure of RDWM

In the RDWM concept, the DAMs are used to achieve high-acceleration and high precise-motions, and a 1DOF RDWM has been already proposed [48]. The DAM contains two actuators that move the top plate and rotate the local pulley, as shown in figure 2.2. When the two actuators rotate in the same direction, a global translational motion is produced. Conversely, when the two actuators rotate in different directions, local pulley rotates to generate precise local motion. As shown in figure 2.4, the top plate in RDWM is controlled by fourteen wires in seven DAMs. The RDWM can move at high speed through a large working space and also undertake specific tasks with high precise using the three fingers on its top plate. The fingers perform grasping tasks using a common DOF and can hold the object using two DOFs for each finger. The structure of a planar RDWM using four DAMs is shown in figure 5.4. Global, high-acceleration motions of the top plate are achieved by applying a large translational force to the mechanism. This force is the sum of the two wire tensions of each DAM. The difference between the wire tensions of each DAM generates a torque for the corresponding local pulley, enabling precise local motions of the top plate mechanism. The basic equations of the planar RDWM using four DAMs are given below:

$$\boldsymbol{F} = \boldsymbol{W}\boldsymbol{T}, \tag{4.1}$$

$$\dot{\boldsymbol{l}} = \boldsymbol{W}^{\mathbf{T}}\boldsymbol{v}, \tag{4.2}$$

where: $\boldsymbol{F} = [\, f_x f_y \, n_z \, n_1 \, n_2 \, n_3 \, n_4 \,]^{\mathrm{T}} \in \boldsymbol{R}^7$ is the resultant force vector. Here f_x and f_y are the resultant forces in the X and Y directions, respectively, for global motion of the top plate; n_z is the resultant moment around the Z-axis for global motion of the top plate; and n_1, n_2, n_3, n_4 are torques on the four local pulleys. $\boldsymbol{T} = [\, T_{11} \, T_{12} \, T_{21} \, T_{22} \, T_{31} \, T_{32} \, T_{41} \, T_{42} \,]^{\mathrm{T}} \in \boldsymbol{R}^8$ is the

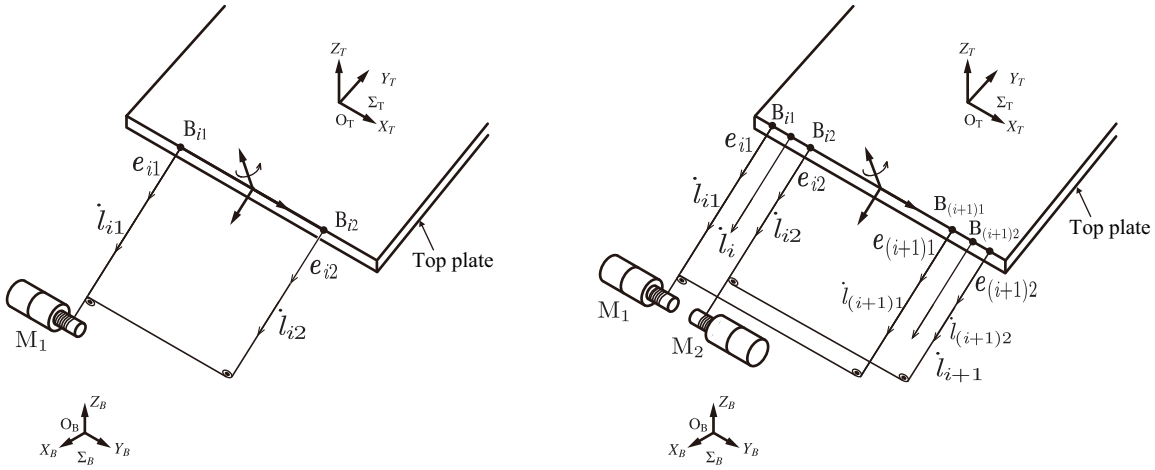

(a) VCM with single actuator module.

(b) VCM with DAM

Figure. 4.1: Velocity Constraint Modules.

wire tension vector, where T_{ij} $(i = 1, 2, 3, 4; j = 1, 2)$ is the tension on each wire, and $\dot{\boldsymbol{l}} = [\, \dot{l}_{11}\, \dot{l}_{12}\, \dot{l}_{21}\, \dot{l}_{22}\, \dot{l}_{31}\, \dot{l}_{32}\, \dot{l}_{41}\, \dot{l}_{42}\,]^{\mathrm{T}} \in \boldsymbol{R}^8$ is the wire velocity vector, where $\dot{l}_{ij}$ $(i = 1, 2, 3, 4; j = 1, 2)$ is the velocity of each wire. $\boldsymbol{v} = [\, \dot{p}_x\, \dot{p}_y\, \dot{\phi}_z\, \dot{\theta}_1\, \dot{\theta}_2\, \dot{\theta}_3\, \dot{\theta}_4\,]^{\mathrm{T}} \in \boldsymbol{R}^7$ is the output velocity vector, where $\dot{p}_x$ and $\dot{p}_y$ are the top plate's velocities in the X and Y directions respectively, $\dot{\phi}_z$ is the top plate's angular velocity around the Z-axis, $\dot{\theta}_1, \dot{\theta}_2, \dot{\theta}_3$ and $\dot{\theta}_4$ are the local pulleys' angular velocities, and $\boldsymbol{W} \in \boldsymbol{R}^{7\times 8}$ is the wire matrix, which can be derived from Eq. (3.6).

The basic equations of actuators are represented as follows:

$$\dot{\boldsymbol{l}} = \boldsymbol{J}\dot{\boldsymbol{q}}, \tag{4.3}$$

$$\boldsymbol{\tau} = \boldsymbol{J}^{\mathbf{T}}\boldsymbol{T}, \tag{4.4}$$

where $\dot{\boldsymbol{q}} = [\, \dot{q}_{11}\, \dot{q}_{12}\, \dot{q}_{21}\, \dot{q}_{22}\, \dot{q}_{31}\, \dot{q}_{32}\, \dot{q}_{41}\, \dot{q}_{42}\,]^{\mathrm{T}} \in \boldsymbol{R}^8$ is the actuator velocity vector. Here $\dot{q}_{ij}$ $(i = 1, 2, 3, 4; j = 1, 2)$ is angular velocity of each actuator, and $\boldsymbol{\tau} = [\, \tau_{11}\, \tau_{12}\, \tau_{21}\, \tau_{22}\, \tau_{31}\, \tau_{32}\, \tau_{41}\, \tau_{42}\,]^{\mathrm{T}} \in \boldsymbol{R}^8$ is the actuator torque vector, where τ_{ij} $(i = 1, 2, 3, 4; j = 1, 2)$ is the torque of each actuator. $\boldsymbol{J} = \mathrm{diag.}(N_{11}, N_{12}, ..., N_{42}) \in \boldsymbol{R}^{8\times 8}$ is a regular matrix of reduction ratios N_{ij} $(i = 1, 2, 3, 4; j = 1, 2)$ of actuator ij^{th} which include the pulley radius information. $\boldsymbol{J}$ is actually the Jacobian matrix between the wire and actuator velocities.

4.1.2 Basic Concept of RDWM with VCM

Figure 4.1(a) shows a VCM with a single actuator module. The VCM is characterized by equality of the two wire velocities $\dot{l}_{i1}$ and $\dot{l}_{i2}$, which restricts the posture of the top plate around the axis perpendicular to the plane containing the two wires. The VCM requires one fewer actuator than driving the top plate in the same direction by two single wires.

Similarly, the VCM is combined with DAM to generate high acceleration motions is shown in figure 4.1(b). Here, the two summation velocities $\dot{l}_i$ and $\dot{l}_{i+1}$ are equal because $\dot{l}_{i1} = \dot{l}_{(i+1)1}$

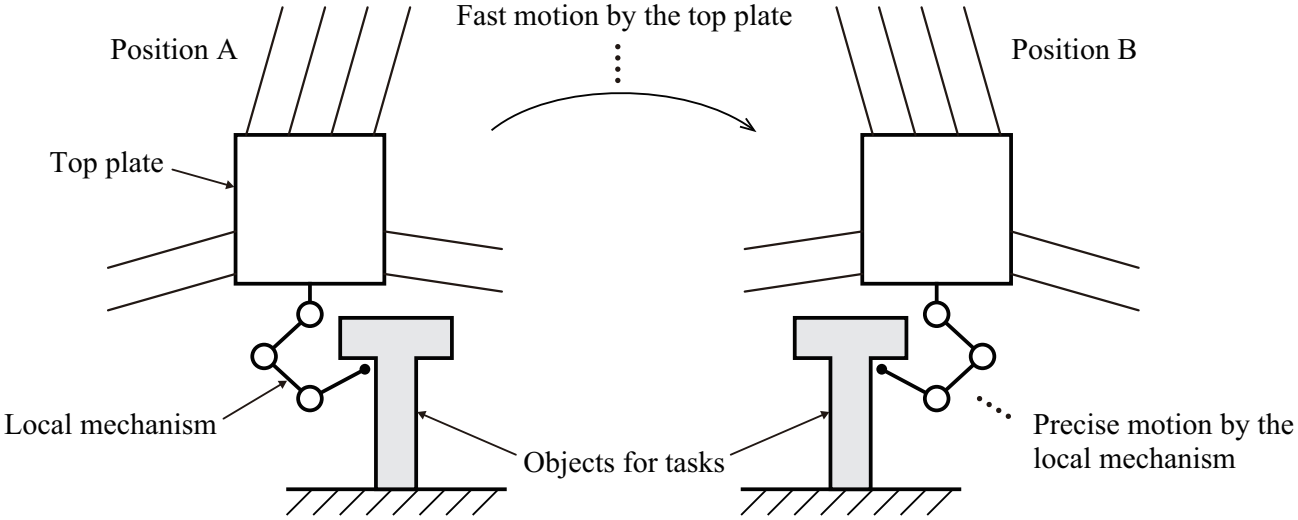

Figure. 4.2: Basic concept of RDWM with VCM.

and $\dot{l}_{i2} = \dot{l}_{(i+1)2}$. This configuration restricts the posture of the top plate around the axis perpendicular to the plane containing the four wires. This VCM requires two fewer actuators than driving the top plate in the same direction by two DAMs.

The above analysis shows that configuring VCMs on RDWM can reduce the required number of actuators. Moreover, the VCMs constraint the posture of the top plate. Therefore, we can propose candidate RDWMs with VCMs that fix the posture of the top plate and allow translational-only motions with fewer actuators than other configurations. However, this research excludes the vibration of the mechanism and investigations on vibration suppression. The wire is assumed as ideally stiffness with no wire elasticity.

Figure 4.2 shows the basic concept of RDWM with VCM. As shown in this figure, the top plate can move at fast speed through a large working space, but its orientation is fixed by the VCMs, which have parallel alignments of two sets of double wires. However, the orientation of the top plate is intrinsically difficult to change, and the end point of the RDWM can be reoriented by precise motions generated by the local mechanism in the proposed structure.

Figure 4.3 shows the proposed structure of the planar RDWM with a VCM. The structure is governed by Eqs. (4.1) and (4.2) and the following basic equations of the actuators:

$$\dot{\boldsymbol{l}} = \boldsymbol{J}_{vc}\dot{\boldsymbol{q}}_{vc}, \tag{4.5}$$

$$\boldsymbol{\tau}_{vc} = \boldsymbol{J}_{vc}^{\mathrm{T}}\boldsymbol{T}, \tag{4.6}$$

where $\dot{\boldsymbol{q}}_{vc} = [\,\dot{q}_{11}\,\dot{q}_{12}\,\dot{q}_{21}\,\dot{q}_{22}\,\dot{q}_{31}\,\dot{q}_{32}\,]^{\mathrm{T}} \in \boldsymbol{R}^6$ is the actuator velocity vector. Here $\dot{q}_{ij}$ $(i = 1,2,3; j = 1,2)$ is the angular velocity of each actuator. $\boldsymbol{\tau}_{vc} = [\,\tau_{11}\,\tau_{12}\,\tau_{21}\,\tau_{22}\,\tau_{31}\,\tau_{32}\,]^{\mathrm{T}} \in \boldsymbol{R}^6$ is the actuator torque vector, where τ_{ij} $(i = 1,2,3; j = 1,2)$ is the torque on each actuator, and $\boldsymbol{J}_{vc} \in \boldsymbol{R}^{8\times 6}$ is the Jacobian matrix between the wire and actuator velocities.

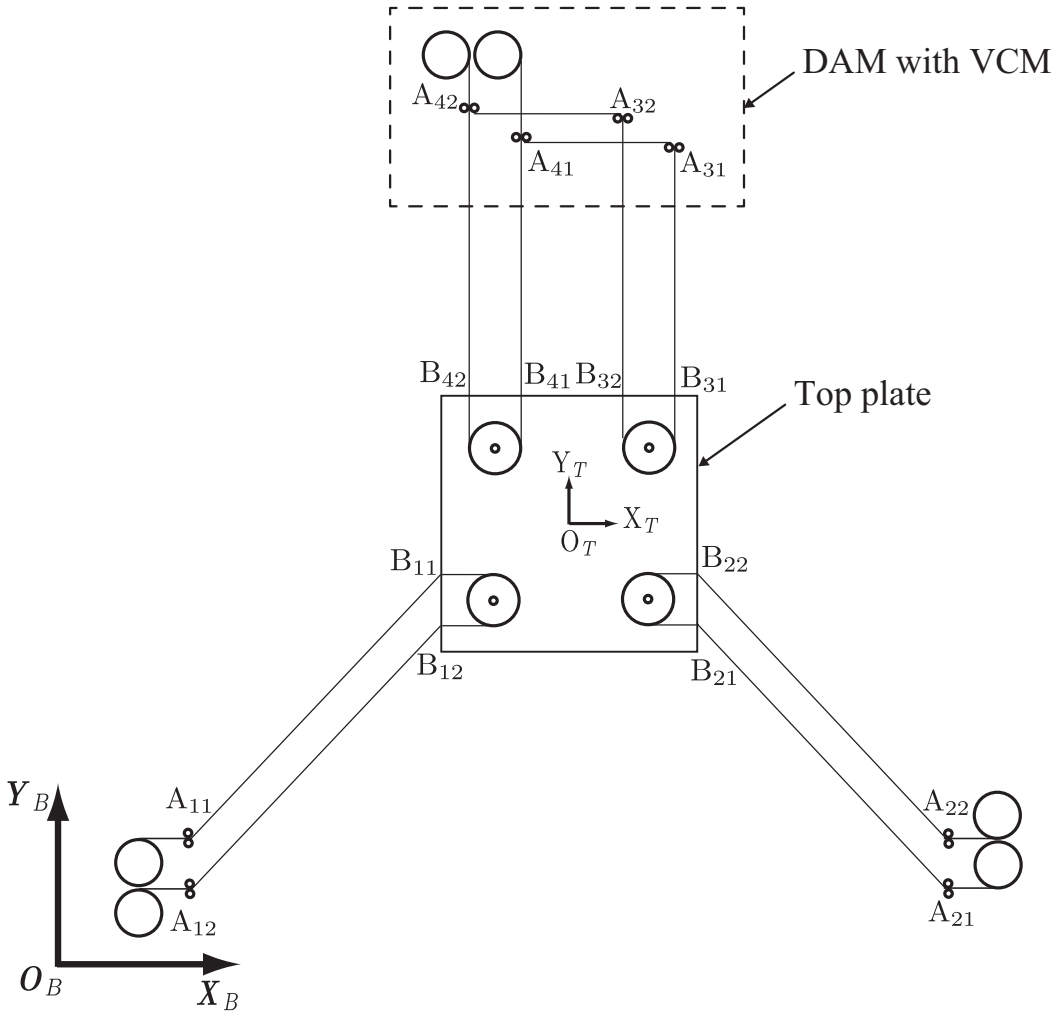

Figure. 4.3: A planar RDWM with a VCM.

In the numerical test cases (see later), the VCMs reduce the number of required actuator units from 8 to 6 in the planar RDWM and from 14 to 8 in the 3D RDWM.

4.1.3 Technical Problems to be Solved

There is an important difference between Eqs. (4.3), (4.4) and Eqs. (4.5), (4.6). The latter pair of equations expresses the constraint imposed by the VCMs. Unlike $\boldsymbol{J}$, the matrix $\boldsymbol{J}_{vc}$ is not regular because it contains the constraint; therefore, the wire tensions are interdependent. The kinematics equations of the whole mechanism are derived from the set of Eqs. (4.2), (4.3) and the set of Eqs. (4.2), (4.5) for the planar RDWM with DAMs and planar RDWM with VCM, respectively:

$$\boldsymbol{J}\dot{\boldsymbol{q}} = \boldsymbol{W}^{\mathbf{T}}\boldsymbol{v}, \tag{4.7}$$

$$\boldsymbol{J}_{vc}\dot{\boldsymbol{q}}_{vc} = \boldsymbol{W}^{\mathbf{T}}\boldsymbol{v}, \tag{4.8}$$

From Eq. (4.7), it is easily to derive $\dot{\boldsymbol{q}} = \boldsymbol{J}^{-1}\boldsymbol{W}^{\mathbf{T}}\boldsymbol{v}$ and the velocity of actuator unit $\dot{\boldsymbol{q}}$ can be got because the matrix $\boldsymbol{J} \in \boldsymbol{R}^{8\times 8}$ is a regular one and is invertible. However, considering Eq. (4.8): it cannot be directly solved as Eq. (4.7) because the matrices $\boldsymbol{J}_{vc} \in \boldsymbol{R}^{8\times 6}$ is not regular and is not invertible. Therefore, the configuration of RDWM with VCM needs to use a kinematical analysis based on convex analysis to solve the problem.

The RDWM candidates cannot be judged solely by checking the vector closure condition (static force analysis). The space (directions and dimensions) of producible velocity of the top plate must be found by kinematic analysis because the VCM excludes the velocity from certain directions. In some cases, the space of producible velocity of the top plate can be intuited from geometrical considerations (see figure 5.5) as mentioned in the subsection "Basic concept of RDWM with VCM". However, in more general cases, this space must be found by an analytical method without relying on intuition. Whether the resultant global-motion force is generated in the desired direction within the space of producible velocity must then be judged by static force analysis. In stepwise fashion, these two analyses will find proper candidate RDWMs with/without VCM. The kinematical analysis was conducted in our previous work [50] and [53] based on [54], but more considered combined analysis is presented here.

4.2. Proposal of the Judgment Procedure to Find RDWM Configuration That Can Produce Desired Velocity

The judgment procedure contains three steps:

Step 1: Checking the vector closure condition.

Step2: Finding the producible velocity space by kinematical analysis (KA).

Step 3: Checking the vector closure condition within the producible velocity space by static force analysis (SFA).

Remark: The essential part of the new form of wire matrix which derived in chapter 3 can be used for vector closure judgment for RDWM with both DAMs and VCMs in step 1.

4.2.1 Outline of the Procedure

To solve the technical problems discussed in the previous section, we propose the following judgment procedure for finding RDWM candidates with/without VCM:

Step 1: Check the necessary condition for vector closure;

Step 2: Find the space of producible velocity (also called the active constraint space $\boldsymbol{S}_{AC}$) by kinematical analysis;

Step 3: Check the vector closure condition within the space of producible velocity.

The above judgment procedure is applicable to RDWM candidates with and without VCM. The contents of each step are described as below:

Using the vector closure condition, step 1 judges whether a resultant force in any direction on the top plate covers the whole motion space. This is a necessary condition.

By kinematical analysis, step 2 derives the active and passive constraint spaces, in which the top plate can and cannot acquire a velocity, respectively.

Using the vector closure condition, step 3 judges whether a resultant force in any direction on the top plate covers the active constraint space derived in step 2.

The proposed judgment procedure can be demonstrated in simple planar configurations, as illustrated in figure 5.4, 5.5 and 5.6.

Intuitively, the top plate in the planar RDWM using four DAMs shown in figure 5.4 can move in the XOY plane and also rotate around the Z-axis. In step 1, the resultant force should be produced in the X and Y directions and around the Z-axis. Step 2, the velocity of the top plate should also be produced in the X and Y directions and around the Z-axis. In step 3, the resultant force force in the static force analysis should again be producible in the X and Y directions and around the Z-axis.

Intuitively the top plate in figure 5.5 can move in the XOY plane but the VCM forbids its rotation around the Z-axis. In step 1, the resultant force should be produced in the X and Y directions and around the Z-axis. The step 2 should restrict the velocity of the top plate to the X and Y directions. In step 3, the static force analysis should restrict the resultant force to the active constraint space (i.e., the X and Y directions).

Intuitively, the configuration of figure 5.6 cannot realize a positive resultant moment around the Z-axis, so appears improper. Step 1 fails to obtain a producible resultant force in all directions. In step 2, the velocity of the top plate should be producible in the X and Y directions and around the Z-axis. However, similar to the step 1, step 3 cannot find a resultant force that is produced in any direction.

4.2.2 Details of Step 1: Checking the Necessary Condition for Holding the Vector Closure

The vector closure condition [13, 55] is used as a necessary condition to judge whether the resultant force can be produced in any direction through out the motion space of the mechanism. For RDWM using DAMs, this condition needs to revised a little bit by using the essential part of the new form of wire matrix which is related to the global motion $\boldsymbol{W}'_G$ and was presented as the main part of chapter 3. The contents of the revised condition is detailed again below:

In an n-dimension space, an RDWM with N_D DAMs ($N_D \geq$ n+1) is said to satisfy the vector closure condition if the wire matrix of global motion $\boldsymbol{W}'_G$ satisfies the following two conditions:

C1) rank($\boldsymbol{W}'_G$) = n.

C2) *There exists a vector $\boldsymbol{T_S} > \boldsymbol{0}$ that satisfies $\boldsymbol{W}'_G \boldsymbol{T_S} = \boldsymbol{0}$.*

Any wire mechanism wherein matrix $\boldsymbol{W}'_G$ satisfies the two conditions C1), C2) will satisfy the vector closure condition and the resultant force can be produced in any direction in the motion space. For checking the vector closure condition, it is sufficient to derive the matrix $\boldsymbol{W}'_G$ by Eq. (4.23) because this matrix alone contributes to the resultant force for producing global motion of the top plate. The rank($\boldsymbol{W}'_G$) in condition C1 defines the number of permitted directions of the resultant forces. If rank($\boldsymbol{W}'_G$) is full ($= n$) the resultant forces can be produced in the whole motion space of the mechanism. In contrast, a partial rank($\boldsymbol{W}'_G$) denotes that the resultant force cannot be produced in one or more directions, so the mechanism configuration should be eliminated. Under condition C2, the matrix $\boldsymbol{W}'_G$ may not be regular because the sizes of wire tension vector $\boldsymbol{T_S}$ and the resultant force vector on the whole motion space $\boldsymbol{F}$ may differ. In this case, the number of roots exceeds the number of equations. If the candidate RDWM is feasible, a positive wire tension $\boldsymbol{T_S}$ such that $\boldsymbol{W}'_G \boldsymbol{T_S} = \boldsymbol{0}$ will exist, meaning that the resultant force can be produced in any direction throughout the whole motion space. Any wire mechanism in which matrix $\boldsymbol{W}'_G$ satisfies both C1 and C2 will satisfy the vector closure condition, and the resultant force can be produced in any direction within the whole motion space.

4.2.3 Details of Step 2: Find the Producible Velocity Space by Kinematical Analysis (KA)

The kinematical analysis judges the motion direction space of the RDWM candidates. This procedure first derives the velocities of the DAMs and VCMs contributing to the top plate's velocity. The derived velocity sets are then combined into a complete set of the top plate's velocities, which is converted from face-form to span-form by convex theory [56–61]. The conversion procedure is summarized in **Appendix D**, and is comprehensively solved by linear programming in [61]. The kinematical analysis is detailed below:

a. Set of top plate velocities contributed by the DAM without VCM

Assuming that the wire velocities satisfy -1[m/s] $\leq \dot{l}_{ij} \leq$ 1[m/s], the DAM characteristic yield the following inequalities:

$$\begin{cases} -1 \leq \dot{l}_{i1} \leq 1, \\ -1 \leq \dot{l}_{i2} \leq 1. \end{cases} \tag{4.9}$$

Eq. (4.9) implies that each wire can produce a non-zero velocity (either positive or negative). The values "1" and "-1" are dummy values with no specific meaning. In matrix form, these inequalities are expressed as:

$$\boldsymbol{A}_{Ldi}\dot{\boldsymbol{l}}_{di} \leq \boldsymbol{b}_{Ldi}, \tag{4.10}$$

where $\dot{\boldsymbol{l}}_{di} = [\, \dot{l}_{i1}\ \dot{l}_{i2}\,]^{\mathrm{T}} \in \boldsymbol{R}^2$ is the wire velocity vector of DAM without VCM and:

$$\boldsymbol{A}_{Ldi} = \begin{bmatrix} -1 & 0 \\ 1 & 0 \\ 0 & -1 \\ 0 & 1 \end{bmatrix} \in \boldsymbol{R}^{4\times 2}, \boldsymbol{b}_{Ldi} = \begin{bmatrix} 1 \\ 1 \\ 1 \\ 1 \end{bmatrix} \in \boldsymbol{R}^4. \tag{4.11}$$

The upper 2×2 block of $\boldsymbol{A}_{Ldi}$ and the upper two rows of $\boldsymbol{b}_{Ldi}$ in Eq. (4.11) correspond to the upper inequality related to $\dot{l}_{i1}$ in Eq. (4.9). Similarly, the lower 2×2 block of $\boldsymbol{A}_{Ldi}$ and the lower two rows of $\boldsymbol{b}_{Ldi}$ in Eq. (4.11) correspond to the lower inequality related to $\dot{l}_{i2}$ in Eq. (4.9).

Considering the kinematic equation $\dot{\boldsymbol{l}}_{di} = \boldsymbol{W}_{Gi}^{\mathrm{T}}\boldsymbol{v}_{di}$, the set of top plate velocities contributed by the DAM without VCM is given by

$$\boldsymbol{V}_{di} = \{\boldsymbol{v}_{di} | \boldsymbol{A}_{Vdi}\boldsymbol{v}_{di} \leq \boldsymbol{b}_{Vdi}\}, \tag{4.12}$$

where the matrix $\boldsymbol{A}_{Vdi}$ in Eq. (4.12) is computed as

$$\boldsymbol{A}_{Vdi} = \boldsymbol{A}_{Ldi}\boldsymbol{W}_{Gi}^{\mathrm{T}},$$

and the matrix $\boldsymbol{W}_{Gi}$ related to the global motion of the top plate of the DAM without VCM is given by

$$\boldsymbol{W}_{Gi} = \begin{bmatrix} {}^{B}\boldsymbol{e}_i & {}^{B}\boldsymbol{e}_i \\ {}^{B}\boldsymbol{p}_{Bi1} \times {}^{B}\boldsymbol{e}_i & {}^{B}\boldsymbol{p}_{Bi2} \times {}^{B}\boldsymbol{e}_i \end{bmatrix} \in \boldsymbol{R}^{n\times 2}; i = 1, \ldots N_D. \tag{4.13}$$

with ${}^{B}\boldsymbol{e}_i = {}^{B}\boldsymbol{e}_{ij}$ $(j = 1, 2)$. Mathematically, the symbol "$\times$" in this equation is the operator to calculate the cross product of two vectors in $\boldsymbol{R}^3$ where each vector contains three elements of X, Y and Z axes. However, in this paper, the symbol "$\times$" is also used to calculate the cross product of two vectors in $\boldsymbol{R}^2$ and the result of this product is a scalar. The detail of its derivation is shown in **Appendix A**. Here, n is the number of global motion DOFs of the top plate; $n = 2$ in the 1D mechanism, $n = 3$ in the planar mechanism and $n = 6$ in the 3D mechanism.

b. Set of top plate velocities contributed by the DAM with VCM

Assuming that the wire velocities satisfy -1[m/s] $\leq \dot{l}_{ij} \leq$ 1[m/s] and considering the characteristic of VCM, we obtain the following inequalities:

$$\begin{cases} -1 \leq \dot{l}_{i1} \leq 1, \\ \dot{l}_{i1} = \dot{l}_{(i+1)1}, \\ -1 \leq \dot{l}_{i2} \leq 1, \\ \dot{l}_{i2} = \dot{l}_{(i+1)2}. \end{cases} \tag{4.14}$$

Equation (4.14) implies that each wire can produce a non-zero velocity (either positive or negative), so the values "1" and "-1" have no specific meaning. In matrix form, these inequalities are expressed as

$$\boldsymbol{A}_{Lvm}\dot{\boldsymbol{l}}_{vm} \leq \boldsymbol{b}_{Lvm}, \tag{4.15}$$

where $\dot{\boldsymbol{l}}_{vm} = [\, \dot{l}_{i1}\ \dot{l}_{i2}\ \dot{l}_{(i+1)1}\ \dot{l}_{(i+1)2}\,]^{\mathrm{T}} \in \boldsymbol{R}^4$ is the wire velocity vector of DAM with VCM and:

$$\boldsymbol{A}_{Lvm} = \begin{bmatrix} -1 & 0 & 0 & 0 \\ 1 & 0 & 0 & 0 \\ 1 & 0 & -1 & 0 \\ -1 & 0 & 1 & 0 \\ 0 & -1 & 0 & 0 \\ 0 & 1 & 0 & 0 \\ 0 & 1 & 0 & -1 \\ 0 & -1 & 0 & 1 \end{bmatrix} \in \boldsymbol{R}^{8\times 4}, \boldsymbol{b}_{Lvm} = \begin{bmatrix} 1 \\ 1 \\ 0 \\ 0 \\ 1 \\ 1 \\ 0 \\ 0 \end{bmatrix} \in \boldsymbol{R}^8. \tag{4.16}$$

In Eq. (4.16), the upper 2×4 block of $\boldsymbol{A}_{Lvm}$ and the first two row of $\boldsymbol{b}_{Lvm}$ correspond to the first inequality related to $\dot{l}_{i1}$ in Eq. (4.14), and the second 2×4 block of $\boldsymbol{A}_{Lvm}$ and the third and fourth rows of $\boldsymbol{b}_{Lvm}$ correspond to the first equality related to $\dot{l}_{i1}$, $\dot{l}_{(i+1)1}$ in Eq. (4.14). Similarly, the third 2×4 block of $\boldsymbol{A}_{Lvm}$ and the fifth and sixth rows of $\boldsymbol{b}_{Lvm}$ in Eq. (4.16) correspond to the second inequality related to $\dot{l}_{i2}$ in Eq. (4.14), and the last 2×4 block of $\boldsymbol{A}_{Lvm}$ and the final two rows of $\boldsymbol{b}_{Lvm}$ correspond to the second equality related to Eq. (4.14).

Considering the kinematic equation, $\dot{\boldsymbol{l}}_{vm} = \boldsymbol{W}_{GVm}^{\mathrm{T}}\boldsymbol{v}_{vm}$, the set of top plate velocities contributed by the DAM with VCM is given by

$$\boldsymbol{V}_{vm} = \{\boldsymbol{v}_{vm} | \boldsymbol{A}_{Vvm}\boldsymbol{v}_{vm} \leq \boldsymbol{b}_{Vvm}\}, \tag{4.17}$$

where the matrix $\boldsymbol{A}_{Vvm}$ in Eq. (4.17) is computed as

$$\boldsymbol{A}_{Vvm} = \boldsymbol{A}_{Lvm}\boldsymbol{W}_{GVm}^{\mathrm{T}},$$

and the matrix $\boldsymbol{W}_{GVm}$ related to the global motion of the top plate of the DAM with VCM is given by

$$\boldsymbol{W}_{GVm} = \begin{bmatrix} {}^{B}\boldsymbol{e}_k & {}^{B}\boldsymbol{e}_k & {}^{B}\boldsymbol{e}_k & {}^{B}\boldsymbol{e}_k \\ {}^{B}\boldsymbol{p}_{Bk1} \times {}^{B}\boldsymbol{e}_k & {}^{B}\boldsymbol{p}_{Bk2} \times {}^{B}\boldsymbol{e}_k & {}^{B}\boldsymbol{p}_{B(k+1)1} \times {}^{B}\boldsymbol{e}_k & {}^{B}\boldsymbol{p}_{B(k+1)2} \times {}^{B}\boldsymbol{e}_k \end{bmatrix} \in \boldsymbol{R}^{n\times 4}; \tag{4.18}$$

$k = N_D + 2m - 1; m = 1, \ldots N_V$.

with ${}^{B}\boldsymbol{e}_k = {}^{B}\boldsymbol{e}_{kj} = \boldsymbol{e}_{(k+1)j}$ $(j = 1, 2)$. Here, k is the ordering number of DAM without VCM when considering a DAM with VCM contains two DAMs without VCM.

c. Face form of the producible velocity space

Combining all velocity sets of the top plate contributed by all modules, the face form of the producible velocity space of the top plate is given by

$$\boldsymbol{V} = \{\boldsymbol{v} | \boldsymbol{A}_V \boldsymbol{v} \leq \boldsymbol{b}_V\}, \tag{4.19}$$

where the velocity matrices of velocity of the top plate are defined as

$$\boldsymbol{A}_V = \boldsymbol{A}_L \boldsymbol{W}_G^{\mathrm{T}}, \tag{4.20}$$

$$\boldsymbol{b}_V = [\, \boldsymbol{b}_{Ld1}^{\mathrm{T}} \ldots \boldsymbol{b}_{LdN_D}^{\mathrm{T}} \boldsymbol{b}_{Lv1}^{\mathrm{T}} \ldots \boldsymbol{b}_{LvN_V}^{\mathrm{T}} \,]^{\mathrm{T}}, \tag{4.21}$$

where, the subscripts Lv and Ld denote the components belong to DAM with and without VCM; the subscripts N_V and N_D are the number of DAM with and without VCM, respectively.

The matrix $\mathbf{A}_L$ is defined as

$$\boldsymbol{A}_L = \text{bdiag.}(\, \boldsymbol{A}_{Ld1}, \ldots, \boldsymbol{A}_{LdN_D}, \boldsymbol{A}_{Lv1}, \ldots, \boldsymbol{A}_{LvN_V}), \tag{4.22}$$

where bdiag.$(\, \boldsymbol{X}_1, \boldsymbol{X}_2, \ldots, \boldsymbol{X}_P)$ denotes a block-diagonal matrix constructed from the sub-matrices $\boldsymbol{X}_1, \boldsymbol{X}_2, \ldots, \boldsymbol{X}_P$ on its diagonal.

The contribution of matrix $\boldsymbol{W}_G$ to the resultant force on the top plate is given by:

$$\boldsymbol{W}_G = [\, \boldsymbol{W}_{G1} \;\ldots\; \boldsymbol{W}_{GN_D} \boldsymbol{W}_{GV1} \;\ldots\; \boldsymbol{W}_{GVN_V} \,]^{\mathrm{T}} \in \boldsymbol{R}^{n \times 2(N_D + 2N_V)} \tag{4.23}$$

where $\boldsymbol{W}_{Gi}$ and $\boldsymbol{W}_{GVm}$ are obtained from Eqs. (4.13) and (4.18).

d. Span form of the producible velocity space

The face form of the producible velocity space does not clarify the directions and number of dimensions of the generated velocities. For this purpose, the face form Eq. (4.19) is converted to the following span form:

$$\boldsymbol{V} = \left\{ \sum_{t=1}^{\beta} \lambda_t \boldsymbol{v}_t | \sum_{t=1}^{\beta} \lambda_t \leq 1, \lambda_t \geq 0, t \in [1, \beta] \right\}, \tag{4.24}$$

using the method proposed in [61]. The results for all vertices are represented in the following matrix $\boldsymbol{A}$:

$$\boldsymbol{A} = [\boldsymbol{v}_1 \;\ldots\ldots\; \boldsymbol{v}_\beta], \tag{4.25}$$

where β is the number of vertices.

Yoshikawa [62] mentioned the concepts of active and passive closure which are critically important for analyzing grasping and manipulation by robotic hands and the constraining mechanisms such as fixtures and vises. Passive and active closure refer to the ability of fixing

and manipulating objects, respectively. In our research, the active constraint space $\boldsymbol{S}_{AC}$ is defined as the space covered by the top plate velocities and movements. Conversely, the passive constraint space $\boldsymbol{S}_{PC}$ is the space wherein the top plate cannot move. Mathematically, these spaces are defined as follows:

$$\boldsymbol{S}_{AC} = \mathcal{R}\left(\boldsymbol{A}\right), \boldsymbol{S}_{PC} = \boldsymbol{S}_{AC}^{\perp} = \mathcal{N}\left(\boldsymbol{A}^{\mathrm{T}}\right). \tag{4.26}$$

4.2.4 Details of Step 3: Check the Vector Closure Condition within the Producible Velocity Space by Static Force Analysis (SFA)

The above mentioned kinematical analysis step obtains the active and passive constraint spaces ($\boldsymbol{S}_{AC}$ and $\boldsymbol{S}_{PC}$, respectively). However, although the vector closure condition is a necessary condition in step 1, this judgment is made over the whole motion space. Consequently, whether the resultant force can be produced in any direction within the active constraint space $\boldsymbol{S}_{AC}$ is not confirmed. Therefore the SFA is used as the sufficient condition for judging RDWM candidates. The SFA procedure is detailed below.

First, the whole motion space coordinate is converted to the producible velocity space coordinate.

The static force relation between $\boldsymbol{F}_G$ and $\boldsymbol{T}$ is given by:

$$\boldsymbol{F}_G = \boldsymbol{W}_G \boldsymbol{T}, \tag{4.27}$$

In the 2D case, $\boldsymbol{F}_G = [f_x f_y n_z]^{\mathrm{T}} \in \boldsymbol{R}^3$ is the resultant force vector that produces the global motion, $\boldsymbol{T} = [\, T_{11}\ T_{12}\ T_{21}\ T_{22}\ T_{31}\ T_{32}\ T_{41}\ T_{42}\,]^{\mathrm{T}} \in \boldsymbol{R}^8$ is the wire tension vector and the matrix $\boldsymbol{W}_G$ is given by Eq. (4.23):

$$\boldsymbol{W}_G = [\, \boldsymbol{W}_{G1}\ \boldsymbol{W}_{G2}\ \boldsymbol{W}_{GV1}\,]^{\mathrm{T}} \in \boldsymbol{R}^{3\times 8}, \tag{4.28}$$

The matrices $\boldsymbol{W}_{Gi}$ and $\boldsymbol{W}_{GV1}$ are derived from Eqs. (4.13) and (4.18), respectively:

$$\boldsymbol{W}_{Gi} = \begin{bmatrix} {}^{B}\boldsymbol{e}_i & {}^{B}\boldsymbol{e}_i \\ {}^{B}\boldsymbol{p}_{Bi1} \times {}^{B}\boldsymbol{e}_i & {}^{B}\boldsymbol{p}_{Bi2} \times {}^{B}\boldsymbol{e}_i \end{bmatrix} \in \boldsymbol{R}^{3\times 2}, i = 1, 2,$$

$$\boldsymbol{W}_{GV1} = \begin{bmatrix} {}^{B}\boldsymbol{e}_3 & {}^{B}\boldsymbol{e}_3 & {}^{B}\boldsymbol{e}_3 & {}^{B}\boldsymbol{e}_3 \\ {}^{B}\boldsymbol{p}_{B31} \times {}^{B}\boldsymbol{e}_3 & {}^{B}\boldsymbol{p}_{B32} \times {}^{B}\boldsymbol{e}_3 & {}^{B}\boldsymbol{p}_{B41} \times {}^{B}\boldsymbol{e}_3 & {}^{B}\boldsymbol{p}_{B42} \times {}^{B}\boldsymbol{e}_3 \end{bmatrix} \in \boldsymbol{R}^{3\times 4}$$

Introducing the coefficient matrix $\boldsymbol{\alpha}$, which represents the tension forces of the DAMs with VCMs under passive constraints, we obtain

$$\begin{bmatrix} \boldsymbol{T}_{31} \\ \boldsymbol{T}_{32} \\ \boldsymbol{T}_{41} \\ \boldsymbol{T}_{42} \end{bmatrix} = \boldsymbol{\alpha} \begin{bmatrix} \boldsymbol{T}_{310} \\ \boldsymbol{T}_{320} \end{bmatrix}, \boldsymbol{\alpha} = \begin{bmatrix} \alpha_{31} & 0 \\ 0 & \alpha_{32} \\ 1-\alpha_{31} & 0 \\ 0 & 1-\alpha_{32} \end{bmatrix} \in \boldsymbol{R}^{4\times 2}, \tag{4.29}$$

where $\boldsymbol{T}_{3i0}, i = 1, 2$ are the independent tensions in the DAM with VCMs. Later, these tensions will be separated into two dependent wire tensions. α_{3i} and $(1 - \alpha_{3i})$ should be zero or positive.

Introducing the constraint matrix $\boldsymbol{C}$, which relates the set of all the wire tensions to the set of all independent wire tensions as follows:

$$\boldsymbol{T} = \boldsymbol{C}\boldsymbol{T}_C, \tag{4.30}$$

$$\boldsymbol{C} = \begin{bmatrix} \boldsymbol{E}_4 & 0 \\ 0 & \boldsymbol{\alpha} \end{bmatrix} \in \boldsymbol{R}^{8\times 6}; \boldsymbol{T}_c = [\ T_{11}\ T_{12}\ T_{21}\ T_{22}\ T_{310}\ T_{320}\ ]^{\mathrm{T}} \in \boldsymbol{R}^6$$

Substituting Eq. (4.30) into Eq. (4.27), the static force under the passive constraints imposed by the VCMs is given by

$$\boldsymbol{F}_G = \boldsymbol{W}_{GC}\boldsymbol{T}_C, \tag{4.31}$$

where

$$\boldsymbol{W}_{GC} = [\ \boldsymbol{W}_{G1}\ \boldsymbol{W}_{G2}\ \boldsymbol{W}_{GC1}\ ]^{\mathrm{T}} \in \boldsymbol{R}^{3\times 6}, \tag{4.32}$$

with

$$\boldsymbol{W}_{GC1} = \begin{bmatrix} {}^B\boldsymbol{e}_3 & {}^B\boldsymbol{e}_3 \\ \{\alpha_{31}{}^B\boldsymbol{p}_{B31} + (1-\alpha_{31}){}^B\boldsymbol{p}_{B41}\} \times {}^B\boldsymbol{e}_3 & \{\alpha_{31}{}^B\boldsymbol{p}_{B31} + (1-\alpha_{31}){}^B\boldsymbol{p}_{B41}\} \times {}^B\boldsymbol{e}_3 \end{bmatrix} \in \boldsymbol{R}^{3\times 2}.$$

In constrast, the producible global velocity, that is, the translational velocity $\dot{\boldsymbol{p}}$ in the global motion space, is determined by kinematical analysis as follows:

$$\boldsymbol{v}_G = \boldsymbol{C}_P\dot{\boldsymbol{p}}, \tag{4.33}$$

where, $\boldsymbol{v}_G = [\ \dot{\boldsymbol{p}}^{\mathrm{T}}\ \dot{\phi}^{\mathrm{T}}\ ]^{\mathrm{T}} \in \boldsymbol{R}^3, \dot{\boldsymbol{p}} \in \boldsymbol{R}^2$. The producible velocity matrix $\boldsymbol{C}_P$, which relates the translational velocity $\dot{\boldsymbol{p}}$ and the global motion velocity $\boldsymbol{v}_G$ is defined as follows:

$$\boldsymbol{C}_P = \begin{bmatrix} 1 & 0 \\ 0 & 1 \\ 0 & 0 \end{bmatrix} \in \boldsymbol{R}^{3\times 2}.$$

As the velocity relation is dual to the static force relation, the resultant force for global motion in the velocity producible space is given by:

$$\boldsymbol{f} = \boldsymbol{C}_P^{\mathrm{T}}\boldsymbol{F}_G, \tag{4.34}$$

Substituting $\boldsymbol{F}_G$ in Eq. (4.31) into Eq. (4.34), the static force relation between $\boldsymbol{f}$ and $\boldsymbol{T}_C$ is obtained as:

$$\boldsymbol{f} = \boldsymbol{C}_P^{\mathrm{T}}\boldsymbol{W}_G\boldsymbol{C}\boldsymbol{T}_C, \tag{4.35}$$

Note that the moments in $\boldsymbol{F}_G$, which include the coefficients α_{3i} will be disappeared.

The same result can be obtained through Eqs. (4.34), (4.27) and (4.30):

$$\boldsymbol{f} = \boldsymbol{W}_{CVC}\boldsymbol{T}_C, \tag{4.36}$$

where $\boldsymbol{W}_{CVC}$ is the matrix of resultant force on the top plate in the constraint space. It is derived as follows:

$$\boldsymbol{W}_{CVC} = \boldsymbol{C}_P^{\mathrm{T}}\boldsymbol{W}_G\boldsymbol{C}, \tag{4.37}$$

In the general case, let us suppose that the RDWM includes N_D DAMs without VCMs and N_V DAMs with VCMs. Then we have $\boldsymbol{F}_G = [\,\boldsymbol{f}^{\mathrm{T}}\ \boldsymbol{n}^{\mathrm{T}}\,]^{\mathrm{T}} \in \boldsymbol{R}^n$, where $\boldsymbol{f} \in \boldsymbol{R}^p$ and $\boldsymbol{n} \in \boldsymbol{R}^{n-p}$, (here,$(n,\ p)$=(2, 1) in 1D, (3, 2) in 2D and (6, 3) in 3D). $\boldsymbol{F}_G$ is the resultant force vector that produce global motion, $\boldsymbol{T} = [\ T_{11}\ T_{12}\ \ldots\ T_{N_D1}\ T_{N_D2}\ T_{(N_D+1)1}\ T_{(N_D+1)2}\ T_{(N_D+2)1}\ T_{(N_D+2)2}\ \ldots\ T_{(N_D+2N_V-1)1}\ T_{(N_D+2N_V-1)2}\ T_{(N_D+2N_V)1}\ T_{(N_D+2N_V)2}\,]^{\mathrm{T}} \in \boldsymbol{R}^{2(N_D+2N_V)}$ is the wire tension vector. The matrix $\boldsymbol{W}_G$ is given by Eq. (4.23):

$$\boldsymbol{W}_G = [\ \boldsymbol{W}_{G1}\ \ldots\ \boldsymbol{W}_{GN_D}\ \boldsymbol{W}_{GV1}\ \ldots\ \boldsymbol{W}_{GVN_V}\,]^{\mathrm{T}} \in \boldsymbol{R}^{n\times 2(N_D+2N_V)}, \tag{4.38}$$

where the matrices $\boldsymbol{W}_{Gi}$ and $\boldsymbol{W}_{GVm}$ are obtained from Eqs. (4.13) and (4.18).

Again introducing the coefficient matrix $\boldsymbol{\alpha}$, which represents the tension forces of the DAMs with VCMs under passive constraints, we obtain

$$\begin{bmatrix} \boldsymbol{T}_{k1} \\ \boldsymbol{T}_{k2} \\ \boldsymbol{T}_{(k+1)1} \\ \boldsymbol{T}_{(k+1)2} \end{bmatrix} = \boldsymbol{\alpha}_m \begin{bmatrix} \boldsymbol{T}_{k10} \\ \boldsymbol{T}_{k20} \end{bmatrix}, \boldsymbol{\alpha}_m = \begin{bmatrix} \alpha_{k1} & 0 \\ 0 & \alpha_{k2} \\ 1-\alpha_{k1} & 0 \\ 0 & 1-\alpha_{k2} \end{bmatrix} \in \boldsymbol{R}^{4\times 2} \tag{4.39}$$

where $k = N_D + 2m - 1; m = 1, \ldots, N_V$.

Here, $\boldsymbol{T}_{ku0}, u = 1, 2$ are the independent tensions in the DAM with VCMs, which later separate into two dependent wire tensions, $\boldsymbol{T}_{(k+u-1)1}$, $\boldsymbol{T}_{(k+u-1)2}$, and α_{ku} $(0 \le \alpha_{ku} \le 1, u = 1, 2)$ is the coefficient that distributes the wire tensions $\boldsymbol{T}_{ku0}$ into two dependent wire tensions.

Introducing the constraint matrix $\boldsymbol{C}$, which relates the set of all the wire tensions to the set of all independent wire tensions as follows:

$$\boldsymbol{T} = \boldsymbol{C}^{\mathrm{T}}\boldsymbol{T}_C, \tag{4.40}$$

where $\boldsymbol{T}_C = [\ T_{11}\ T_{12}\ \ldots\ T_{N_D1}\ T_{N_D2}\ T_{(N_D+1)10}\ T_{(N_D+1)20}\ T_{(N_D+3)10}\ T_{(N_D+3)20}\ \ldots\ T_{(N_D+2N_V-1)10}\ T_{(N_D+2N_V-1)20}\,]^{\mathrm{T}} \in \boldsymbol{R}^{2(N_D+N_V)}$ is the vector of independent wire tensions.

Here,

$$\boldsymbol{C} = \mathrm{bdiag.}(\ \boldsymbol{E}_{2N_D},\ \boldsymbol{\alpha}_1,\ \ldots,\ \boldsymbol{\alpha}_{N_V}) \in \boldsymbol{R}^{2(N_D+2N_V)\times 2(N_D+N_V)} \tag{4.41}$$

$\boldsymbol{E}_{2N_D} \in \boldsymbol{R}^{2N_D\times 2N_D}$ is the identity matrix.

Substituting Eq. (4.40) into Eq. (4.27), the static force relation under the passive constraints imposed by the VCMs is given by

$$\boldsymbol{F}_G = \boldsymbol{W}_{GC}\boldsymbol{T}_C, \tag{4.42}$$

where

$$\boldsymbol{W}_{GC} = [\ \boldsymbol{W}_{G1}\ \ldots\ \boldsymbol{W}_{GN_D}\ \boldsymbol{W}_{GC1}\ \ldots\ \boldsymbol{W}_{GCN_D}\,]^{\mathrm{T}} \in \boldsymbol{R}^{n\times 2(N_D+2N_V)}, \tag{4.43}$$

here

$$\boldsymbol{W}_{Gi} = \begin{bmatrix} {}^B\boldsymbol{e}_i & {}^B\boldsymbol{e}_i \\ {}^B\boldsymbol{p}_{Bi1}\times {}^B\boldsymbol{e}_i & {}^B\boldsymbol{p}_{Bi2}\times {}^B\boldsymbol{e}_i \end{bmatrix} \in \boldsymbol{R}^{\mathrm{n}\times 2} i = 1, \ldots N_D,$$

$$\boldsymbol{W}_{GCm} = \begin{bmatrix} {}^{B}\boldsymbol{e}_k & {}^{B}\boldsymbol{e}_k \\ \left\{\alpha_{k1}{}^{B}\boldsymbol{p}_{Bk1} + (1-\alpha_{k1}){}^{B}\boldsymbol{p}_{B(k+1)1}\right\} \times {}^{B}\boldsymbol{e}_k & \left\{\alpha_{k2}{}^{B}\boldsymbol{p}_{Bk2} + (1-\alpha_{k2}){}^{B}\boldsymbol{p}_{B(k+1)2}\right\} \times {}^{B}\boldsymbol{e}_k \end{bmatrix}$$

$\in \boldsymbol{R}^{\mathrm{n}\times 2}$, $(k = N_D + 2m - 1; m = 1, \ldots N_V)$.

Again, the producible global velocity (translational velocity $\dot{\boldsymbol{p}}$ in the global motion space) is derived from kinematical analysis:

$$\boldsymbol{v}_G = \boldsymbol{C}_P \dot{\boldsymbol{p}}, \tag{4.44}$$

where, $\boldsymbol{v}_G = [\,\dot{\boldsymbol{p}}^{\mathrm{T}}\ \dot{\boldsymbol{\phi}}^{\mathrm{T}}\,]^{\mathrm{T}} \in \boldsymbol{R}^n, \dot{\boldsymbol{p}} \in \boldsymbol{R}^p$. The producible velocity matrix $\boldsymbol{C}_P$, which relates the translational velocity $\dot{\boldsymbol{p}}$ and the global motion velocity $\boldsymbol{v}_G$ is defined as follows:

$$\boldsymbol{C}_P = \begin{bmatrix} \boldsymbol{E}_{p\times p} \\ \boldsymbol{O}_{(n\text{-}p)\times p} \end{bmatrix} \in \boldsymbol{R}^{n\times p},$$

($(n,\ p)$=(2, 1) in 1D, (3, 2) in 2D and (6, 3) in 3D).

As the velocity relation is dual to the static force relation, the resultant force for global motion in the velocity producible space is given by:

$$\boldsymbol{f} = \boldsymbol{C}_P^{\mathrm{T}} \boldsymbol{F}_G, \tag{4.45}$$

Substituting $\boldsymbol{F}_G$ in Eq. (4.42) into Eq. (4.45), the static force relation between $\boldsymbol{f}$ and $\boldsymbol{T}_C$ is obtained as:

$$\boldsymbol{f} = \boldsymbol{C}_P^{\mathrm{T}} \boldsymbol{W}_G \boldsymbol{C} \boldsymbol{T}_C, \tag{4.46}$$

Note that the moments in $\boldsymbol{F}_G$, which include the coefficients α_{kbu} will be disappeared.

The same result can be obtained through Eqs. (4.45), (4.27) and (4.40):

$$\boldsymbol{f} = \boldsymbol{W}_{CVC} \boldsymbol{T}_C, \tag{4.47}$$

w where $\boldsymbol{W}_{CVC}$ is the matrix of resultant force on the top plate in the constraint space. It is derived as follows:

$$\boldsymbol{W}_{CVC} = \boldsymbol{C}_P^{\mathrm{T}} \boldsymbol{W}_G \boldsymbol{C}, \tag{4.48}$$

Second, Eq. (4.36) or Eq. (4.47) will be used in SFA for judging whether the resultant force can be produced in any direction within the active constraint space $\boldsymbol{S}_{AC}$. The procedure is described below.

C1) Find rank($\boldsymbol{W}_{CVC}$).

C2) *Find a vector* $\boldsymbol{T}_C > \boldsymbol{0}$ *that satisfies* $\boldsymbol{W}_{CVC}\boldsymbol{T}_C = \boldsymbol{0}$.

The rank($\boldsymbol{W}_{CVC}$) in Condition C1 defines the number of directions where the resultant forces are produced in the active constraint space $\boldsymbol{S}_{AC}$. If rank($\boldsymbol{W}_{CVC}$) is full, the resultant forces can be produced in any direction in $\boldsymbol{S}_{AC}$. In contrast, if rank($\boldsymbol{W}_{CVC}$) is not full, the resultant force (and hence the velocity of the top plate) will be forbidden in one or more directions. In this case, the SFA fails and the RDWM candidate should be eliminated. Under condition C2, the matrix $\boldsymbol{W}_{CVC}$ is non-regular because the sizes of the wire tension vector in

the constraint coordinate $\boldsymbol{T}_C$ and the resultant force vector in the active constraint space $\boldsymbol{f}$ are mismatched. Consequently, the number of roots exceeds the number of equations. If the candidate RDWM configuration is feasible, we can find a positive value of the wire tension $\boldsymbol{T}_C$ satisfying $\boldsymbol{W}_{CVC}\boldsymbol{T}_C = \boldsymbol{0}$. If the RDWM candidate passes the SFA, the resultant force can be produced in any direction within the active constraint space.

The proposed procedure with three steps specify the necessary and sufficient conditions for judging the RDWM candidates, respectively. If a candidate RDWM satisfies the above procedure, it can generate the desired motions. Hence, the proposed judgment determines proper configurations of the RDWM.

4.3. Discussion and Conclusion

This chapter discussed the method for developing a wire driven mechanism wherein the top plate can generate the desired producible velocity space with the reduction number of actuators. It explained the basic concept of using VCM in RDWM for keeping the top plate's orientation with the reducing number of actuators. Then it proposed the judgment procedure with three steps to check if the RDWM candidates using VCM can produce the desired velocity. Using just the essential component of the new form of wire matrix in the 1^{st} step of the judgment procedure will make it simpler and easier. The numerical examples in the next chapter will make clear and verify the proposed method of using the essential component as well as the validity of the judgment procedure for RDWM.

Chapter 5

Numerical Examples

5.1. Introduction

This chapter applies the proposed theories presented in chapter 3 and chapter 4 for finding the proper configuration of RDWM that produces the velocity in a specific space. Assuming that the designer would like to develop a wire driven mechanism for the aim of producing high speed and high precise motion in which the top plate can move in the producible velocity space. The DAMs will be used for producing high speed global motion and high precise local motion as the concept of RDWM presented in chapter 3. Then for producing velocity in a specific space as well as for reducing the number of actuators, the designer will introduce the VCMs into the configuration of the mechanism as discussed in chapter 4. The examples presented in the next sections illustrate how to apply DAMs and VCMs in RDWM as well as how to use the proposed judgment method for finding the proper configuration RDWM that can generate the producible velocity space.

5.2. Proper Configuration of the 1D Wire Mechanism with One VCM

The 1D wire mechanism with one VCM is shown in figure 5.1. Here, the top plate under the gravity force will be suspended by one VCM. The gravity force $p = mg$ has any positive value which depends on the mass of the top plate m under the acceleration of gravity g. For the purpose of simplifying, let's assume that the gravity force has the magnitude $p = 1$ [N].

Positions of wire end points on the top plate w.r.t the top plate coordinate.

$$ {}^{T}\boldsymbol{p}_{B1} = [-6 \;\; 10]^{\mathrm{T}}, \qquad {}^{T}\boldsymbol{p}_{B2} = [6 \;\; 10]^{\mathrm{T}}, $$

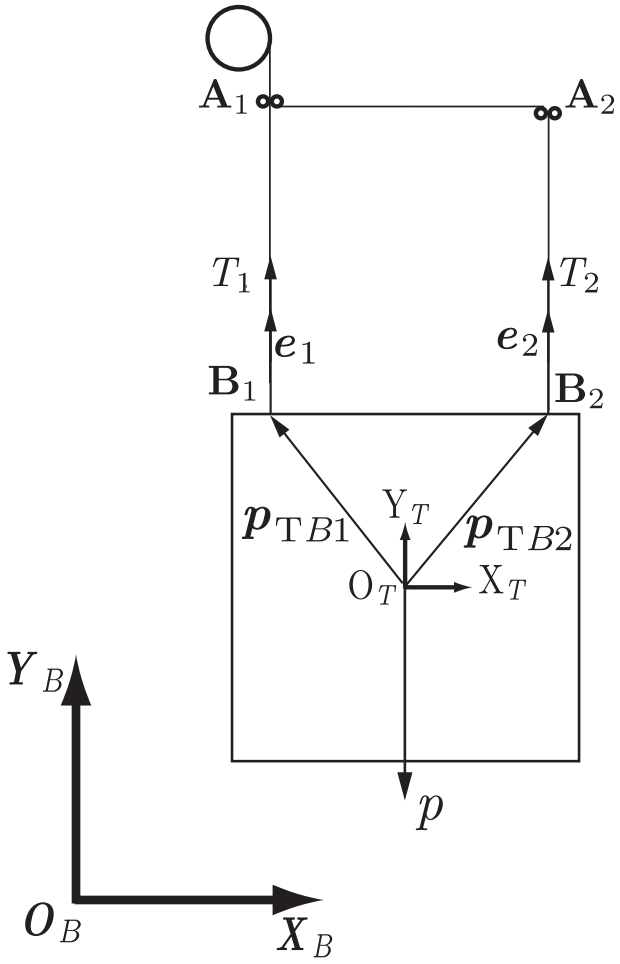

Figure. 5.1: 1D wire mechanism with one VCM.

Set of positions ${}^{B}\boldsymbol{p}_{T}$ and orientations ${}^{B}\boldsymbol{R}_{T}$ of the top plate

$$ {}^{B}\boldsymbol{p}_{T} = [50 \;\; 50]^{\mathrm{T}} \,, \; {}^{B}\boldsymbol{R}_{T} = \begin{bmatrix} 1 & 0 \\ 0 & 1 \end{bmatrix} \in \boldsymbol{R}^{2\times 2}. $$

Positions of wire end points on the top plate

From Eq. (3.10):

$$ {}^{B}\boldsymbol{p}_{B1} = [44 \;\; 60]^{\mathrm{T}} \,, \; {}^{B}\boldsymbol{p}_{B2} = [56 \;\; 60]^{\mathrm{T}} $$

Position of wire end points on the frame

The following positions of the wire end points on the frame are shown as follows:

$$ {}^{B}\boldsymbol{p}_{A1} = [44 \;\; 90]^{\mathrm{T}} \,, \quad {}^{B}\boldsymbol{p}_{A2} = [56 \;\; 90]^{\mathrm{T}} \,. $$

Calculating the wire vectors ${}^{B}\boldsymbol{e}_{i}$

The wire vectors ${}^{B}\boldsymbol{e}_{i}$ were calculated by Eq. (3.11).

$$ {}^{B}\boldsymbol{e}_{1} = \; {}^{B}\boldsymbol{e}_{2} = [0 \;\; 1]^{\mathrm{T}} $$

Necessary condition check (Step 1)

In step 1, the matrix $\boldsymbol{W}_{G}$ that contributes to the resultant force on the top plate is given by Eq. (4.23) with only one VCM contain two wires as follows:

$$ \boldsymbol{W}_{G} = \begin{bmatrix} 0 & 0 \\ 1 & 1 \\ -6 & 6 \end{bmatrix} \in \boldsymbol{R}^{3\times 2}. \tag{5.1} $$

The first row of $\boldsymbol{W}_{G}$ above has all zero elements so the top plate cannot move in X direction. Then, $\boldsymbol{W}_{G}$ can be written again as follows:

$$ \boldsymbol{W}_{G} = \begin{bmatrix} 1 & 1 \\ -6 & 6 \end{bmatrix} \in \boldsymbol{R}^{2\times 2}. \tag{5.2} $$

For checking vector closure condition, the gravity force on the top plate is introduced. Then the matrix $\widetilde{\boldsymbol{W}}_{G}$ contains the gravity component is shown as follows:

$$ \widetilde{\boldsymbol{W}} = \begin{bmatrix} 1 & 1 & -1 \\ -6 & 6 & 0 \end{bmatrix} \in \boldsymbol{R}^{2\times 3}. \tag{5.3} $$

Correspond to the matrix $\widetilde{\boldsymbol{W}}_{G}$ is a vector $\widetilde{\boldsymbol{T}} = [\, T_1 \;\; T_2 \;\; p\,]^{\mathrm{T}} \in \boldsymbol{R}^{3}$ which contains the wire tensions T_1, T_2 and the gravity force p. It is easily seen that:

i) $\mathrm{rank}(\widetilde{\boldsymbol{W}}) = 2$.

ii) The vector $\widetilde{\boldsymbol{T}}_{0} = [\, 0.5 \;\; 0.5 \;\; 1\,]^{\mathrm{T}} \in \boldsymbol{R}^{3} > \boldsymbol{0}$ satisfies $\widetilde{\boldsymbol{W}}\,\widetilde{\boldsymbol{T}}_{0} = \boldsymbol{0}$.

Therefore, this 1D wire mechanism satisfies step 1 and the analysis proceeds to the step 2 as follows.

KA (Step 2)

The matrices of contribution of VCM to the velocity of the top plate is given as follows:

$$\boldsymbol{A}_L = \begin{bmatrix} -1 & 0 \\ 1 & 0 \\ 1 & 1 \\ -1 & 1 \end{bmatrix} \in \boldsymbol{R}^{4\times 2}, \boldsymbol{b}_L = \begin{bmatrix} 1 \\ 1 \\ 0 \\ 0 \end{bmatrix} \in \boldsymbol{R}^4. \tag{5.4}$$

The matrices of top plate velocities $\boldsymbol{A}_V$ and $\boldsymbol{b}_V$ are given by Eqs. (4.20) and (4.21), respectively. The result are given below:

$$\boldsymbol{A}_V = \begin{bmatrix} -1 & 6 \\ 1 & -6 \\ 0 & 12 \\ 0 & -12 \end{bmatrix} \in \boldsymbol{R}^{4\times 2}, \boldsymbol{b}_V = \begin{bmatrix} 1 \\ 1 \\ 0 \\ 0 \end{bmatrix} \in \boldsymbol{R}^4. \tag{5.5}$$

From the above $\boldsymbol{A}_V, \boldsymbol{b}_V$, the convex sets mentioned in Eqs. (4.19) and (4.24) can be solved. The vertex sets in matrix $\boldsymbol{A}$, the active constraint space $\boldsymbol{S}_{AC}$ and passive constraint space $\boldsymbol{S}_{PC}$ of the 1D wire mechanism are found by Eqs. (4.25) and (4.26). The result are shown below.

$$\boldsymbol{A} = \begin{bmatrix} -1 & 1 \\ 0 & 0 \end{bmatrix} \in \boldsymbol{R}^{2\times 2} \tag{5.6}$$

$$\boldsymbol{S}_{AC} = \mathcal{R}\left(\begin{bmatrix} 1 \\ 0 \end{bmatrix}\right), \boldsymbol{S}_{PC} = \mathcal{R}\left(\begin{bmatrix} 0 \\ 1 \end{bmatrix}\right). \tag{5.7}$$

Eq. (5.7) shows that in this case, the active constraint space $\boldsymbol{S}_{AC}$ produced by the top plate allows motion in the Y direction and the orientation is fixed around the Z-axis.

SFA (Step 3)

The matrix $\widetilde{\boldsymbol{W}}_{CVC}$ that relates the wire tension vector in the constraint coordinate is derived from Eq. (4.48) then it is used for SFA. The contents of the matrix $\widetilde{\boldsymbol{W}}_{CVC}$ are given below:

$$\widetilde{\boldsymbol{W}}_{CVC} = \begin{bmatrix} 1 & 1 & -1 \end{bmatrix} \in \boldsymbol{R}^{1\times 3}, \tag{5.8}$$

$\widetilde{\boldsymbol{W}}_{CVC}$ contains some of the elements of matrix $\widetilde{\boldsymbol{W}}_G$. We then have:

i) rank($\widetilde{\boldsymbol{W}}_{CVC}$) = 1.

ii) The vector $\widetilde{\boldsymbol{T}}_0 = [0.5\ 0.5\ 1]^{\mathrm{T}} \in \boldsymbol{R}^3 > \boldsymbol{0}$ satisfies $\widetilde{\boldsymbol{W}}_{CVC}\widetilde{\boldsymbol{T}}_0 = \boldsymbol{0}$.

The above analysis reveals that $\widetilde{\boldsymbol{W}}_{CVC}$ is a full-ranked matrix. Moreover, there is a vector $\widetilde{\boldsymbol{T}}_0$ that satisfies $\widetilde{\boldsymbol{W}}_{CVC}\widetilde{\boldsymbol{T}}_0 = \boldsymbol{0}$. Consequently, this wire mechanism satisfies step 3 and the resultant force can be produced in any direction within the active constraint space $\boldsymbol{S}_{AC}$.

Because it passes all three of the judgment steps, this wire mechanism is a proper configuration that achieves the desired active constraint space $\boldsymbol{S}_{AC}$ in Y direction.

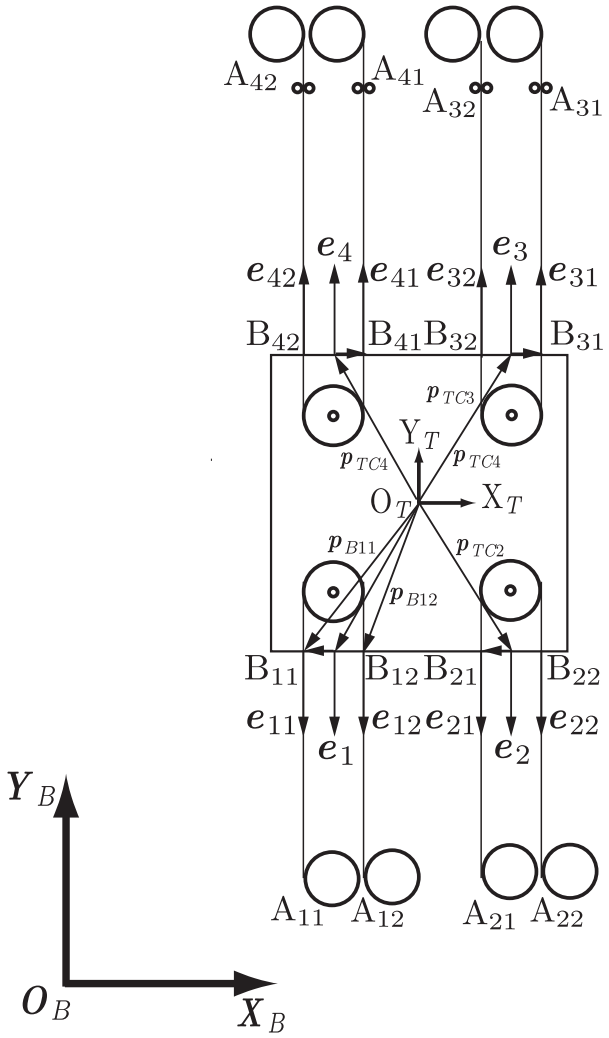

Figure. 5.2: The mechanism does not satisfy the 1^{st} point of the step 1.

5.3. Proper Configuration of the Planar RDWM with Fixed Orientation Around the Z-axis while Maintaining Translational Motion in the X and Y Directions

Suppose a planar RDWM wherein the desired active constraint space $\boldsymbol{S}_{AC}$ is the XOY plane and the passive constraint space $\boldsymbol{S}_{PC}$ is the orientation around the Z-axis of the top plate is required. Various configurations of the planar RDWM are proposed and assessed by the judgment procedure developed in chapter 4. All length-based parameters in this analysis are in [cm].

5.3.1 First configuration: The Mechanism Does Not Satisfy the 1^{st} Point of Step 1

A planar RDWM does not satisfy the 1^{st} point of the step 1 of the judgment procedure is shown in figure 5.2. Here, the unit of the values of parameters related to length are assumed to be [cm]. The processes for deriving the matrix $\boldsymbol{W}'_{G2}$ and the judgment procedure are shown below:

Defining ${}^{T}\boldsymbol{p}_{TCi}$, $\boldsymbol{R}_i$, ${}^{T}\boldsymbol{p}_{TDi}$ and ${}^{T}\boldsymbol{p}_{Bij}$

Select the parameters for the mechanism in figure 5.2 as follows:

$$\begin{aligned} {}^{T}\boldsymbol{p}_{TC1} &= [-6 \quad -10]^{\mathrm{T}}, \quad {}^{T}\boldsymbol{p}_{TC2} = [6 \quad -10]^{\mathrm{T}}, \\ {}^{T}\boldsymbol{p}_{TC3} &= [6 \quad 10]^{\mathrm{T}}, \qquad {}^{T}\boldsymbol{p}_{TC4} = [-6 \quad 10]^{\mathrm{T}}. \end{aligned}$$

Radii of the pulleys: $R_1 = R_2 = R_3 = R_4 = 2$.

$$\begin{aligned} {}^{T}\boldsymbol{p}_{TD1} &= [-2 \quad 0]^{\mathrm{T}}, \quad {}^{T}\boldsymbol{p}_{TD2} = [-2 \quad 0]^{\mathrm{T}}, \\ {}^{T}\boldsymbol{p}_{TD3} &= [2 \quad 0]^{\mathrm{T}}, \qquad {}^{T}\boldsymbol{p}_{TD4} = [2 \quad 0]^{\mathrm{T}}. \end{aligned}$$

Position of wire end points on the top plate w.r.t the top plate coordinate:

$$\begin{aligned} {}^{T}\boldsymbol{p}_{B11} &= [-8 \quad -10]^{\mathrm{T}}, \quad {}^{T}\boldsymbol{p}_{B12} = [-4 \quad -10]^{\mathrm{T}}, \\ {}^{T}\boldsymbol{p}_{B21} &= [4 \quad -10]^{\mathrm{T}}, \quad {}^{T}\boldsymbol{p}_{B22} = [8 \quad -10]^{\mathrm{T}}, \\ {}^{T}\boldsymbol{p}_{B31} &= [8 \quad 10]^{\mathrm{T}}, \quad {}^{T}\boldsymbol{p}_{B32} = [4 \quad 10]^{\mathrm{T}}, \\ {}^{T}\boldsymbol{p}_{B41} &= [-4 \quad 10]^{\mathrm{T}}, \quad {}^{T}\boldsymbol{p}_{B42} = [-8 \quad 10]^{\mathrm{T}}. \end{aligned}$$

Set of position ${}^{B}\boldsymbol{p}_{T}$ and orientation ${}^{B}\boldsymbol{R}_{T}$ of the top plate

$$ {}^{B}\boldsymbol{p}_{T} = [50 \quad 50]^{\mathrm{T}}, \; {}^{B}\boldsymbol{R}_{T} = \begin{bmatrix} 1 & 0 \\ 0 & 1 \end{bmatrix}. \tag{5.9}$$

Position of wire end points on the top plate

From Eq. (3.10), we have:

$$\begin{aligned} {}^{B}\boldsymbol{p}_{B11} &= [42 \quad 40]^{\mathrm{T}}, \; {}^{B}\boldsymbol{p}_{B12} = [46 \quad 40]^{\mathrm{T}}, \\ {}^{B}\boldsymbol{p}_{B21} &= [54 \quad 40]^{\mathrm{T}}, \; {}^{B}\boldsymbol{p}_{B22} = [58 \quad 40]^{\mathrm{T}}, \\ {}^{B}\boldsymbol{p}_{B31} &= [58 \quad 60]^{\mathrm{T}}, \; {}^{B}\boldsymbol{p}_{B32} = [54 \quad 60]^{\mathrm{T}}, \\ {}^{B}\boldsymbol{p}_{B41} &= [46 \quad 60]^{\mathrm{T}}, \; {}^{B}\boldsymbol{p}_{B42} = [42 \quad 60]^{\mathrm{T}}. \end{aligned}$$

Position of wire end points on the frame

The DAMs are arranged on the frame such that the positions of the wire end points on the frame are as below:

$$\begin{aligned} {}^{B}\boldsymbol{p}_{A11} &= [42 \quad 20]^{\mathrm{T}}, \; {}^{B}\boldsymbol{p}_{A12} = [46 \quad 20]^{\mathrm{T}}, \\ {}^{B}\boldsymbol{p}_{A21} &= [54 \quad 20]^{\mathrm{T}}, \; {}^{B}\boldsymbol{p}_{A22} = [58 \quad 20]^{\mathrm{T}}, \\ {}^{B}\boldsymbol{p}_{A31} &= [58 \quad 90]^{\mathrm{T}}, \; {}^{B}\boldsymbol{p}_{A32} = [54 \quad 90]^{\mathrm{T}}, \\ {}^{B}\boldsymbol{p}_{A41} &= [46 \quad 90]^{\mathrm{T}}, \; {}^{B}\boldsymbol{p}_{A42} = [42 \quad 90]^{\mathrm{T}}. \end{aligned}$$

Calculating the wire vectors ${}^{B}\boldsymbol{e}_{ij}$

The wire vectors ${}^{B}\boldsymbol{e}_{ij}$ can be calculated using Eq. (3.11), and the results are shown below:

$$\begin{aligned} {}^{B}\boldsymbol{e}_{11} = {}^{B}\boldsymbol{e}_{12} = {}^{B}\boldsymbol{e}_{21} = {}^{B}\boldsymbol{e}_{22} &= [0 \quad -1]^{\mathrm{T}}, \\ {}^{B}\boldsymbol{e}_{31} = {}^{B}\boldsymbol{e}_{32} = {}^{B}\boldsymbol{e}_{41} = {}^{B}\boldsymbol{e}_{42} &= [0 \quad 1]^{\mathrm{T}}. \end{aligned}$$

Checking if the two wires in the DAMs are in parallel

With this configuration, the two wires in the DAMs are in parallel.

Derivation of the matrix $\boldsymbol{W}'_{G2}$

From Eqs. (3.6) and (3.16) with n=3, N_D=4, it is easy to see that the matrices $\boldsymbol{W}_2$ and $\boldsymbol{W}'_2$ have size 7×8. As mentioned in the chapters 3 and 4, both of them will not be used in the proposed judgment method. For reference, those matrices can be seen in Eqs. (C.1) and (C.4) of the **Appendix C**, only the matrix $\boldsymbol{W}'_{G2}$ will be used for the judgment and it is derived as follows:

From Eq. (3.12), the vectors ${}^B\boldsymbol{e}_i$ can be derived as:

$$\begin{aligned} {}^B\boldsymbol{e}_1 = {}^B\boldsymbol{e}_2 &= [0 \quad -1]^{\mathrm{T}}, \\ {}^B\boldsymbol{e}_3 = {}^B\boldsymbol{e}_4 &= [0 \quad 1]^{\mathrm{T}}, \end{aligned}$$

From Eq. (3.13), the vectors ${}^B\boldsymbol{p}_{TCi}$ can be derived as:

$$\begin{aligned} {}^B\boldsymbol{p}_{TC1} &= [44 \quad 40]^{\mathrm{T}}, \quad {}^B\boldsymbol{p}_{TC2} = [56 \quad 40]^{\mathrm{T}}, \\ {}^B\boldsymbol{p}_{TC3} &= [56 \quad 60]^{\mathrm{T}}, \quad {}^B\boldsymbol{p}_{TC4} = [44 \quad 60]^{\mathrm{T}}. \end{aligned}$$

Then the wire matrix $\boldsymbol{W}'_{G2}$ from Eq. (3.17) becomes:

$$\boldsymbol{W}'_{G2} = \begin{bmatrix} 0 & 0 & 0 & 0 \\ -1 & -1 & 1 & 1 \\ 6 & -6 & 6 & -6 \end{bmatrix}_{3\times 4}, \tag{5.10}$$

The matrix $\boldsymbol{W}'_{G2}$ has size 3×4, with the row is equal to the number of DOFs in the planar global motion space and the column given by the four DOFs in the local motion space. It is about a quarter of the size of the wire matrix $\boldsymbol{W}_2$. The matrix $\boldsymbol{W}'_{G2}$ will then be applied in the step 1 of the judgment procedure as follows:

Necessary condition check (Step 1)

Easily to see in this case that rank($\boldsymbol{W}'_{G2}$) = 2, it is smaller than the number of dimension space of this wire mechanism(=3). Therefore, this mechanism can only realize the motion in two dimensions and it cannot realize motion in the remaining one. The first row of $\boldsymbol{W}'_{G2}$ corresponds to the resultant force in X direction, and all the elements of the row are zero, which causes the rank($\boldsymbol{W}'_{G2}$) to reduce one. The resultant force in X direction is zero so the motion in X direction can not be realized. This mechanism does not satisfy the 1^{st} point which also means it does not satisfy the vector closure condition as the necessary condition. Therefore, the mechanism fails step 1, so the judgment procedure is terminated and this RDWM candidate is eliminated.

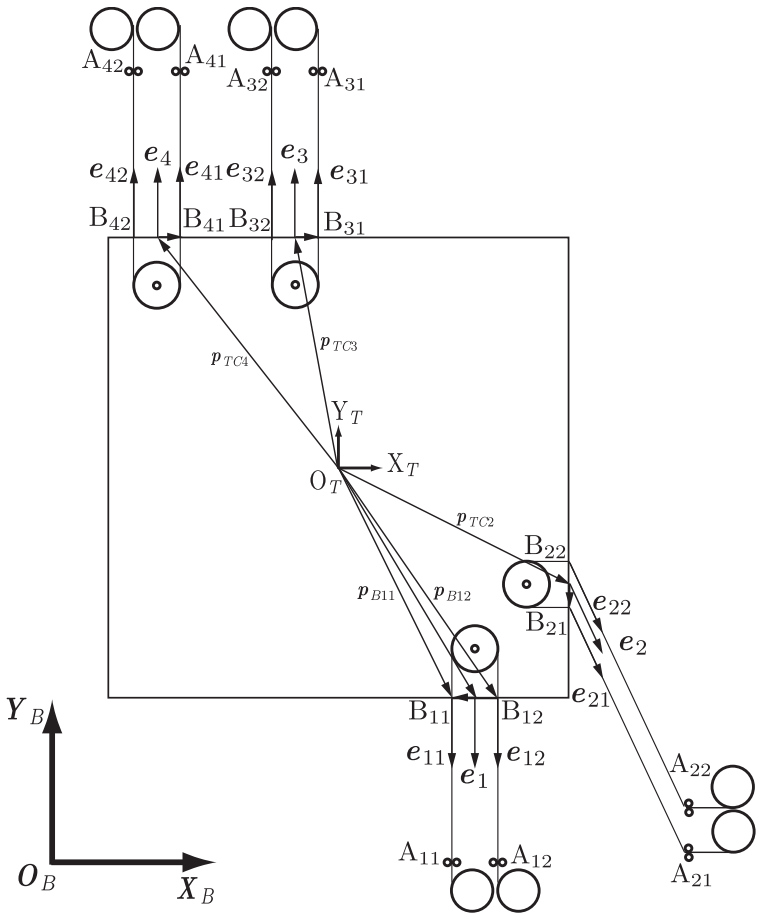

Figure. 5.3: The mechanism does not satisfy the 2^{nd} point of the step 1.

5.3.2 Second configuration: The Mechanism does not satisfy the 2^{nd} point of Step 1

A planar RDWM does not satisfy the 2^{nd} point of the step 1 of the judgment procedure is shown in figure 5.3. Here, the unit of the values of parameters related to length are also assumed to be [cm]. The processes for deriving the matrix $\boldsymbol{W}'_{G2}$ and the judgment procedure are shown below:

Defining ${}^{T}\boldsymbol{p}_{TCi}$, $\boldsymbol{R}_i$, ${}^{T}\boldsymbol{p}_{TDi}$ and ${}^{T}\boldsymbol{p}_{Bij}$

Select the parameters for the mechanism in figure 5.3 as follows:

$$
\begin{aligned}
{}^{T}\boldsymbol{p}_{TC1} &= [16 \quad -20]^{\mathrm{T}}, \quad {}^{T}\boldsymbol{p}_{TC2} = [20 \quad -10]^{\mathrm{T}}, \\
{}^{T}\boldsymbol{p}_{TC3} &= [-4 \quad 20]^{\mathrm{T}}, \quad {}^{T}\boldsymbol{p}_{TC4} = [-16 \quad 20]^{\mathrm{T}}.
\end{aligned}
$$

Radii of the pulleys: $R_1 = R_2 = R_3 = R_4 = 2$.

$$
\begin{aligned}
{}^{T}\boldsymbol{p}_{TD1} &= [-2 \quad 0]^{\mathrm{T}}, \quad {}^{T}\boldsymbol{p}_{TD2} = [0 \quad -2]^{\mathrm{T}}, \\
{}^{T}\boldsymbol{p}_{TD3} &= [2 \quad 0]^{\mathrm{T}}, \quad {}^{T}\boldsymbol{p}_{TD4} = [2 \quad 0]^{\mathrm{T}}.
\end{aligned}
$$

Position of wire end points on the top plate w.r.t the top plate coordinate:

$$
\begin{aligned}
{}^{T}\boldsymbol{p}_{B11} &= [14 \quad -20]^{\mathrm{T}}, \quad {}^{T}\boldsymbol{p}_{B12} = [18 \quad -20]^{\mathrm{T}}, \\
{}^{T}\boldsymbol{p}_{B21} &= [20 \quad -12]^{\mathrm{T}}, \quad {}^{T}\boldsymbol{p}_{B22} = [20 \quad -8]^{\mathrm{T}}, \\
{}^{T}\boldsymbol{p}_{B31} &= [-2 \quad 20]^{\mathrm{T}}, \quad {}^{T}\boldsymbol{p}_{B32} = [-6 \quad 20]^{\mathrm{T}}, \\
{}^{T}\boldsymbol{p}_{B41} &= [-14 \quad 20]^{\mathrm{T}}, \quad {}^{T}\boldsymbol{p}_{B42} = [-18 \quad 20]^{\mathrm{T}}.
\end{aligned}
$$

Set of position ${}^{B}\boldsymbol{p}_{T}$ and orientation ${}^{B}\boldsymbol{R}_{T}$ of the top plate

$$
{}^{B}\boldsymbol{p}_{T} = [50 \quad 50]^{\mathrm{T}}, \; {}^{B}\boldsymbol{R}_{T} = \begin{bmatrix} 1 & 0 \\ 0 & 1 \end{bmatrix}. \tag{5.11}
$$

Position of wire end points on the top plate

From Eq. (3.10), we have:

$$
\begin{aligned}
{}^{B}\boldsymbol{p}_{B11} &= [64 \quad 30]^{\mathrm{T}}, \; {}^{B}\boldsymbol{p}_{B12} = [68 \quad 30]^{\mathrm{T}}, \\
{}^{B}\boldsymbol{p}_{B21} &= [70 \quad 38]^{\mathrm{T}}, \; {}^{B}\boldsymbol{p}_{B22} = [70 \quad 42]^{\mathrm{T}}, \\
{}^{B}\boldsymbol{p}_{B31} &= [48 \quad 70]^{\mathrm{T}}, \; {}^{B}\boldsymbol{p}_{B32} = [44 \quad 70]^{\mathrm{T}}, \\
{}^{B}\boldsymbol{p}_{B41} &= [36 \quad 70]^{\mathrm{T}}, \; {}^{B}\boldsymbol{p}_{B42} = [32 \quad 70]^{\mathrm{T}}.
\end{aligned}
$$

Position of wire end points on the frame

The DAMs are arranged on the frame such that the positions of the wire end points on the frame are as below:

$$
\begin{aligned}
{}^{B}\boldsymbol{p}_{A11} &= [64 \quad 0]^{\mathrm{T}}, \quad {}^{B}\boldsymbol{p}_{A12} = [68 \quad 0]^{\mathrm{T}}, \\
{}^{B}\boldsymbol{p}_{A21} &= [118 \quad 2]^{\mathrm{T}}, \quad {}^{B}\boldsymbol{p}_{A22} = [118 \quad 6]^{\mathrm{T}}, \\
{}^{B}\boldsymbol{p}_{A31} &= [48 \quad 100]^{\mathrm{T}}, \; {}^{B}\boldsymbol{p}_{A32} = [44 \quad 100]^{\mathrm{T}}, \\
{}^{B}\boldsymbol{p}_{A41} &= [36 \quad 100]^{\mathrm{T}}, \; {}^{B}\boldsymbol{p}_{A42} = [32 \quad 100]^{\mathrm{T}}.
\end{aligned}
$$

Calculating the wire vectors ${}^{B}\boldsymbol{e}_{ij}$

The wire vectors ${}^{B}\boldsymbol{e}_{ij}$ can be calculated using Eq. (3.11), and the results are shown below:

$$
\begin{aligned}
&{}^{B}\boldsymbol{e}_{11} = {}^{B}\boldsymbol{e}_{12} = [0 \quad -1]^{\mathrm{T}},\ {}^{B}\boldsymbol{e}_{21} = {}^{B}\boldsymbol{e}_{22} = [4/5 \quad -3/5]^{\mathrm{T}},\\
&{}^{B}\boldsymbol{e}_{31} = {}^{B}\boldsymbol{e}_{32} = {}^{B}\boldsymbol{e}_{41} = {}^{B}\boldsymbol{e}_{42} = [0 \quad 1]^{\mathrm{T}}.
\end{aligned}
$$

Checking if the two wires in the DAMs are in parallel

With this configuration, the two wires in the DAMs are in parallel.

Derivation of the matrix $\boldsymbol{W}'_{G2}$

From Eqs. (3.6) and (3.16) with n=3, N_D=4, it is easy to see that the matrices $\boldsymbol{W}_2$ and $\boldsymbol{W}'_2$ have size 7×8. Similarly to the previous example, those matrices can be seen in Eqs. (C.9) and (C.12) of the **Appendix C** for reference, only the matrix $\boldsymbol{W}'_{G2}$ will be used for the judgment and it is derived as follows:

From Eq. (3.12), the vectors ${}^{B}\boldsymbol{e}_i$ can be derived as:

$$
{}^{B}\boldsymbol{e}_1 = [0 \quad -1]^{\mathrm{T}},\ {}^{B}\boldsymbol{e}_2 = [4/5 \quad -3/5]^{\mathrm{T}},{}^{B}\boldsymbol{e}_3 = {}^{B}\boldsymbol{e}_4 = [0 \quad 1]^{\mathrm{T}}.
$$

From Eq. (3.13), the vectors ${}^{B}\boldsymbol{p}_{TCi}$ can be derived as:

$$
\begin{aligned}
&{}^{B}\boldsymbol{p}_{TC1} = [66 \quad 30]^{\mathrm{T}},\ {}^{B}\boldsymbol{p}_{TC2} = [70 \quad 40]^{\mathrm{T}},\\
&{}^{B}\boldsymbol{p}_{TC3} = [46 \quad 70]^{\mathrm{T}},\ {}^{B}\boldsymbol{p}_{TC4} = [34 \quad 70]^{\mathrm{T}}.
\end{aligned}
$$

Then the wire matrix $\boldsymbol{W}'_{G2}$ from Eq. (3.17) becomes:

$$
\boldsymbol{W}'_{G2} = \frac{1}{5}\begin{bmatrix} 0 & 4 & 0 & 0 \\ -5 & -3 & 5 & 5 \\ -80 & -20 & -20 & -80 \end{bmatrix}_{3\times 4}, \tag{5.12}
$$

Similarly to the previous example, the matrix $\boldsymbol{W}'_{G2}$ related to the global motion in this case also equals just a quarter of the normal wire matrix $\boldsymbol{W}_2$. The matrix $\boldsymbol{W}'_{G2}$ will then be applied in the step 1 of the judgment procedure as follows:

Necessary condition check (Step 1)

Easily to see in this case that rank($\boldsymbol{W}'_{G2}$) = 3. It equals to the number of dimension space of the wire mechanism(=3) so it satisfies the 1^{st} point of vector closure condition. However considering the 3^{rd} row of $\boldsymbol{W}'_{G2}$, this row corresponds to the resultant moment. It has all elements with negative values so with any positive wire tension $\boldsymbol{T}_0$, the resultant moment will be produced only negative value. Therefore no wire tension $\boldsymbol{T}_0$ satisfies $\boldsymbol{W}'_{G2}\boldsymbol{T}_0 = 0$. This mechanism does not satisfy the 2^{nd} point which also means it does not satisfy vector closure condition as the necessary condition. Therefore, the mechanism fails step 1, so the judgment procedure is terminated and this RDWM candidate is eliminated.

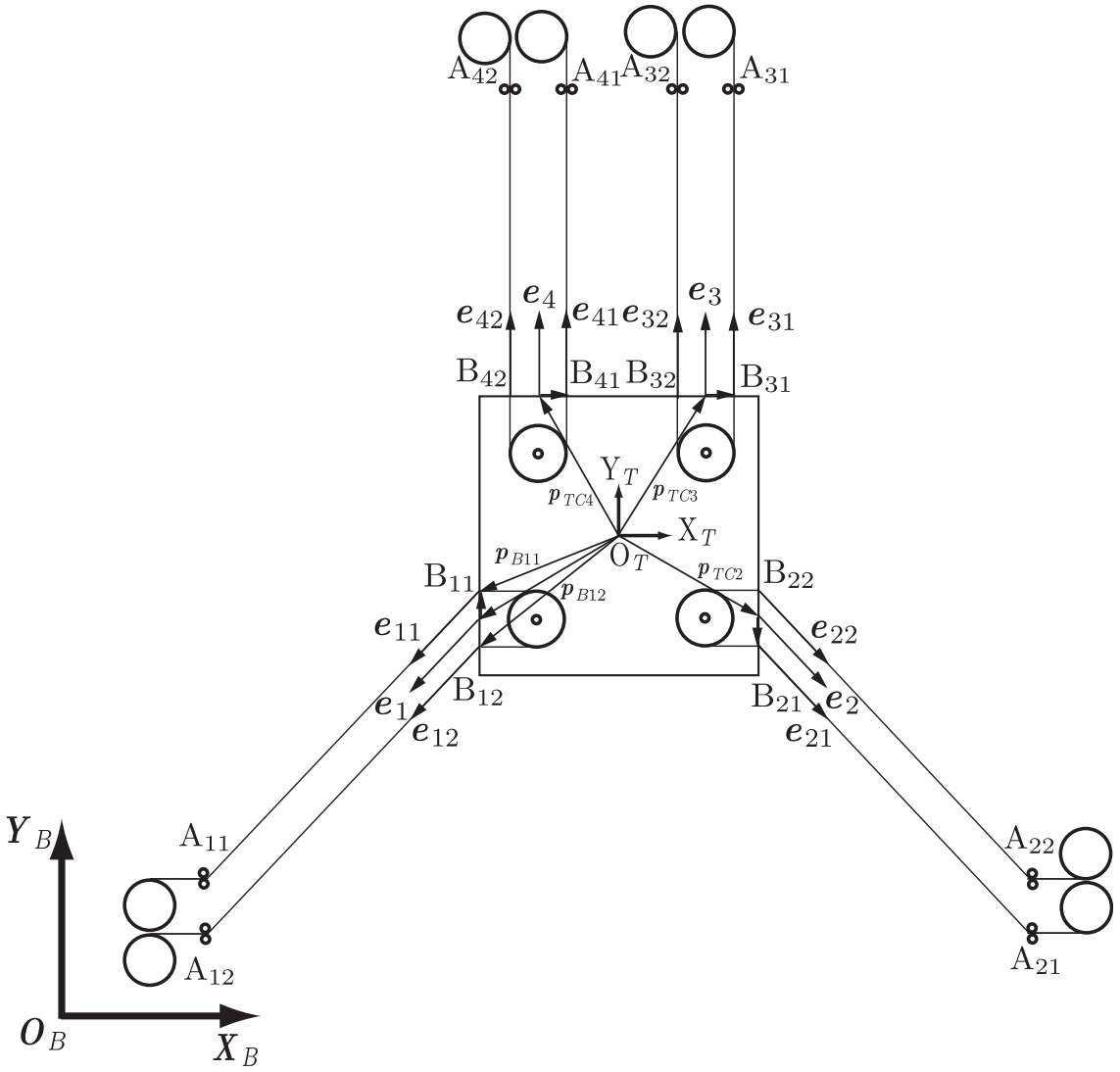

Figure. 5.4: A planar RDWM using DAMs.

5.3.3 Third configuration: planar RDWM with four DAMs

A planar RDWM with DAMs is shown in figure 5.4. Here, the unit of the values of parameters related to length are assumed to be [cm]. The processes for deriving the matrix $\boldsymbol{W}'_{G2}$ and the judgment procedure are shown below:

Defining ${}^{T}\boldsymbol{p}_{TCi}$, $\boldsymbol{R}_i$, ${}^{T}\boldsymbol{p}_{TDi}$ and ${}^{T}\boldsymbol{p}_{Bij}$

$$
\begin{aligned}
{}^{T}\boldsymbol{p}_{TC1} &= [-10 \;\; -6]^{\mathrm{T}}, \quad {}^{T}\boldsymbol{p}_{TC2} = [10 \;\; -6]^{\mathrm{T}}, \\
{}^{T}\boldsymbol{p}_{TC3} &= [6 \;\; 10]^{\mathrm{T}}, \qquad {}^{T}\boldsymbol{p}_{TC4} = [-6 \;\; 10]^{\mathrm{T}}.
\end{aligned}
$$

The pulley radii are $R_1 = R_2 = R_3 = R_4 = 2$.

$$
\begin{aligned}
{}^{T}\boldsymbol{p}_{TD1} &= [0 \;\; 2]^{\mathrm{T}}, \quad {}^{T}\boldsymbol{p}_{TD2} = [0 \;\; -2]^{\mathrm{T}}, \\
{}^{T}\boldsymbol{p}_{TD3} &= [2 \;\; 0]^{\mathrm{T}}, \quad {}^{T}\boldsymbol{p}_{TD4} = [2 \;\; 0]^{\mathrm{T}}.
\end{aligned}
$$

Position of wire end points on the top plate w.r.t the top plate coordinate:

From Eq. (3.9):

$$
\begin{aligned}
{}^{T}\boldsymbol{p}_{B11} &= [-10 \;\; -4]^{\mathrm{T}}, \quad {}^{T}\boldsymbol{p}_{B12} = [-10 \;\; -8]^{\mathrm{T}}, \\
{}^{T}\boldsymbol{p}_{B21} &= [10 \;\; -8]^{\mathrm{T}}, \quad {}^{T}\boldsymbol{p}_{B22} = [10 \;\; -4]^{\mathrm{T}}, \\
{}^{T}\boldsymbol{p}_{B31} &= [8 \;\; 10]^{\mathrm{T}}, \quad {}^{T}\boldsymbol{p}_{B32} = [4 \;\; 10]^{\mathrm{T}}, \\
{}^{T}\boldsymbol{p}_{B41} &= [-4 \;\; 10]^{\mathrm{T}}, \quad {}^{T}\boldsymbol{p}_{B42} = [-8 \;\; 10]^{\mathrm{T}}.
\end{aligned}
$$

Set of positions ${}^{B}\boldsymbol{p}_{T}$ and orientations ${}^{B}\boldsymbol{R}_{T}$ of the top plate

$$
{}^{B}\boldsymbol{p}_{T} = [50 \;\; 50]^{\mathrm{T}}, \; {}^{B}\boldsymbol{R}_{T} = \begin{bmatrix} 1 & 0 \\ 0 & 1 \end{bmatrix} \in \boldsymbol{R}^{2\times 2}.
$$

Positions of wire end points on the top plate

From Eq. (3.10):

$$
\begin{aligned}
{}^{B}\boldsymbol{p}_{B11} &= [40 \;\; 46]^{\mathrm{T}}, \; {}^{B}\boldsymbol{p}_{B12} = [40 \;\; 42]^{\mathrm{T}}, \\
{}^{B}\boldsymbol{p}_{B21} &= [60 \;\; 42]^{\mathrm{T}}, \; {}^{B}\boldsymbol{p}_{B22} = [60 \;\; 46]^{\mathrm{T}}, \\
{}^{B}\boldsymbol{p}_{B31} &= [58 \;\; 60]^{\mathrm{T}}, \; {}^{B}\boldsymbol{p}_{B32} = [54 \;\; 60]^{\mathrm{T}}, \\
{}^{B}\boldsymbol{p}_{B41} &= [46 \;\; 60]^{\mathrm{T}}, \; {}^{B}\boldsymbol{p}_{B42} = [42 \;\; 60]^{\mathrm{T}}.
\end{aligned}
$$

Position of wire end points on the frame

The following positions of the wire end points on the frame were ensured by appropriately arranging the DAMs on the frame:

$$
\begin{aligned}
{}^{B}\boldsymbol{p}_{A11} &= [10 \;\; 23.5]^{\mathrm{T}}, \quad {}^{B}\boldsymbol{p}_{A12} = [10 \;\; 19.5]^{\mathrm{T}}, \\
{}^{B}\boldsymbol{p}_{A21} &= [90 \;\; 19.5]^{\mathrm{T}}, \quad {}^{B}\boldsymbol{p}_{A22} = [90 \;\; 23.5]^{\mathrm{T}}, \\
{}^{B}\boldsymbol{p}_{A31} &= [58 \;\; 90]^{\mathrm{T}}, \quad {}^{B}\boldsymbol{p}_{A32} = [54 \;\; 90]^{\mathrm{T}}, \\
{}^{B}\boldsymbol{p}_{A41} &= [46 \;\; 90]^{\mathrm{T}}, \quad {}^{B}\boldsymbol{p}_{A42} = [42 \;\; 90]^{\mathrm{T}}.
\end{aligned}
$$

Calculating the wire vectors ${}^{B}\boldsymbol{e}_{ij}$

The wire vectors ${}^{B}\boldsymbol{e}_{ij}$ were calculated by Eq. (3.11).

$$\begin{aligned}
{}^{B}\boldsymbol{e}_{11} &= {}^{B}\boldsymbol{e}_{12} = [-4/5 \quad -3/5]^{\mathrm{T}}, \\
{}^{B}\boldsymbol{e}_{21} &= {}^{B}\boldsymbol{e}_{22} = [4/5 \quad -3/5]^{\mathrm{T}}, \\
{}^{B}\boldsymbol{e}_{31} &= {}^{B}\boldsymbol{e}_{32} = [0 \quad 1]^{\mathrm{T}}, \\
{}^{B}\boldsymbol{e}_{41} &= {}^{B}\boldsymbol{e}_{42} = [0 \quad 1]^{\mathrm{T}}.
\end{aligned}$$

Checking if the two wires in the DAMs are in parallel

With this configuration, the two wires in the DAMs are in parallel.

Derivation of the matrix $\boldsymbol{W}_{\boldsymbol{G}}^{'}$

From Eqs. (3.6) and (3.16) with n=3, N_D=4, it is easy to see that the matrices $\boldsymbol{W}_2$ and $\boldsymbol{W}_2^{'}$ have size 7×8. Similarly to the previous examples, those matrices can be seen in Eqs. (C.17) and (C.20) of the **Appendix C** for reference, only the matrix $\boldsymbol{W}_{G2}^{'}$ will be used for the judgment and it is derived as follows:

From Eq. (3.12), the vectors ${}^{B}\boldsymbol{e}_i$ can be derived as:

$${}^{B}\boldsymbol{e}_1 = [0 \quad 1]^{\mathrm{T}}, \; {}^{B}\boldsymbol{e}_2 = [-4/5 \quad -3/5]^{\mathrm{T}}, {}^{B}\boldsymbol{e}_3 = [4/5 \quad -3/5]^{\mathrm{T}}, \; {}^{B}\boldsymbol{e}_4 = [0 \quad 1]^{\mathrm{T}}$$

From Eq. (3.13), the vectors ${}^{B}\boldsymbol{p}_{TCi}$ can be derived as:

$$\begin{aligned}
{}^{B}\boldsymbol{p}_{TC1} &= [40 \quad 44]^{\mathrm{T}}, \quad {}^{B}\boldsymbol{p}_{TC2} = [60 \quad 44]^{\mathrm{T}}, \\
{}^{B}\boldsymbol{p}_{TC3} &= [56 \quad 60]^{\mathrm{T}}, \quad {}^{B}\boldsymbol{p}_{TC4} = [44 \quad 60]^{\mathrm{T}}.
\end{aligned}$$

Then the matrix $\boldsymbol{W}_{G2}^{'}$ from Eq. (3.17) becomes:

$$\boldsymbol{W}_{G2}^{'} = \frac{1}{5}\begin{bmatrix} -4 & 4 & 0 & 0 \\ -3 & -3 & 1 & 1 \\ 6 & -6 & 30 & -30 \end{bmatrix}_{3\times 4}, \tag{5.13}$$

Similarly to the previous examples, the matrix $\boldsymbol{W}_{G2}^{'}$ related to the global motion in this case also equals just a quarter of the normal wire matrix $\boldsymbol{W}_2$. The matrix $\boldsymbol{W}_{G2}^{'}$ will then be applied in the step 1 of the judgment procedure as follows:

Necessary condition check (Step 1)

From the expression in the judgment of a candidate section, only the matrix that contributes to global motion $\boldsymbol{W}_{G2}^{'}$ is needed to check the vector closure condition. Using the matrix of global motion from Eq. (5.13), we have:

i) rank($\boldsymbol{W}_{G2}^{'}$) = 3.

ii) With $\boldsymbol{T}_{S2} = \begin{bmatrix} 5 & 5 & 3 & 3 \end{bmatrix}^{\mathrm{T}} > \boldsymbol{0}$, easy to get $\boldsymbol{W}_{G2}^{'}\boldsymbol{T}_{S2} = \boldsymbol{0}$.

The above analysis shows that rank($\boldsymbol{W}_{G2}^{'}$) equals to the number of dimension spaces of the wire mechanism. As there is a vector $\boldsymbol{T}_{S2}$ that satisfies $\boldsymbol{W}_{G2}^{'}\boldsymbol{T}_{S2} = \boldsymbol{0}$, the matrix $\boldsymbol{W}_{G2}^{'}$

satisfies the vector closure condition and the mechanism can produce the resultant force in any direction within its motion space. The results mean that the planar RDWM with four sets of DAMs in this example has the same structure as that of a conventional wire mechanism with four sets of single actuator modules, where each wire is equivalent to a set of two wires for each DAM in the planar RDWM, when judging the vector closure condition. Therefore, this planar RDWM candidate satisfies step 1 and the analysis proceeds to the step 2 as follows.

KA (Step 2)

In step 2, the matrix $\boldsymbol{W}_{G2}$ that contributes to the resultant force on the top plate is given by Eq. (4.23) as follows:

$$\boldsymbol{W}_{G2} = \frac{1}{5}\begin{bmatrix} -4 & -4 & 4 & 4 & 0 & 0 & 0 & 0 \\ -3 & -3 & -3 & -3 & 5 & 5 & 5 & 5 \\ 14 & -2 & 2 & -14 & 40 & 20 & -20 & -40 \end{bmatrix} \in \boldsymbol{R}^{3\times 8}. \tag{5.14}$$

The matrix of total contribution of DAMs to the velocity of the top plate is given by Eq. (4.22):

$$\boldsymbol{A}_L = \text{bdiag.}(\, \boldsymbol{A}_{Ld1},\, \boldsymbol{A}_{Ld2},\, \boldsymbol{A}_{Ld3},\, \boldsymbol{A}_{Ld4}) \in \boldsymbol{R}^{16\times 8}. \tag{5.15}$$

Eq. (4.11) presents the contents of $\boldsymbol{A}_{Ld1}$, $\boldsymbol{A}_{Ld2}$, $\boldsymbol{A}_{Ld3}$, $\boldsymbol{A}_{Ld4}$ and $\boldsymbol{b}_{Ld1}$, $\boldsymbol{b}_{Ld2}$, $\boldsymbol{b}_{Ld3}$, $\boldsymbol{b}_{Ld4}$. The matrices of top plate velocities $\boldsymbol{A}_V$ and $\boldsymbol{b}_V$ are given by Eqs. (4.20) and (4.21), respectively. The result are given below:

$$\boldsymbol{A}_V = \frac{1}{5}\begin{bmatrix} 4 & 3 & -14 \\ -4 & -3 & 14 \\ 4 & 3 & 2 \\ -4 & -3 & -2 \\ -4 & 3 & -2 \\ 4 & -3 & 2 \\ -4 & 3 & 14 \\ 4 & -3 & -14 \\ 0 & -5 & -40 \\ 0 & 5 & 40 \\ 0 & -5 & -20 \\ 0 & 5 & 20 \\ 0 & -5 & 20 \\ 0 & 5 & -20 \\ 0 & -5 & 40 \\ 0 & 5 & -40 \end{bmatrix} \in \boldsymbol{R}^{16\times 3}, \boldsymbol{b}_V = \begin{bmatrix} 1 \\ 1 \\ 1 \\ 1 \\ 1 \\ 1 \\ 1 \\ 1 \\ 1 \\ 1 \\ 1 \\ 1 \\ 1 \\ 1 \\ 1 \\ 1 \end{bmatrix} \in \boldsymbol{R}^{16}. \tag{5.16}$$

From the above $\boldsymbol{A}_V, \boldsymbol{b}_V$, we solve the convex sets mentioned in Eqs. (4.19) and (4.24). The vertex sets in matrix $\boldsymbol{A}$, the active constraint space $\boldsymbol{S}_{AC}$ and passive constraint space $\boldsymbol{S}_{PC}$ of the planar RDWM with four sets of DAM are found by Eqs. (4.25) and (4.26). The result are

shown below.

$$\boldsymbol{A} = \begin{bmatrix} -1.25 & 1.25 & -1.1875 & -0.5 & 0.5 & 1.1875 & 0.5 & -0.5 & -0.8125 & 0.8125 \\ 0 & 0 & 0 & -1 & 1 & 0 & -1 & 1 & 0 & 0 \\ 0 & 0 & -0.125 & 0 & 0 & 0.125 & 0 & 0 & 0.125 & -0.125 \end{bmatrix} \in \boldsymbol{R}^{3\times 10} \tag{5.17}$$

$$\boldsymbol{S}_{AC} = \mathcal{R}\left(\boldsymbol{E}_3\right), \boldsymbol{S}_{PC} = \emptyset. \tag{5.18}$$

Eq. (5.18) shows that in this case, the active constraint space $\boldsymbol{S}_{AC}$ produced by the top plate allows motion in the X, and Y directions and the rotation around the Z-axis.

SFA (Step 3)

The above KA revealed that the active constraint space $\boldsymbol{S}_{AC}$ is the whole motion space of the mechanism. Therefore, the matrix $\boldsymbol{W}_{CVC}$ which relates the wire tension vector to the resultant force vector in the constraint coordinates is exactly the matrix $\boldsymbol{W}_G$ in Eq. (5.14). Then, similar to step 1, we easily observe that:

i) rank($\boldsymbol{W}_{CVC}$) = 3.

ii) The wire tension vector $\boldsymbol{T}_{C0} = [\,5\ 5\ 5\ 5\ 3\ 3\ 3\ 3\,]^{\mathrm{T}} \in \boldsymbol{R}^8 > \boldsymbol{0}$ satisfies $\boldsymbol{W}_{CVC}\boldsymbol{T}_{C0} = \boldsymbol{0}$.

The matrix $\boldsymbol{W}_{CVC}$ is full-ranked in the above analysis. Moreover, there is a vector $\boldsymbol{T}_{C0}$ that satisfies $\boldsymbol{W}_{CVC}\boldsymbol{T}_{C0} = \boldsymbol{0}$. Therefore, this RDWM candidate passes step 3 and the resultant force can be produced in any direction within the active constraint space $\boldsymbol{S}_{AC}$.

As this configuration of planar RDWM does not contrain the velocity, velocities can be generated in any direction (step 2). Consequently, the contents of step 3 are identical to those of step 1.

Therefore, to find proper configurations of a RDWM without VCM, only step 1 is enough. However, not only step 1 but also steps 2, 3 are necessary for the case of RDWM with VCM as revealed next.

5.3.4 Fourth configuration: planar RDWM with two DAMs and one DAM with a VCM

We now propose a planar RDWM configured with two DAMs without VCMs and one DAM with a VCM (see figure 5.5). This configuration is identical to the planar RDWM with four DAMs in the last example, except that the top two DAMs are replaced by a DAM with a VCM.

The values of the parameters ${}^{T}\boldsymbol{p}_{TCi}$, R_i, ${}^{T}\boldsymbol{p}_{TDi}$, ${}^{T}\boldsymbol{p}_{Bij}$, ${}^{B}\boldsymbol{p}_{T}$, ${}^{B}\boldsymbol{R}_{T}$ and ${}^{B}\boldsymbol{p}_{Bij}$ were those assigned to the planar RDWM with four DAMs.

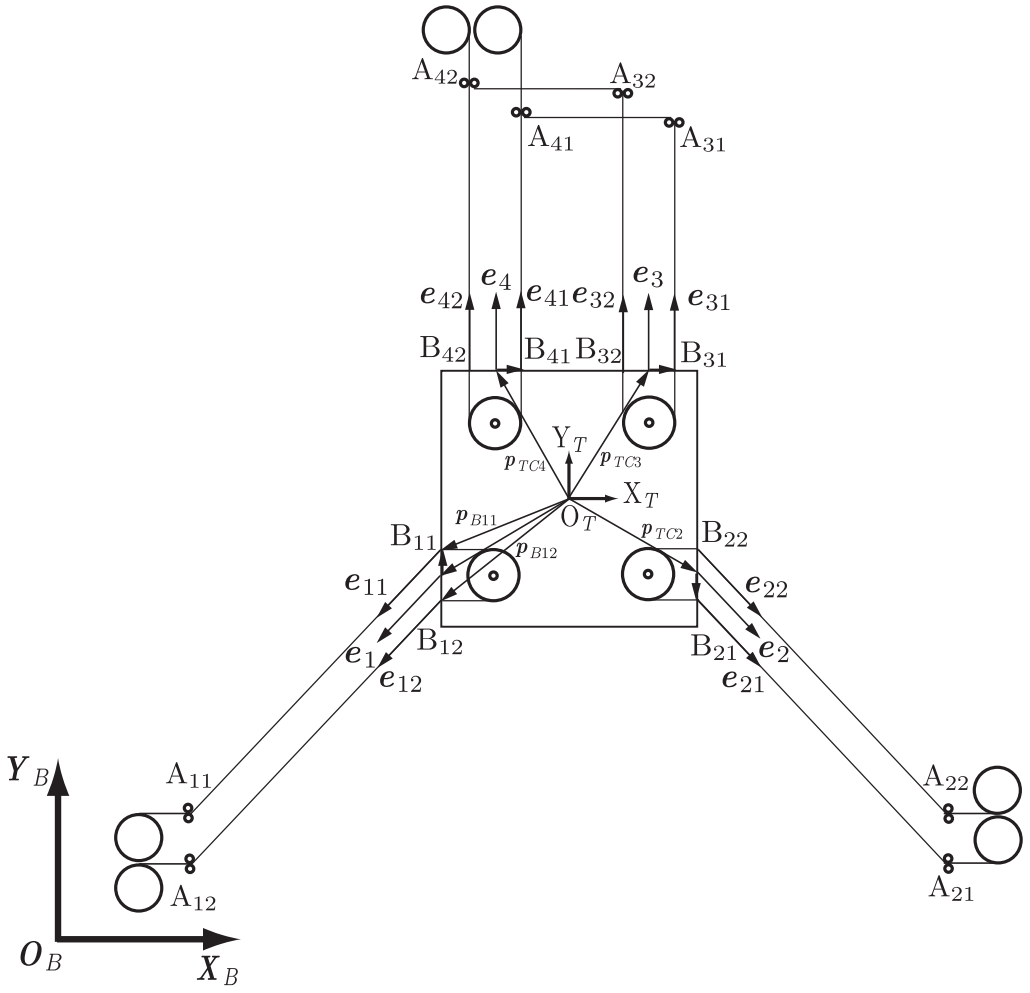

Figure. 5.5: A planar RDWM with a VCM.

Positions of wire end points on the frame

The following positions of the wire end points on the frame were ensured by appropriately arranging the DAMs and VCM on the frame:

$$
\begin{aligned}
{}^{B}\boldsymbol{p}_{A11} &= [10 \;\; 23.5]^{\mathrm{T}}, \; {}^{B}\boldsymbol{p}_{A12} = [10 \;\; 19.5]^{\mathrm{T}}, \\
{}^{B}\boldsymbol{p}_{A21} &= [90 \;\; 19.5]^{\mathrm{T}}, \; {}^{B}\boldsymbol{p}_{A22} = [90 \;\; 23.5]^{\mathrm{T}}, \\
{}^{B}\boldsymbol{p}_{A31} &= [58 \;\; 85]^{\mathrm{T}}, \quad {}^{B}\boldsymbol{p}_{A32} = [54 \;\; 90]^{\mathrm{T}}, \\
{}^{B}\boldsymbol{p}_{A41} &= [46 \;\; 85]^{\mathrm{T}}, \quad {}^{B}\boldsymbol{p}_{A42} = [42 \;\; 90]^{\mathrm{T}}.
\end{aligned}
$$

Calculating the wire vectors ${}^{B}\boldsymbol{e}_{ij}$

The wire vectors ${}^{B}\boldsymbol{e}_{ij}$ calculated by Eq. (3.11), were identical to those of the planar RDWM with four DAMs.

Derivation of the matrix $\boldsymbol{W}_{G}^{'}$

From Eqs. (B.1) and (B.4) with n=3, N_D=2 and N_V=1, it is easy to see that the matrices $\boldsymbol{W}_2$ and $\boldsymbol{W}_2^{'}$ have size 7×8. Similarly to the previous examples, those matrices can be seen in Eqs. (C.25) and (C.28) of the **Appendix C** for reference, only the matrix $\boldsymbol{W}_{G2}^{'}$ will be used for the judgment and it is derived as follows:

From Eq. (3.12), the vectors ${}^{B}\boldsymbol{e}_i$ can be derived as:

$$
{}^{B}\boldsymbol{e}_1 = [0 \;\; 1]^{\mathrm{T}}, \; {}^{B}\boldsymbol{e}_2 = [-4/5 \;\; -3/5]^{\mathrm{T}}, {}^{B}\boldsymbol{e}_3 = [4/5 \;\; -3/5]^{\mathrm{T}}, \; {}^{B}\boldsymbol{e}_4 = [0 \;\; 1]^{\mathrm{T}}
$$

From Eq. (3.13), the vectors ${}^{B}\boldsymbol{p}_{TCi}$ can be derived as:

$$
\begin{aligned}
{}^{B}\boldsymbol{p}_{TC1} &= [40 \;\; 44]^{\mathrm{T}}, \; {}^{B}\boldsymbol{p}_{TC2} = [60 \;\; 44]^{\mathrm{T}}, \\
{}^{B}\boldsymbol{p}_{TC3} &= [56 \;\; 60]^{\mathrm{T}}, \; {}^{B}\boldsymbol{p}_{TC4} = [44 \;\; 60]^{\mathrm{T}}.
\end{aligned}
$$

Then the matrix $\boldsymbol{W}_{G2}^{'}$ from Eq. (B.5) becomes:

$$
\boldsymbol{W}_{G2}^{'} = \frac{1}{5} \begin{bmatrix} -4 & 4 & 0 & 0 \\ -3 & -3 & 1 & 1 \\ 6 & -6 & 30 & -30 \end{bmatrix}_{3\times 4}, \tag{5.19}
$$

Similarly to the previous examples, the matrix $\boldsymbol{W}_{G2}^{'}$ related to the global motion in this case also equals just a quarter of the normal wire matrix $\boldsymbol{W}_2$. The matrix $\boldsymbol{W}_{G2}^{'}$ will then be applied in the step 1 of the judgment procedure as follows:

Necessary condition check (Step 1)

The matrix $\boldsymbol{W}_{G2}^{'}$ of this configuration is given by Eq. (5.19) and step 1 proceeds as described for the configuration of RDWM with four DAMs.

KA (Step 2)

The matrix $\boldsymbol{W}_G$ of this configuration is given by Eq. (5.14). Then, the matrix of total contributions of the DAMs and VCM to the top plate's velocity is given by Eq. (4.22):

$$\boldsymbol{A}_L = \text{bdiag.}(\boldsymbol{A}_{Ld1},\ \boldsymbol{A}_{Ld2},\ \boldsymbol{A}_{Lv}) \in \boldsymbol{R}^{8\times 4}. \tag{5.20}$$

Here the contents of $\boldsymbol{A}_{Ld1}$, $\boldsymbol{A}_{Ld2}$, $\boldsymbol{A}_{Lv}$ and $\boldsymbol{b}_{Ld1}$, $\boldsymbol{b}_{Ld2}$, $\boldsymbol{b}_{Lv}$ are shown in Eqs. (4.11) and (4.16). The matrices of top plate's velocities $\boldsymbol{A}_V, \boldsymbol{b}_V$ are obtained from Eqs. (4.20) and (4.21), and the results are shown below:

$$\boldsymbol{A}_V = \frac{1}{5}\begin{bmatrix} 4 & 3 & -14 \\ -4 & -3 & 14 \\ 4 & 3 & 2 \\ -4 & -3 & -2 \\ -4 & 3 & -2 \\ 4 & -3 & 2 \\ -4 & 3 & 14 \\ 4 & -3 & -14 \\ 0 & -5 & -40 \\ 0 & 5 & 40 \\ 0 & 0 & 60 \\ 0 & 0 & -60 \\ 0 & -5 & -20 \\ 0 & 5 & 20 \\ 0 & 0 & 60 \\ 0 & 0 & -60 \end{bmatrix} \in \boldsymbol{R}^{16\times 3}, \boldsymbol{b}_V = \begin{bmatrix} 1 \\ 1 \\ 1 \\ 1 \\ 1 \\ 1 \\ 1 \\ 1 \\ 1 \\ 1 \\ 0 \\ 0 \\ 1 \\ 1 \\ 0 \\ 0 \end{bmatrix} \in \boldsymbol{R}^{16}. \tag{5.21}$$

From the above $\boldsymbol{A}_V, \boldsymbol{b}_V$, we solve the convex sets mentioned in Eqs. (4.19) and (4.24). The vertex sets in matrix $\boldsymbol{A}$, the active constraint space $\boldsymbol{S}_{AC}$ and the passive constraint space $\boldsymbol{S}_{PC}$ of the planar RDWM with two DAMs and one DAM with a VCM are obtained by Eqs. (4.25) and (4.26) and are respectively given by

$$\boldsymbol{A} = \begin{bmatrix} -1.25 & 1.25 & -0.5 & 0.5 & 0.5 & -0.5 \\ 0 & 0 & -1 & 1 & -1 & 1 \\ 0 & 0 & 0 & 0 & 0 & 0 \end{bmatrix} \in \boldsymbol{R}^{3\times 6}, \tag{5.22}$$

$$\boldsymbol{S}_{AC} = \mathcal{R}\left(\begin{bmatrix} 1 & 0 \\ 0 & 1 \\ 0 & 0 \end{bmatrix}\right), \boldsymbol{S}_{PC} = \mathcal{R}\left(\begin{bmatrix} 0 \\ 0 \\ 1 \end{bmatrix}\right). \tag{5.23}$$

Equation (5.23) indicates that the top plate can move in the X and Y directions but its orientation is fixed around the Z-axis. Therefore, this configuration satisfies the step 2 and the analysis proceeds to step 3.

SFA (Step 3)

The matrix $\boldsymbol{W}_{CVC}$ that relates the wire tension vector in the constraint coordinate is derived from Eq. (4.48) then it is used for SFA. The contents of this matrix are given below:

$$\boldsymbol{W}_{CVC} = \frac{1}{5}\begin{bmatrix} -4 & -4 & 4 & 4 & 0 & 0 \\ -3 & -3 & -3 & -3 & 5 & 5 \end{bmatrix} \in \boldsymbol{R}^{2\times 6}, \tag{5.24}$$

$\boldsymbol{W}_{CVC}$ contains some of the elements of matrix $\boldsymbol{W}_G$. We then have:

i) rank($\boldsymbol{W}_{CVC}$) = 2.

ii) The wire tension vector $\boldsymbol{T}_{C0} = [\,3\ 2\ 3\ 2\ 3\ 3\,]^{\mathrm{T}} \in \boldsymbol{R}^6 > \boldsymbol{0}$ satisfies $\boldsymbol{W}_{CVC}\boldsymbol{T}_{C0} = \boldsymbol{0}$.

The above analysis reveals that $\boldsymbol{W}_{CVC}$ is a full-ranked matrix. Moreover, there is a vector $\boldsymbol{T}_{C0}$ that satisfies $\boldsymbol{W}_{CVC}\boldsymbol{T}_{C0} = \boldsymbol{0}$. Consequently, this RDWM candidate satisfies step 3 and the resultant force can be produced in any direction within the active constraint space $\boldsymbol{S}_{AC}$.

Because it passes all three of the judgment steps, this planar RDWM candidate with two DAMs and one DAM with a VCM is a proper configuration that achieves the desired active constraint space $\boldsymbol{S}_{AC}$ in X and Y directions. This configuration requires two fewer actuators than the planar RDWM with four DAMs.

5.3.5 Fifth configuration: improper planar RDWM with two DAMs and one DAM with a VCM

Figure 5.6 shows an improper planar RDWM with two DAMs and one DAM with a VCM. This configuration has the same modules as configuration 2, but the modules arrangement is inappropriate.

Defining ${}^{T}\boldsymbol{p}_{TCi}$, $\boldsymbol{R}_i$, ${}^{T}\boldsymbol{p}_{TDi}$ and ${}^{T}\boldsymbol{p}_{Bij}$

$$
\begin{array}{ll}
{}^{T}\boldsymbol{p}_{TC1} = [16\ \ -20]^{\mathrm{T}}, & {}^{T}\boldsymbol{p}_{TC2} = [20\ \ -10]^{\mathrm{T}}, \\
{}^{T}\boldsymbol{p}_{TC3} = [-4\ \ 20]^{\mathrm{T}}, & {}^{T}\boldsymbol{p}_{TC4} = [-16\ \ 20]^{\mathrm{T}}.
\end{array}
$$

The pulley radii are: $R_1 = R_2 = R_3 = R_4 = 2$.

$$
\begin{array}{ll}
{}^{T}\boldsymbol{p}_{TD1} = [-2\ \ 0]^{\mathrm{T}}, & {}^{T}\boldsymbol{p}_{TD2} = [0\ \ -2]^{\mathrm{T}}, \\
{}^{T}\boldsymbol{p}_{TD3} = [2\ \ 0]^{\mathrm{T}}, & {}^{T}\boldsymbol{p}_{TD4} = [2\ \ 0]^{\mathrm{T}}.
\end{array}
$$

The position of the wire end points on the top plate w.r.t the top plate coordinate were calculated by Eq. (3.9):

$$
\begin{array}{ll}
{}^{T}\boldsymbol{p}_{B11} = [14\ \ -20]^{\mathrm{T}}, & {}^{T}\boldsymbol{p}_{B12} = [18\ \ -20]^{\mathrm{T}}, \\
{}^{T}\boldsymbol{p}_{B21} = [20\ \ -12]^{\mathrm{T}}, & {}^{T}\boldsymbol{p}_{B22} = [20\ \ -8]^{\mathrm{T}}, \\
{}^{T}\boldsymbol{p}_{B31} = [-2\ \ 20]^{\mathrm{T}}, & {}^{T}\boldsymbol{p}_{B32} = [-6\ \ 20]^{\mathrm{T}}, \\
{}^{T}\boldsymbol{p}_{B41} = [-14\ \ 20]^{\mathrm{T}}, & {}^{T}\boldsymbol{p}_{B42} = [-18\ \ 20]^{\mathrm{T}}.
\end{array}
$$

Set of positions ${}^{B}\boldsymbol{p}_{T}$ and orientations ${}^{B}\boldsymbol{R}_{T}$ of the top plate

$$
{}^{B}\boldsymbol{p}_{T} = [50\ \ 50]^{\mathrm{T}},\ {}^{B}\boldsymbol{R}_{T} = \begin{bmatrix} 1 & 0 \\ 0 & 1 \end{bmatrix} \in \boldsymbol{R}^{2\times 2}.
$$

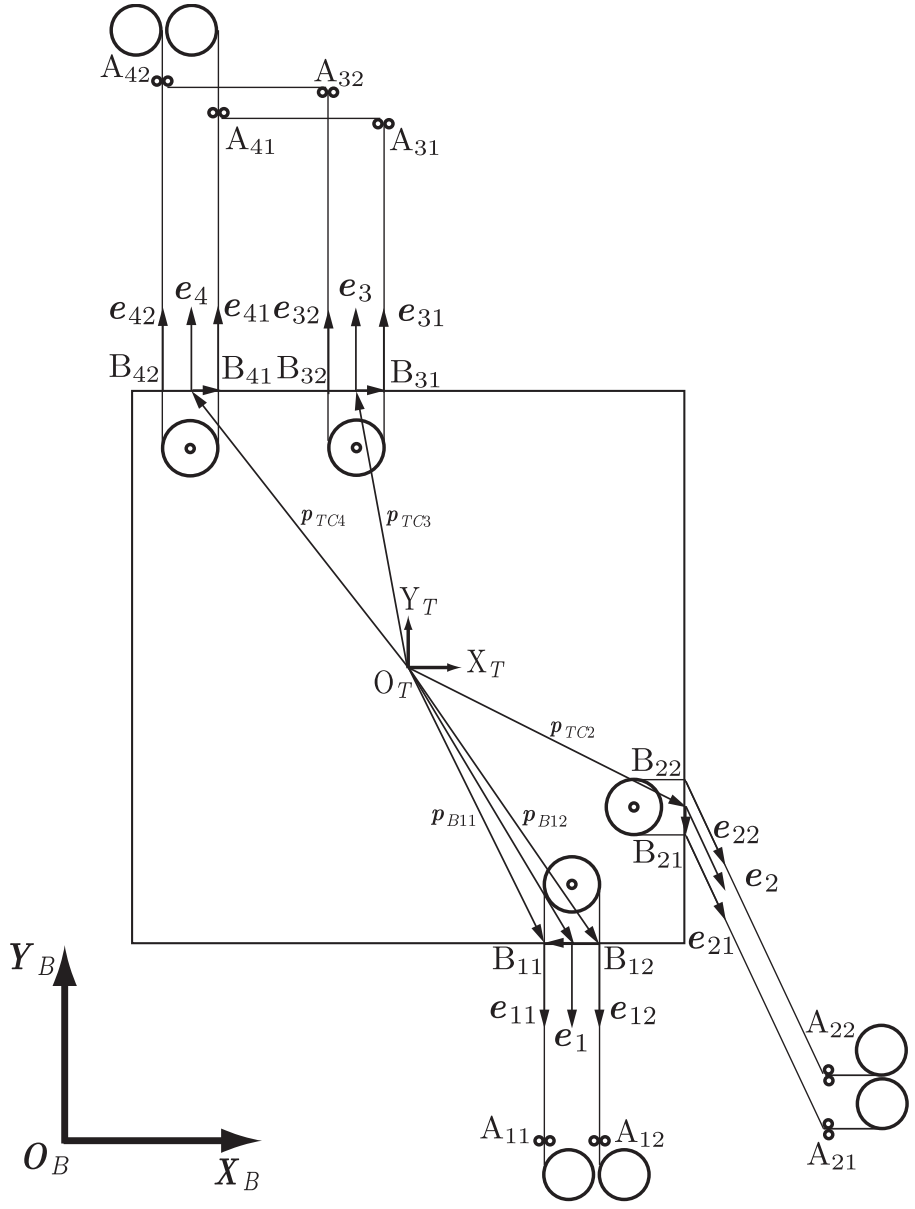

Figure. 5.6: Improper planar RDWM configuration with two DAMs and one VCM.

Positions of wire end points on the top plate

From Eq. (3.10):

$$
\begin{aligned}
{}^{B}\boldsymbol{p}_{B11} &= [64 \;\; 30]^{\mathrm{T}}, \; {}^{B}\boldsymbol{p}_{B12} = [68 \;\; 30]^{\mathrm{T}}, \\
{}^{B}\boldsymbol{p}_{B21} &= [70 \;\; 38]^{\mathrm{T}}, \; {}^{B}\boldsymbol{p}_{B22} = [70 \;\; 42]^{\mathrm{T}}, \\
{}^{B}\boldsymbol{p}_{B31} &= [48 \;\; 70]^{\mathrm{T}}, \; {}^{B}\boldsymbol{p}_{B32} = [44 \;\; 70]^{\mathrm{T}}, \\
{}^{B}\boldsymbol{p}_{B41} &= [36 \;\; 70]^{\mathrm{T}}, \; {}^{B}\boldsymbol{p}_{B42} = [32 \;\; 70]^{\mathrm{T}}.
\end{aligned}
$$

Positions of wire end points on the frame

The positions of the wire end points on the frame were ensured by appropriately arranging the DAMs and VCMs on the frame:

$$
\begin{aligned}
{}^{B}\boldsymbol{p}_{A11} &= [64 \;\; 0]^{\mathrm{T}}, \quad {}^{B}\boldsymbol{p}_{A12} = [68 \;\; 0]^{\mathrm{T}}, \\
{}^{B}\boldsymbol{p}_{A21} &= [118 \;\; 2]^{\mathrm{T}}, \quad {}^{B}\boldsymbol{p}_{A22} = [118 \;\; 6]^{\mathrm{T}}, \\
{}^{B}\boldsymbol{p}_{A31} &= [48 \;\; 95]^{\mathrm{T}}, \quad {}^{B}\boldsymbol{p}_{A32} = [44 \;\; 100]^{\mathrm{T}}, \\
{}^{B}\boldsymbol{p}_{A41} &= [36 \;\; 95]^{\mathrm{T}}, \quad {}^{B}\boldsymbol{p}_{A42} = [32 \;\; 100]^{\mathrm{T}}.
\end{aligned}
$$

Calculating the wire vectors ${}^{B}\boldsymbol{e}_{ij}$

The wire vectors ${}^{B}\boldsymbol{e}_{ij}$ calculated by Eq. (3.11) are shown below:

$$
\begin{aligned}
{}^{B}\boldsymbol{e}_{11} &= {}^{B}\boldsymbol{e}_{12} = [0 \;\; -1]^{\mathrm{T}}, \\
{}^{B}\boldsymbol{e}_{21} &= {}^{B}\boldsymbol{e}_{22} = [4/5 \;\; -3/5]^{\mathrm{T}}, \\
{}^{B}\boldsymbol{e}_{31} &= {}^{B}\boldsymbol{e}_{32} = [0 \;\; 1]^{\mathrm{T}}, \\
{}^{B}\boldsymbol{e}_{41} &= {}^{B}\boldsymbol{e}_{42} = [0 \;\; 1]^{\mathrm{T}}.
\end{aligned}
$$

Derivation of the matrix $\boldsymbol{W}_{G}^{'}$

From Eqs. (B.1) and (B.4) with n=3, N_D=2 and N_V=1, it is easy to see that the matrices $\boldsymbol{W}_2$ and $\boldsymbol{W}_2^{'}$ have size 7×8. Similarly to the previous examples, those matrices can be seen in Eqs. (C.33) and (C.36) of the **Appendix C** for reference, only the matrix $\boldsymbol{W}_{G2}^{'}$ will be used for the judgment and it is derived as follows:

From Eq. (3.12), the vectors ${}^{B}\boldsymbol{e}_i$ can be derived as:

$$
{}^{B}\boldsymbol{e}_1 = [0 \;\; -1]^{\mathrm{T}}, \; {}^{B}\boldsymbol{e}_2 = [4/5 \;\; -3/5]^{\mathrm{T}}, {}^{B}\boldsymbol{e}_3 = [0 \;\; 1]^{\mathrm{T}}, \; {}^{B}\boldsymbol{e}_4 = [0 \;\; 1]^{\mathrm{T}}
$$

From Eq. (3.13), the vectors ${}^{B}\boldsymbol{p}_{TCi}$ can be derived as:

$$
\begin{aligned}
{}^{B}\boldsymbol{p}_{TC1} &= [16 \;\; -20]^{\mathrm{T}}, \; {}^{B}\boldsymbol{p}_{TC2} = [20 \;\; -10]^{\mathrm{T}}, \\
{}^{B}\boldsymbol{p}_{TC3} &= [-4 \;\; 20]^{\mathrm{T}}, \; {}^{B}\boldsymbol{p}_{TC4} = [-16 \;\; 20]^{\mathrm{T}}.
\end{aligned}
$$

Then the matrix $\boldsymbol{W}_{G2}^{'}$ from Eq. (B.5) becomes:

$$
\boldsymbol{W}_{G2}^{'} = \frac{1}{5} \begin{bmatrix} 0 & 4 & 0 & 0 \\ -5 & -3 & 5 & 5 \\ -80 & -20 & -20 & -80 \end{bmatrix} \in \boldsymbol{R}^{3\times 4}. \tag{5.25}
$$

Similarly to the previous examples, the matrix $\boldsymbol{W}'_{G2}$ related to the global motion in this case also equals just a quarter of the normal wire matrix $\boldsymbol{W}_2$. The matrix $\boldsymbol{W}'_{G2}$ will then be applied in the step 1 of the judgment procedure as follows:

Necessary condition check (Step 1)

In step 1, the matrix $\boldsymbol{W}'_{G2}$ of contributions to the resultant force exerted on the top plate will be used for judgment. It is easily determined that although rank($\boldsymbol{W}'_{G2}$) = 3 (satisfying the necessary condition C1), this configuration fails C2. The resultant moments around the Z-axis (third row of matrix $\boldsymbol{W}'_{G2}$) are all negative, meaning that any positive wire tension vector will produce a clockwise moment. Therefore, the mechanism fails step 1, so the judgment procedure is terminated and this RDWM candidate is eliminated.

5.4. Proper Configuration of 3D RDWM with Fixed Orientations Around X-, Y-, and Z-axes while Maintaining Translational Motions in the X, Y and Z Directions

Similar to the previous example, we now develop a 3D RDWM wherein the desired active constraint space $\boldsymbol{S}_{AC}$ enables motions of the top plate in the X, Y and Z directions, and the passive constraint space $\boldsymbol{S}_{PC}$ prohibits orientation of the top plate around the three axes. We propose two 3D configurations and apply the judgment procedures in chapter 4 to determine whether the mechanisms can produce the desired active constrained motion space. As before, the unit of all length-related parameters is [cm].

5.4.1 First configuration: 3D RDWM with seven DAMs

A 3D RDWM with DAMs is shown in figure 5.7. Here, the unit of the values of parameters related to length are assumed to be [cm]. Because of space limitations, the DAMs are not shown; only the end points of the wires on those modules are shown, with the important representative vectors. The processes for deriving the matrix $\boldsymbol{W}'_{G3}$ and the judgment procedure are shown below:

Defining ${}^{T}\boldsymbol{p}_{TCi}$, $\boldsymbol{R}_i$, ${}^{T}\boldsymbol{p}_{TDi}$, and ${}^{T}\boldsymbol{p}_{Bij}$

$$
\begin{aligned}
{}^{T}\boldsymbol{p}_{TC1} &= [-10 \;\; -6 \;\; 10]^{\mathrm{T}}, & {}^{T}\boldsymbol{p}_{TC2} &= [10 \;\; -6 \;\; 10]^{\mathrm{T}}, \\
{}^{T}\boldsymbol{p}_{TC3} &= [6 \;\; 10 \;\; 10]^{\mathrm{T}}, & {}^{T}\boldsymbol{p}_{TC4} &= [-6 \;\; 10 \;\; 10]^{\mathrm{T}}, \\
{}^{T}\boldsymbol{p}_{TC5} &= [-10 \;\; 6 \;\; -10]^{\mathrm{T}}, & {}^{T}\boldsymbol{p}_{TC6} &= [0 \;\; -10 \;\; -10]^{\mathrm{T}}, \\
{}^{T}\boldsymbol{p}_{TC7} &= [10 \;\; 6 \;\; -10]^{\mathrm{T}}.
\end{aligned}
$$

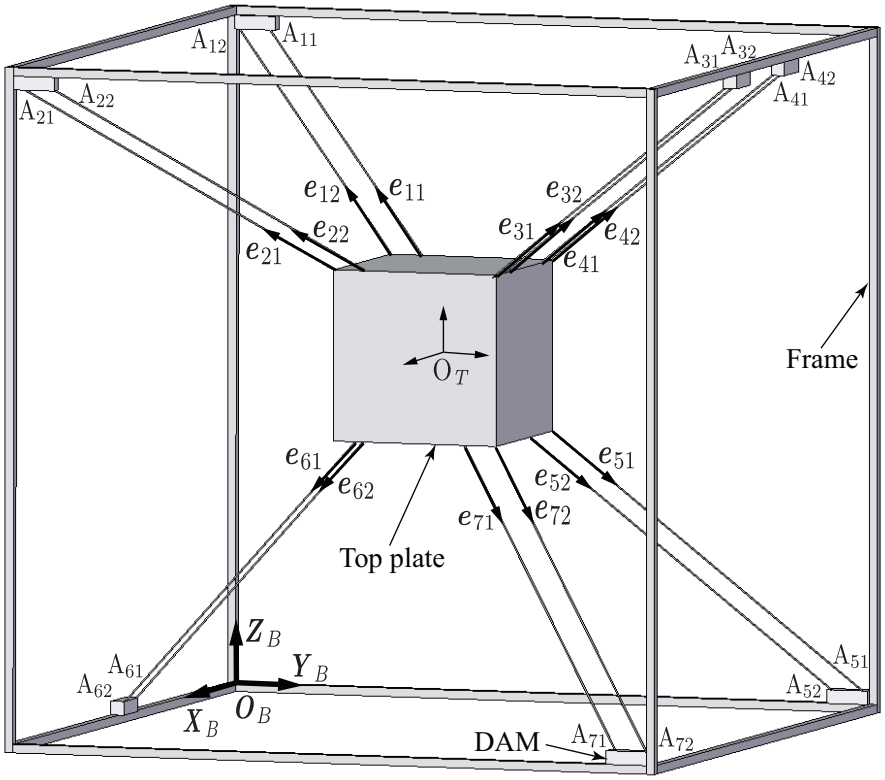

Figure. 5.7: A 3D RDWM using DAMs.

The pulley radii are: $R_1 = R_2 = R_3 = R_4 = R_5 = R_6 = R_7 = 2$.

$$
\begin{aligned}
&{}^{T}\boldsymbol{p}_{TD1} = [0 \;\; 2 \;\; 0]^{\mathrm{T}}, && {}^{T}\boldsymbol{p}_{TD2} = [0 \;\; -2 \;\; 0]^{\mathrm{T}},\\
&{}^{T}\boldsymbol{p}_{TD3} = [2 \;\; 0 \;\; 0]^{\mathrm{T}}, && {}^{T}\boldsymbol{p}_{TD4} = [2 \;\; 0 \;\; 0]^{\mathrm{T}},\\
&{}^{T}\boldsymbol{p}_{TD5} = [0 \;\; 2 \;\; 0]^{\mathrm{T}}, && {}^{T}\boldsymbol{p}_{TD6} = [-2 \;\; 0 \;\; 0]^{\mathrm{T}},\\
&{}^{T}\boldsymbol{p}_{TD7} = [0 \;\; -2 \;\; 0]^{\mathrm{T}}.
\end{aligned}
$$

The positions of the wire end points on the top plate w.r.t the top plate coordinate were calculated by Eq. (3.9):

$$
\begin{aligned}
&{}^{T}\boldsymbol{p}_{B11} = [-10 \;\; -4 \;\; 10]^{\mathrm{T}}, && {}^{T}\boldsymbol{p}_{B12} = [-10 \;\; -8 \;\; 10]^{\mathrm{T}},\\
&{}^{T}\boldsymbol{p}_{B21} = [10 \;\; -8 \;\; 10]^{\mathrm{T}}, && {}^{T}\boldsymbol{p}_{B22} = [10 \;\; -4 \;\; 10]^{\mathrm{T}},\\
&{}^{T}\boldsymbol{p}_{B31} = [8 \;\; 10 \;\; 10]^{\mathrm{T}}, && {}^{T}\boldsymbol{p}_{B32} = [4 \;\; 10 \;\; 10]^{\mathrm{T}},\\
&{}^{T}\boldsymbol{p}_{B41} = [-4 \;\; 10 \;\; 10]^{\mathrm{T}}, && {}^{T}\boldsymbol{p}_{B42} = [-8 \;\; 10 \;\; 10]^{\mathrm{T}},\\
&{}^{T}\boldsymbol{p}_{B51} = [-10 \;\; 8 \;\; -10]^{\mathrm{T}}, && {}^{T}\boldsymbol{p}_{B52} = [-10 \;\; 4 \;\; -10]^{\mathrm{T}},\\
&{}^{T}\boldsymbol{p}_{B61} = [-2 \;\; -10 \;\; -10]^{\mathrm{T}}, && {}^{T}\boldsymbol{p}_{B62} = [2 \;\; -10 \;\; -10]^{\mathrm{T}},\\
&{}^{T}\boldsymbol{p}_{B71} = [10 \;\; 4 \;\; -10]^{\mathrm{T}}, && {}^{T}\boldsymbol{p}_{B72} = [10 \;\; 8 \;\; -10]^{\mathrm{T}}.
\end{aligned}
$$

Sets of position ${}^{B}\boldsymbol{p}_{T}$ and orientations ${}^{B}\boldsymbol{R}_{T}$ of the top plate

$$
{}^{B}\boldsymbol{p}_{T} = [50 \;\; 50 \;\; 50]^{\mathrm{T}}, \; {}^{B}\boldsymbol{R}_{T} = \begin{bmatrix} 1 & 0 & 0 \\ 0 & 1 & 0 \\ 0 & 0 & 1 \end{bmatrix} \in \boldsymbol{R}^{3\times 3}.
$$

Positions of wire end points on the top plate

From Eq. (3.10):

$$
\begin{aligned}
&{}^{B}\boldsymbol{p}_{B11} = [40\ \ 46\ \ 60]^{\mathrm{T}},\ {}^{B}\boldsymbol{p}_{B12} = [40\ \ 42\ \ 60]^{\mathrm{T}},\\
&{}^{B}\boldsymbol{p}_{B21} = [60\ \ 42\ \ 60]^{\mathrm{T}},\ {}^{B}\boldsymbol{p}_{B22} = [60\ \ 46\ \ 60]^{\mathrm{T}},\\
&{}^{B}\boldsymbol{p}_{B31} = [58\ \ 60\ \ 60]^{\mathrm{T}},\ {}^{B}\boldsymbol{p}_{B32} = [54\ \ 60\ \ 60]^{\mathrm{T}},\\
&{}^{B}\boldsymbol{p}_{B41} = [46\ \ 60\ \ 60]^{\mathrm{T}},\ {}^{B}\boldsymbol{p}_{B42} = [42\ \ 60\ \ 60]^{\mathrm{T}},\\
&{}^{B}\boldsymbol{p}_{B51} = [40\ \ 58\ \ 40]^{\mathrm{T}},\ {}^{B}\boldsymbol{p}_{B52} = [40\ \ 54\ \ 40]^{\mathrm{T}},\\
&{}^{B}\boldsymbol{p}_{B61} = [48\ \ 40\ \ 40]^{\mathrm{T}},\ {}^{B}\boldsymbol{p}_{B62} = [52\ \ 40\ \ 40]^{\mathrm{T}},\\
&{}^{B}\boldsymbol{p}_{B71} = [60\ \ 54\ \ 40]^{\mathrm{T}},\ {}^{B}\boldsymbol{p}_{B72} = [60\ \ 58\ \ 40]^{\mathrm{T}}.
\end{aligned}
$$

Positions of wire end points on the frame

The positions of the wire end points on the frame were ensured by appropriately arranging the DAMs on the frame:

$$
\begin{aligned}
&{}^{B}\boldsymbol{p}_{A11} = [10\ \ 46\ \ 100]^{\mathrm{T}},\ {}^{B}\boldsymbol{p}_{A12} = [10\ \ 42\ \ 100]^{\mathrm{T}},\\
&{}^{B}\boldsymbol{p}_{A21} = [90\ \ 42\ \ 100]^{\mathrm{T}},\ {}^{B}\boldsymbol{p}_{A22} = [90\ \ 46\ \ 100]^{\mathrm{T}},\\
&{}^{B}\boldsymbol{p}_{A31} = [58\ \ 90\ \ 100]^{\mathrm{T}},\ {}^{B}\boldsymbol{p}_{A32} = [54\ \ 90\ \ 100]^{\mathrm{T}},\\
&{}^{B}\boldsymbol{p}_{A41} = [46\ \ 90\ \ 100]^{\mathrm{T}},\ {}^{B}\boldsymbol{p}_{A42} = [42\ \ 90\ \ 100]^{\mathrm{T}},\\
&{}^{B}\boldsymbol{p}_{A51} = [10\ \ 58\ \ 0]^{\mathrm{T}},\quad {}^{B}\boldsymbol{p}_{A52} = [10\ \ 54\ \ 0]^{\mathrm{T}},\\
&{}^{B}\boldsymbol{p}_{A61} = [48\ \ 10\ \ 0]^{\mathrm{T}},\quad {}^{B}\boldsymbol{p}_{A62} = [52\ \ 10\ \ 0]^{\mathrm{T}},\\
&{}^{B}\boldsymbol{p}_{A71} = [90\ \ 54\ \ 0]^{\mathrm{T}},\quad {}^{B}\boldsymbol{p}_{A72} = [90\ \ 58\ \ 0]^{\mathrm{T}}.
\end{aligned}
$$

Calculating the wire vectors ${}^{B}\boldsymbol{e}_{ij}$

The wire vectors ${}^{B}\boldsymbol{e}_{ij}$ were calculated by Eq. (3.11) and are listed below:

$$
\begin{aligned}
&{}^{B}\boldsymbol{e}_{11} = {}^{B}\boldsymbol{e}_{12} = [-3/5\ \ 0\ \ 4/5]^{\mathrm{T}},\\
&{}^{B}\boldsymbol{e}_{21} = {}^{B}\boldsymbol{e}_{22} = [3/5\ \ 0\ \ 4/5]^{\mathrm{T}},\\
&{}^{B}\boldsymbol{e}_{31} = {}^{B}\boldsymbol{e}_{32} = [0\ \ 3/5\ \ 4/5]^{\mathrm{T}},\\
&{}^{B}\boldsymbol{e}_{41} = {}^{B}\boldsymbol{e}_{42} = [0\ \ 3/5\ \ 4/5]^{\mathrm{T}},\\
&{}^{B}\boldsymbol{e}_{51} = {}^{B}\boldsymbol{e}_{52} = [-3/5\ \ 0\ \ -4/5]^{\mathrm{T}},\\
&{}^{B}\boldsymbol{e}_{61} = {}^{B}\boldsymbol{e}_{62} = [0\ \ -3/5\ \ -4/5]^{\mathrm{T}},\\
&{}^{B}\boldsymbol{e}_{71} = {}^{B}\boldsymbol{e}_{72} = [3/5\ \ 0\ \ -4/5]^{\mathrm{T}}.
\end{aligned}
$$

Checking if the two wires in the DAMs are in parallel

With this configuration, the two wires in the DAMs are in parallel.

Derivation of the matrix $\boldsymbol{W}'_{G}$

From Eqs. (3.6) and (3.16) with n=6, N_D=7, it is easy to see that the matrices $\boldsymbol{W}_3$ and $\boldsymbol{W}'_3$ have size 13×14. Similarly to the previous examples, those matrices can be seen in Eqs. (C.41) and (C.44) of the **Appendix C** for reference, only the matrix $\boldsymbol{W}'_{G3}$ will be used for the judgment and it is derived as follows:

From Eq. (3.12), the vectors ${}^{B}\boldsymbol{e}_i$ can be derived as:

$$
\begin{array}{ll}
{}^{B}\boldsymbol{e}_1 = [-3/5 \;\; 0 \;\; 4/5]^{\mathrm{T}}, & {}^{B}\boldsymbol{e}_2 = [3/5 \;\; 0 \;\; 4/5]^{\mathrm{T}}, \\
{}^{B}\boldsymbol{e}_3 = [0 \;\; 3/5 \;\; 4/5]^{\mathrm{T}}, & {}^{B}\boldsymbol{e}_4 = [0 \;\; 3/5 \;\; 4/5]^{\mathrm{T}}, \\
{}^{B}\boldsymbol{e}_5 = [-3/5 \;\; 0 \;\; -4/5]^{\mathrm{T}}, & {}^{B}\boldsymbol{e}_6 = [0 \;\; -3/5 \;\; -4/5]^{\mathrm{T}}, \\
{}^{B}\boldsymbol{e}_7 = [3/5 \;\; 0 \;\; -4/5]^{\mathrm{T}}. &
\end{array}
$$

From Eq. (3.13), the vectors ${}^{B}\boldsymbol{p}_{TCi}$ can be derived as:

$$
\begin{array}{ll}
{}^{B}\boldsymbol{p}_{TC1} = [40 \;\; 44 \;\; 60]^{\mathrm{T}}, & {}^{B}\boldsymbol{p}_{TC2} = [60 \;\; 44 \;\; 60]^{\mathrm{T}}, \\
{}^{B}\boldsymbol{p}_{TC3} = [56 \;\; 60 \;\; 60]^{\mathrm{T}}, & {}^{B}\boldsymbol{p}_{TC4} = [44 \;\; 60 \;\; 60]^{\mathrm{T}}. \\
{}^{B}\boldsymbol{p}_{TC5} = [40 \;\; 56 \;\; 40]^{\mathrm{T}}, & {}^{B}\boldsymbol{p}_{TC6} = [50 \;\; 25 \;\; 40]^{\mathrm{T}}, \\
{}^{B}\boldsymbol{p}_{TC7} = [60 \;\; 56 \;\; 40]^{\mathrm{T}}. &
\end{array}
$$

Then the matrix $\boldsymbol{W}'_{G3}$ from Eq. (3.17) becomes:

$$
\boldsymbol{W}'_{G3} = \frac{1}{5}
\begin{bmatrix}
-3 & 3 & 0 & 0 & -3 & 0 & 3 \\
0 & 0 & 3 & 3 & 0 & -3 & 0 \\
4 & 4 & 4 & 4 & -4 & -4 & -4 \\
-24 & -24 & 10 & 10 & -24 & 10 & -24 \\
10 & -10 & -24 & 24 & -10 & 0 & 10 \\
-18 & 18 & 18 & -18 & 18 & 0 & -18
\end{bmatrix}_{6\times 7}, \tag{5.26}
$$

The matrix $\boldsymbol{W}'_{G3}$ has size 6×7, where the number of rows is equal to the six DOFs in the 3D global motion space and the number of columns is equal to the seven DOFs in the local motion space. It is about a quarter of the size of the wire matrix $\boldsymbol{W}_3$. The matrix $\boldsymbol{W}'_{G3}$ will then be applied in the step 1 of the judgment procedure as follows:

Necessary condition check (Step 1)

From the expression in the judgment of a candidate section, only the matrix that contributes to global motion $\boldsymbol{W}'_{G3}$ is needed to check the vector closure condition. Using the matrix of global motion from Eq. (5.26), we have:

i) rank($\boldsymbol{W}'_{G3}$) = 6.

ii) With $\boldsymbol{T}_{S3} = \begin{bmatrix} 5 & 5 & 12 & 12 & 5 & 24 & 5 \end{bmatrix}^{\mathrm{T}} > \boldsymbol{0}$, easy to get $\boldsymbol{W}'_{G3}\boldsymbol{T}_{S3} = \boldsymbol{0}$.

The above analysis shows that rank($\boldsymbol{W}'_{G3}$) equals to the number of dimension spaces of the wire mechanism. As there is a vector $\boldsymbol{T}_{S3}$ that satisfies $\boldsymbol{W}'_{G3}\boldsymbol{T}_{S3} = \boldsymbol{0}$, the matrix $\boldsymbol{W}'_{G3}$ satisfies the vector closure condition and the mechanism can produce the resultant force in any direction within its motion space. The results mean that the 3D RDWM with seven sets of DAMs in this example has the same structure as a conventional wire mechanism with seven sets of single actuator modules, wherein each wire in the conventional wire mechanism is equivalent to a set of two wires of each DAM in the 3D RDWM, in judgment with the vector closure condition. Therefore, this 3D RDWM candidate satisfies step 1 and the analysis proceeds to step 2 as follows.

KA (Step 2)

Step 2 analyzes the following matrix $\boldsymbol{W}_G$ of contributions to the resultant force on the top plate. This matrix, obtained from Eq. (4.23) is given by:

$$\boldsymbol{W}_{G3} = \frac{1}{5}\begin{bmatrix} -3 & -3 & 3 & 3 & 0 & 0 & 0 & 0 & -3 & -3 & 0 & 0 & 3 & 3 \\ 0 & 0 & 0 & 0 & 3 & 3 & 3 & 3 & 0 & 0 & -3 & -3 & 0 & 0 \\ 4 & 4 & 4 & 4 & 4 & 4 & 4 & 4 & -4 & -4 & -4 & -4 & -4 & -4 \\ -16 & -32 & -32 & -16 & 10 & 10 & 10 & 10 & -32 & -16 & 10 & 10 & -16 & -32 \\ 10 & 10 & -10 & -10 & -32 & -16 & 16 & 32 & -10 & -10 & -8 & 8 & 10 & 10 \\ -12 & -24 & 24 & 12 & 24 & 12 & -12 & -24 & 24 & 12 & 6 & -6 & -12 & -24 \end{bmatrix} \in \boldsymbol{R}^{6\times 14}. \tag{5.27}$$

From Eq. (4.22), the matrix of total VCM contributions to the velocity of the top plate is given by:

$$\boldsymbol{A}_L = \text{bdiag.}(\, \boldsymbol{A}_{Ld1},\, \boldsymbol{A}_{Ld2},\, \boldsymbol{A}_{Ld3},\, \boldsymbol{A}_{Ld4},\, \boldsymbol{A}_{Ld5},\, \boldsymbol{A}_{Ld6},\, \boldsymbol{A}_{Ld7}\,) \in \boldsymbol{R}^{14\times 7}. \tag{5.28}$$

The contents of $\boldsymbol{A}_{Ldi}$ and $\boldsymbol{b}_{Ldi}$ are shown in Eq. (4.11). The matrices of the top plate's velocity $\boldsymbol{A}_V$ and $\boldsymbol{b}_V$ were then obtained by Eqs. (4.20) and (4.21). The result shown below:

$$\boldsymbol{A}_V = \frac{1}{5}\begin{bmatrix} 3 & 0 & -4 & 16 & -10 & 12 \\ -3 & 0 & 4 & -16 & 10 & -12 \\ 3 & 0 & -4 & 32 & -10 & 24 \\ -3 & 0 & 4 & -32 & 10 & -24 \\ -3 & 0 & -4 & 32 & 10 & -24 \\ 3 & 0 & 4 & -32 & -2 & 24 \\ -3 & 0 & -4 & 16 & 10 & -12 \\ 3 & 0 & 4 & -16 & -10 & 60 \\ 0 & -3 & -4 & -10 & 32 & -24 \\ 0 & 3 & 4 & 10 & -32 & 24 \\ 0 & -3 & -4 & -10 & 16 & -12 \\ 0 & 3 & 4 & 10 & -16 & 12 \\ 0 & -3 & -4 & -10 & -16 & 12 \\ 0 & 3 & 4 & 10 & 16 & -12 \\ 0 & -3 & -4 & -10 & -32 & 24 \\ 0 & 3 & 4 & 10 & 32 & -24 \\ 3 & 0 & 4 & 32 & 10 & -24 \\ -3 & 0 & -4 & -32 & -10 & 24 \\ 3 & 0 & 4 & 16 & 10 & -12 \\ -3 & 0 & -4 & -16 & -10 & 12 \\ 0 & 3 & 4 & -10 & 8 & -6 \\ 0 & -3 & -4 & 10 & -8 & 6 \\ 0 & 3 & 4 & -10 & -8 & 6 \\ 0 & -3 & -4 & 10 & 8 & -6 \\ -3 & 0 & 4 & 16 & -10 & 12 \\ 3 & 0 & -4 & -16 & 10 & -12 \\ -3 & 0 & 4 & 32 & -10 & 24 \\ 3 & 0 & -4 & -32 & 10 & -24 \end{bmatrix} \in \boldsymbol{R}^{28\times 6},\ \boldsymbol{b}_V = \begin{bmatrix} 1 \\ 1 \\ 1 \\ 1 \\ 1 \\ 1 \\ 1 \\ 1 \\ 1 \\ 1 \\ 1 \\ 1 \\ 1 \\ 1 \\ 1 \\ 1 \\ 1 \\ 1 \\ 1 \\ 1 \\ 1 \\ 1 \\ 1 \\ 1 \\ 1 \\ 1 \\ 1 \\ 1 \\ 1 \end{bmatrix} \in \boldsymbol{R}^{28}. \tag{5.29}$$

From the $\boldsymbol{A}_V, \boldsymbol{b}_V$ in the above Eq. (5.29), the convex set in Eqs. (4.19) and (4.24) can be solved. The results includes the vertex sets in matrix $\boldsymbol{A}$ (sized 6×172). Then, the active constraint space $\boldsymbol{S}_{AC}$, the passive constraint space $\boldsymbol{S}_{PC}$ of the 3D RDWM with seven DAM sets are obtained by Eq. (4.26). The result is shown below:

$$\boldsymbol{S}_{AC} = \mathcal{R}\left(\boldsymbol{E}_6\right), \boldsymbol{S}_{PC} = \emptyset. \tag{5.30}$$

Equation (5.30) means that in this configuration, the active constraint space $\boldsymbol{S}_{AC}$ produced by the top plate allows motions of the top plate in the X, Y, and Z directions and also rotations around all three axes.

SFA (Step 3)

The above KA reveals that the active constraint space $\boldsymbol{S}_{AC}$ is the whole motion space of the mechanism. Therefore, the matrix $\boldsymbol{W}_{CVC}$ which relates the wire tension vector to the resultant force vector in the constraint coordinates is exactly the matrix $\boldsymbol{W}_{G3}$. Then, similar to step 1, we can easily determine that this RDWM candidate satisfies step 3 and generates a resultant force in any direction within the active constraint space $\boldsymbol{S}_{AC}$.

5.4.2 Second configuration: 3D RDWM with four sets of DAMs with VCMs

Finally, we configure a 3D RDWM with four sets of DAMs each with a VCM (see figure 5.8). The processes for deriving the matrix $\boldsymbol{W}'_{G3}$ and the judgment procedure are shown below:

Defining ${}^{T}\boldsymbol{p}_{TCi}$, $\boldsymbol{R}_i$, ${}^{T}\boldsymbol{p}_{TDi}$, and ${}^{T}\boldsymbol{p}_{Bij}$

$$\begin{array}{ll}
{}^{T}\boldsymbol{p}_{TC1} = [-6 \;\; -9 \;\; 6]^{\mathrm{T}}, & {}^{T}\boldsymbol{p}_{TC2} = [6 \;\; -9 \;\; -6]^{\mathrm{T}}, \\
{}^{T}\boldsymbol{p}_{TC3} = [9 \;\; -6 \;\; 6]^{\mathrm{T}}, & {}^{T}\boldsymbol{p}_{TC4} = [9 \;\; 6 \;\; -6]^{\mathrm{T}}, \\
{}^{T}\boldsymbol{p}_{TC5} = [6 \;\; 9 \;\; 6]^{\mathrm{T}}, & {}^{T}\boldsymbol{p}_{TC6} = [-6 \;\; 9 \;\; -6]^{\mathrm{T}}, \\
{}^{T}\boldsymbol{p}_{TC7} = [-9 \;\; 6 \;\; 6]^{\mathrm{T}}, & {}^{T}\boldsymbol{p}_{TC8} = [-9 \;\; -6 \;\; -6]^{\mathrm{T}}.
\end{array}$$

The pulley radii are given by $R_1 = R_2 = R_3 = R_4 = R_5 = R_6 = R_7 = R_8 = 2\sqrt{2}$.

$$\begin{array}{ll}
{}^{T}\boldsymbol{p}_{TD1} = [-2 \;\; 0 \;\; 2]^{\mathrm{T}}, & {}^{T}\boldsymbol{p}_{TD2} = [-2 \;\; 0 \;\; 2]^{\mathrm{T}}, \\
{}^{T}\boldsymbol{p}_{TD3} = [0 \;\; -2 \;\; 2]^{\mathrm{T}}, & {}^{T}\boldsymbol{p}_{TD4} = [0 \;\; -2 \;\; 2]^{\mathrm{T}}, \\
{}^{T}\boldsymbol{p}_{TD5} = [2 \;\; 0 \;\; 2]^{\mathrm{T}}, & {}^{T}\boldsymbol{p}_{TD6} = [2 \;\; 0 \;\; 2]^{\mathrm{T}}, \\
{}^{T}\boldsymbol{p}_{TD7} = [0 \;\; 2 \;\; 2]^{\mathrm{T}}, & {}^{T}\boldsymbol{p}_{TD8} = [0 \;\; 2 \;\; 2]^{\mathrm{T}}.
\end{array}$$

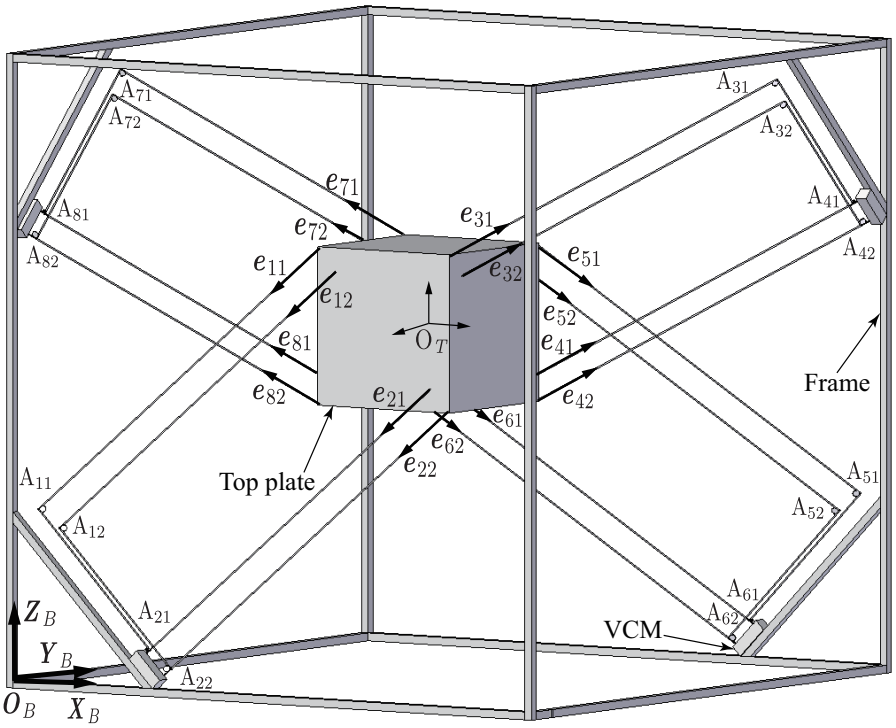

Figure. 5.8: 3D RDWM with four VCMs.

The positions of the wire end points on the top plate w.r.t the top plate coordinate were calculated by Eq. (3.9):

$$
\begin{aligned}
&{}^{T}\boldsymbol{p}_{B11} = [-8 \;\; -9 \;\; 8]^{\mathrm{T}}, && {}^{T}\boldsymbol{p}_{B12} = [-4 \;\; -9 \;\; 4]^{\mathrm{T}},\\
&{}^{T}\boldsymbol{p}_{B21} = [4 \;\; -9 \;\; -4]^{\mathrm{T}}, && {}^{T}\boldsymbol{p}_{B22} = [8 \;\; -9 \;\; -8]^{\mathrm{T}},\\
&{}^{T}\boldsymbol{p}_{B31} = [9 \;\; -8 \;\; 8]^{\mathrm{T}}, && {}^{T}\boldsymbol{p}_{B32} = [9 \;\; -4 \;\; 4]^{\mathrm{T}},\\
&{}^{T}\boldsymbol{p}_{B41} = [9 \;\; 4 \;\; -4]^{\mathrm{T}}, && {}^{T}\boldsymbol{p}_{B42} = [9 \;\; 8 \;\; -8]^{\mathrm{T}},\\
&{}^{T}\boldsymbol{p}_{B51} = [8 \;\; 9 \;\; 8]^{\mathrm{T}}, && {}^{T}\boldsymbol{p}_{B52} = [4 \;\; 9 \;\; 4]^{\mathrm{T}},\\
&{}^{T}\boldsymbol{p}_{B61} = [-4 \;\; 9 \;\; -4]^{\mathrm{T}}, && {}^{T}\boldsymbol{p}_{B62} = [-8 \;\; 9 \;\; -8]^{\mathrm{T}},\\
&{}^{T}\boldsymbol{p}_{B71} = [-9 \;\; 8 \;\; 8]^{\mathrm{T}}, && {}^{T}\boldsymbol{p}_{B72} = [-9 \;\; 4 \;\; 4]^{\mathrm{T}},\\
&{}^{T}\boldsymbol{p}_{B81} = [-9 \;\; -4 \;\; -4]^{\mathrm{T}}, && {}^{T}\boldsymbol{p}_{B82} = [-9 \;\; -8 \;\; -8]^{\mathrm{T}}.
\end{aligned}
$$

Sets of positions ${}^{B}\boldsymbol{p}_{T}$ and orientations ${}^{B}\boldsymbol{R}_{T}$ of the top plate

$$
{}^{B}\boldsymbol{p}_{T} = [50 \;\; 50 \;\; 50]^{\mathrm{T}}, \; {}^{B}\boldsymbol{R}_{T} = \begin{bmatrix} 1 & 0 & 0 \\ 0 & 1 & 0 \\ 0 & 0 & 1 \end{bmatrix} \in \boldsymbol{R}^{3\times 3}.
$$

Positions of wire end points on the top plate

From Eq. (3.10):

$$
\begin{array}{ll}
{}^{B}\boldsymbol{p}_{B11} = [42\ \ 41\ \ 58]^{\mathrm{T}}, & {}^{B}\boldsymbol{p}_{B12} = [46\ \ 41\ \ 54]^{\mathrm{T}}, \\
{}^{B}\boldsymbol{p}_{B21} = [54\ \ 41\ \ 46]^{\mathrm{T}}, & {}^{B}\boldsymbol{p}_{B22} = [58\ \ 41\ \ 42]^{\mathrm{T}}, \\
{}^{B}\boldsymbol{p}_{B31} = [59\ \ 42\ \ 58]^{\mathrm{T}}, & {}^{B}\boldsymbol{p}_{B32} = [59\ \ 46\ \ 54]^{\mathrm{T}}, \\
{}^{B}\boldsymbol{p}_{B41} = [59\ \ 54\ \ 46]^{\mathrm{T}}, & {}^{B}\boldsymbol{p}_{B42} = [59\ \ 58\ \ 42]^{\mathrm{T}}, \\
{}^{B}\boldsymbol{p}_{B51} = [58\ \ 59\ \ 58]^{\mathrm{T}}, & {}^{B}\boldsymbol{p}_{B52} = [54\ \ 59\ \ 54]^{\mathrm{T}}, \\
{}^{B}\boldsymbol{p}_{B61} = [46\ \ 59\ \ 46]^{\mathrm{T}}, & {}^{B}\boldsymbol{p}_{B62} = [42\ \ 59\ \ 42]^{\mathrm{T}}, \\
{}^{B}\boldsymbol{p}_{B71} = [41\ \ 58\ \ 58]^{\mathrm{T}}, & {}^{B}\boldsymbol{p}_{B72} = [41\ \ 54\ \ 54]^{\mathrm{T}}, \\
{}^{B}\boldsymbol{p}_{B81} = [41\ \ 46\ \ 46]^{\mathrm{T}}, & {}^{B}\boldsymbol{p}_{B82} = [41\ \ 42\ \ 42]^{\mathrm{T}}.
\end{array}
$$

Positions of wire end points on the frame

The positions of the wire end points on the frame were ensured by appropriately arranging the VCMs on the frame:

$$
\begin{array}{ll}
{}^{B}\boldsymbol{p}_{A11} = [21.5\ \ 0\ \ 17]^{\mathrm{T}}, & {}^{B}\boldsymbol{p}_{A12} = [25.5\ \ 0\ \ 13]^{\mathrm{T}}, \\
{}^{B}\boldsymbol{p}_{A21} = [33.5\ \ 0\ \ 5]^{\mathrm{T}}, & {}^{B}\boldsymbol{p}_{A22} = [37.5\ \ 0\ \ 1]^{\mathrm{T}}, \\
{}^{B}\boldsymbol{p}_{A31} = [100\ \ 83\ \ 78.5]^{\mathrm{T}}, & {}^{B}\boldsymbol{p}_{A32} = [100\ \ 87\ \ 74.5]^{\mathrm{T}}, \\
{}^{B}\boldsymbol{p}_{A41} = [100\ \ 95\ \ 66.5]^{\mathrm{T}}, & {}^{B}\boldsymbol{p}_{A42} = [100\ \ 99\ \ 62.5]^{\mathrm{T}}, \\
{}^{B}\boldsymbol{p}_{A51} = [78.5\ \ 100\ \ 17]^{\mathrm{T}}, & {}^{B}\boldsymbol{p}_{A52} = [74.5\ \ 100\ \ 13]^{\mathrm{T}}, \\
{}^{B}\boldsymbol{p}_{A61} = [66.5\ \ 100\ \ 5]^{\mathrm{T}}, & {}^{B}\boldsymbol{p}_{A62} = [62.5\ \ 100\ \ 1]^{\mathrm{T}}, \\
{}^{B}\boldsymbol{p}_{A71} = [0\ \ 17\ \ 78.5]^{\mathrm{T}}, & {}^{B}\boldsymbol{p}_{A72} = [0\ \ 13\ \ 74.5]^{\mathrm{T}}, \\
{}^{B}\boldsymbol{p}_{A81} = [0\ \ 5\ \ 66.5]^{\mathrm{T}}, & {}^{B}\boldsymbol{p}_{A82} = [0\ \ 1\ \ 62.5]^{\mathrm{T}}.
\end{array}
$$

Calculating the wire vectors ${}^{B}\boldsymbol{e}_{ij}$

The wire vectors ${}^{B}\boldsymbol{e}_{ij}$ calculated by Eq. (3.11) are shown below:

$$
\begin{aligned}
{}^{B}\boldsymbol{e}_{11} = {}^{B}\boldsymbol{e}_{12} = {}^{B}\boldsymbol{e}_{21} = {}^{B}\boldsymbol{e}_{22} &= [-1/3\ \ -2/3\ \ -2/3]^{\mathrm{T}}, \\
{}^{B}\boldsymbol{e}_{31} = {}^{B}\boldsymbol{e}_{32} = {}^{B}\boldsymbol{e}_{41} = {}^{B}\boldsymbol{e}_{42} &= [2/3\ \ 2/3\ \ 1/3]^{\mathrm{T}}, \\
{}^{B}\boldsymbol{e}_{51} = {}^{B}\boldsymbol{e}_{52} = {}^{B}\boldsymbol{e}_{61} = {}^{B}\boldsymbol{e}_{62} &= [1/3\ \ 2/3\ \ -2/3]^{\mathrm{T}}, \\
{}^{B}\boldsymbol{e}_{71} = {}^{B}\boldsymbol{e}_{72} = {}^{B}\boldsymbol{e}_{81} = {}^{B}\boldsymbol{e}_{82} &= [-2/3\ \ -2/3\ \ 1/3]^{\mathrm{T}}.
\end{aligned}
$$

Derivation of the matrix $\boldsymbol{W}_{G}^{'}$

From Eqs. (B.1) and (B.4) with n=6, N_V=4, it is easy to see that the matrices $\boldsymbol{W}_3$ and $\boldsymbol{W}_3^{'}$ have size 14×16. Similarly to the previous examples, those matrices can be seen in Eqs. (C.49) and (C.52) of the **Appendix C** for reference, only the matrix $\boldsymbol{W}_{G3}^{'}$ will be used for the judgment and it is derived as follows:

From Eq. (3.12), the vectors ${}^{B}\boldsymbol{e}_{i}$ can be derived as:

$$
\begin{aligned}
{}^{B}\boldsymbol{e}_{11} = {}^{B}\boldsymbol{e}_{12} = {}^{B}\boldsymbol{e}_{21} = {}^{B}\boldsymbol{e}_{22} &= [-1/3\ \ -2/3\ \ -2/3]^{\mathrm{T}}, \\
{}^{B}\boldsymbol{e}_{31} = {}^{B}\boldsymbol{e}_{32} = {}^{B}\boldsymbol{e}_{41} = {}^{B}\boldsymbol{e}_{42} &= [2/3\ \ 2/3\ \ 1/3]^{\mathrm{T}}, \\
{}^{B}\boldsymbol{e}_{51} = {}^{B}\boldsymbol{e}_{52} = {}^{B}\boldsymbol{e}_{61} = {}^{B}\boldsymbol{e}_{62} &= [1/3\ \ 2/3\ \ -2/3]^{\mathrm{T}}, \\
{}^{B}\boldsymbol{e}_{71} = {}^{B}\boldsymbol{e}_{72} = {}^{B}\boldsymbol{e}_{81} = {}^{B}\boldsymbol{e}_{82} &= [-2/3\ \ -2/3\ \ 1/3]^{\mathrm{T}}.
\end{aligned}
$$

From Eq. (3.13), the vectors ${}^{B}\boldsymbol{p}_{TCi}$ can be derived as:

$$
\begin{array}{ll}
{}^{T}\boldsymbol{p}_{TC1} = [-6 \;\; -9 \;\; 6]^{\mathrm{T}}, & {}^{T}\boldsymbol{p}_{TC2} = [6 \;\; -9 \;\; -6]^{\mathrm{T}}, \\
{}^{T}\boldsymbol{p}_{TC3} = [9 \;\; -6 \;\; 6]^{\mathrm{T}}, & {}^{T}\boldsymbol{p}_{TC4} = [9 \;\; 6 \;\; -6]^{\mathrm{T}}, \\
{}^{T}\boldsymbol{p}_{TC5} = [6 \;\; 9 \;\; 6]^{\mathrm{T}}, & {}^{T}\boldsymbol{p}_{TC6} = [-6 \;\; 9 \;\; -6]^{\mathrm{T}}, \\
{}^{T}\boldsymbol{p}_{TC7} = [-9 \;\; 6 \;\; 6]^{\mathrm{T}}, & {}^{T}\boldsymbol{p}_{TC8} = [-9 \;\; -6 \;\; -6]^{\mathrm{T}}.
\end{array}
$$

Then the matrix $\boldsymbol{W}'_{G3}$ from Eq. (B.5) becomes:

$$
\boldsymbol{W}'_{G3} = \frac{1}{3}\begin{bmatrix}
-1 & -1 & 2 & 2 & 1 & 1 & -2 & -2 \\
-2 & -2 & 2 & 2 & 2 & 2 & -2 & -2 \\
-2 & -2 & 1 & 1 & -2 & -2 & 1 & 1 \\
30 & 6 & -18 & 18 & -30 & -6 & 18 & -18 \\
-18 & -18 & 3 & -21 & 18 & -18 & -3 & 21 \\
3 & -21 & 30 & 6 & 3 & -21 & 30 & 6
\end{bmatrix} \in \boldsymbol{R}^{6\times 8}. \tag{5.31}
$$

The matrix $\boldsymbol{W}'_{G3}$ has size 6×8, where the number of rows is equal to the six DOFs in the 3D global motion space and the number of columns is equal to the seven DOFs in the local motion space. It is about a quarter of the size of the wire matrix $\boldsymbol{W}_3$. The matrix $\boldsymbol{W}'_{G3}$ will then be applied in the step 1 of the judgment procedure as follows:

Necessary condition check (Step 1)

From the expression in the judgment of a candidate section, only the matrix that contributes to global motion $\boldsymbol{W}'_{G3}$ is needed to check the vector closure condition. Using the matrix of global motion from Eq. (5.26), we have:

i) $\mathrm{rank}(\boldsymbol{W}'_{G3}) = 6$.

ii) The wire tension vector $\boldsymbol{T}_{S0} = [\,5\ 35\ 10\ 70\ 5\ 35\ 10\ 70\,]^{\mathrm{T}} \in \boldsymbol{R}^8 > \boldsymbol{0}$ satisfies $\boldsymbol{W}'_{G3}\boldsymbol{T}_{S0} = \boldsymbol{0}$.

Therefore, this 3D RDWM candidate satisfies step 1 and the analysis proceeds to step 2.

KA (Step 2)

Step 2 analyzes the following matrix $\boldsymbol{W}_{G3}$ of contributions to the resultant force on the top plate. This matrix, obtained from Eq. (4.23) is given by:

$$
\boldsymbol{W}_{G3} = \frac{1}{3}\begin{bmatrix}
-1 & -1 & -1 & -1 & 2 & 2 & 2 & 2 & 1 & 1 & 1 & 1 & -2 & -2 \\
-2 & -2 & -2 & -2 & 2 & 2 & 2 & 2 & 2 & 2 & 2 & 2 & -2 & -2 \\
-2 & -2 & -2 & -2 & 1 & 1 & 1 & 1 & -2 & -2 & -2 & -2 & 1 & 1 \\
34 & 26 & 10 & 2 & -24 & -12 & 12 & 24 & -34 & -26 & -10 & -2 & 24 & 12 \\
-24 & -12 & 12 & 24 & 7 & -1 & -17 & -25 & 24 & 12 & -12 & -24 & -7 & 1 \\
7 & -1 & -17 & -25 & 34 & 26 & 10 & 2 & 7 & -1 & -17 & -25 & 34 & 26
\end{bmatrix}
\begin{bmatrix}
-2 & -2 \\
-2 & -2 \\
1 & 1 \\
-12 & -24 \\
17 & 25 \\
10 & 2
\end{bmatrix} \in \boldsymbol{R}^{6\times 16}. \tag{5.32}
$$

From Eq. (4.22), the matrix of total VCM contributions to the top plate's velocity is given by:

$$\boldsymbol{A}_L = \text{bdiag.}(\, \boldsymbol{A}_{Lv1},\ \boldsymbol{A}_{Lv2},\ \boldsymbol{A}_{Lv3},\ \boldsymbol{A}_{Lv4}\,) \in \boldsymbol{R}^{16\times 8}. \tag{5.33}$$

The contents of $\boldsymbol{A}_{Lvm}$ and $\boldsymbol{b}_{Lvm}$ are shown in Eq. (4.16). The velocity matrices of the top plate $\boldsymbol{A}_V$ and $\boldsymbol{b}_V$, obtained by Eqs. (4.20) and (4.21) are given by:

$$\boldsymbol{A}_V = \frac{1}{3}\begin{bmatrix}
1 & 2 & 2 & -34 & 24 & -7 \\
-1 & -2 & -2 & 34 & -24 & 7 \\
0 & 0 & 0 & 24 & -36 & 24 \\
0 & 0 & 0 & -24 & 36 & -24 \\
1 & 2 & 2 & -26 & 12 & 1 \\
-1 & -2 & -2 & 26 & -12 & -1 \\
0 & 0 & 0 & 24 & -36 & 24 \\
0 & 0 & 0 & -24 & 36 & -24 \\
-2 & -2 & -1 & 24 & -7 & -34 \\
2 & 2 & 1 & -24 & 7 & 34 \\
0 & 0 & 0 & -36 & 24 & 24 \\
0 & 0 & 0 & 36 & -24 & -24 \\
-2 & -2 & -1 & 12 & 1 & -26 \\
2 & 2 & 1 & -12 & -1 & 26 \\
0 & 0 & 0 & -36 & 24 & 24 \\
0 & 0 & 0 & 36 & -24 & -24 \\
-1 & -2 & 2 & 34 & -24 & -7 \\
1 & 2 & -2 & -34 & 24 & 7 \\
0 & 0 & 0 & -24 & 36 & 24 \\
0 & 0 & 0 & 24 & -36 & -24 \\
-1 & -2 & 2 & 26 & -12 & 1 \\
1 & 2 & -2 & -26 & 12 & -1 \\
0 & 0 & 0 & -24 & 36 & 24 \\
0 & 0 & 0 & 24 & -36 & -24 \\
2 & 2 & -1 & -24 & 6 & -34 \\
-2 & -2 & 1 & 24 & -6 & 34 \\
0 & 0 & 0 & 36 & -24 & 24 \\
0 & 0 & 0 & -36 & 24 & -24 \\
2 & 2 & -1 & -12 & -1 & -26 \\
-2 & -2 & 1 & 12 & 1 & 26 \\
0 & 0 & 0 & 36 & -24 & 24 \\
0 & 0 & 0 & -36 & 24 & -24
\end{bmatrix} \in \boldsymbol{R}^{32\times 6}, \boldsymbol{b}_V = \begin{bmatrix}
1 \\ 1 \\ 1 \\ 1 \\ 1 \\ 1 \\ 1 \\ 1 \\ 1 \\ 1 \\ 1 \\ 1 \\ 1 \\ 1 \\ 1 \\ 1 \\ 1 \\ 1 \\ 1 \\ 1 \\ 1 \\ 1 \\ 1 \\ 1 \\ 1 \\ 1 \\ 1 \\ 1 \\ 1 \\ 1 \\ 1 \\ 1
\end{bmatrix} \in \boldsymbol{R}^{32}. \tag{5.34}$$

Solving the convex set in Eqs. (4.19) and (4.24) with the above $\boldsymbol{A}_V$ and $\boldsymbol{b}_V$, the vertex sets in matrix $\boldsymbol{A}$ of the 3D RDWM with four sets of VCM are calculated as:

$$\boldsymbol{A} = \begin{bmatrix}
0 & 1.5 & 6 & -6 & -0 & -1.5 & 1.5 & -1.5 \\
-1.5 & -0.75 & -4.5 & 4.5 & 1.5 & 0.75 & -0.75 & 0.75 \\
0 & 1.5 & 0 & -0 & 0 & -1.5 & -1.5 & 1.5 \\
0 & 0 & 0 & 0 & 0 & 0 & 0 & 0 \\
0 & 0 & 0 & 0 & 0 & 0 & 0 & 0 \\
0 & 0 & 0 & 0 & 0 & 0 & 0 & 0
\end{bmatrix} \in \boldsymbol{R}^{6\times 8}. \tag{5.35}$$

As the previous examples, step 2 derives the active constraint space $\boldsymbol{S}_{AC}$ and the passive constraint space $\boldsymbol{S}_{PC}$ of the 3D RDWM using four sets of DAMs with VCMs by Eq. (4.26).

The result is shown below:

$$\boldsymbol{S}_{AC} = \mathcal{R}\left(\begin{bmatrix} \boldsymbol{E}_3 \\ \boldsymbol{O}_3 \end{bmatrix}\right), \boldsymbol{S}_{PC} = \mathcal{R}\left(\begin{bmatrix} \boldsymbol{O}_3 \\ \boldsymbol{E}_3 \end{bmatrix}\right). \tag{5.36}$$

Equation (5.36) shows that the configured 3D RDWM can move in the X, Y and Z directions but cannot rotate around the X-, Y- and Z-axes. Therefore, this configuration satisfies step 2 and the analysis proceeds to step 3.

SFA (Step 3)

The matrix $\boldsymbol{W}_{CVC}$ which relates the wire tension vector to the resultant force vector in the constrained coordinate is derived from Eq. (4.48) and subjected to SFA. The content of this matrix are shown below:

$$\boldsymbol{W}_{CVC} = \frac{1}{3}\begin{bmatrix} -1 & -1 & 2 & 2 & 1 & 1 & -2 & -2 \\ -2 & -2 & 2 & 2 & 2 & 2 & -2 & -2 \\ -2 & -2 & 1 & 1 & -2 & -2 & 1 & 1 \end{bmatrix} \in \boldsymbol{R}^{3\times 8}, \tag{5.37}$$

The matrix $\boldsymbol{W}_{CVC}$ contains some of the elements of matrix $\boldsymbol{W}_G$. We then have:

i) rank($\boldsymbol{W}_{CVC}$) = 3.

ii) The wire tension vector $\boldsymbol{T}_{C0} = [\,7\ 1\ 14\ 2\ 5\ 3\ 6\ 10\,]^{\mathrm{T}} \in \boldsymbol{R}^8 > \boldsymbol{0}$ satisfying $\boldsymbol{W}_{CVC}\boldsymbol{T}_{C0} = \boldsymbol{0}$.

The above analysis shows that $\boldsymbol{W}_{CVC}$ is a full- ranked matrix. Moreover, as there exists a vector $\boldsymbol{T}_{C0}$ satisfying $\boldsymbol{W}_{CVC}\boldsymbol{T}_{C0} = \boldsymbol{0}$, this RDWM candidate satisfies step 3 and the resultant force can be produced in any direction within the active constraint space $\boldsymbol{S}_{AC}$. Because it passes all three steps of the judgment procedure, the four sets of DAMs with VCMs form a proper 3D RDWM configuration that generates the desired active constraint space $\boldsymbol{S}_{AC}$ in the X, Y and Z directions. This configuration requires six fewer actuators than the 3D RDWM with seven DAMs.

5.5. Discussion and Conclusion

This chapter applied the proposed methods in chapters 3 and 4 for finding the appropriate RDWM configuration by analyzing some examples of the RDWM candidates. The numerical examples showed the advantages of the proposed judgment method in checking RDWM candidates. It specially showed the effects in the case of dealing with the multi-dimension mechanisms as the 3D cases in the last two examples. In the case where seven DAMs without VCM are used, we only have to deal with a 6×7 matrix instead of a 13×14 one. Then, in the case where four DAMs with VCMs are used, we only have to deal with a 6×8 matrix instead of a 14×16 one. By this reduction of matrix size, the number of equalities which are required to be solved in step 1 is halved; therefore, the procedure will be simpler and easier. This will let the designers to focus on thinking about arranging the configurations and then they can check those configurations with faster, simpler and easier way. The numerical examples also verified

that the VCMs effectively reduce the number of actuators while maintaining the orientation of the top plate. Especially, in the 3D RDWM configured with four sets of DAMs with VCMs, the sets of tensions in the four directions generate translational forces in any direction on the top plate, enabling global translational motions in 3D space.

Chapter 6

Experiment of the 1D RDWM

6.1. Objective of the Experiment

This experiment is set up with the objective to verify how global motion and local motions can be produced by using DAMs. This experiment will be the initial step to experimentally investigate the 3D RDWM.

6.2. Experiment Set Up

6.2.1 Configuration of the 1D RDWM

Figure 6.1 shows the overview of the 1D RDWM experimental prototype, the motions of the top plate and two fingers are controlled by four motors. Based on this overview, the 1D RDWM experimental prototype is developed and presented as follows:

Figure 6.2 shows the frame of the 1D RDWM which was fabricated by SK Machinery Ltd. Co utilizing their drum unit products. It contains the two DAMs in two sides. A cross bar connects the two DAMs. In the top of the cross bar is a linear rail where the top plate in figure 6.3 will move and perform task on the top of it. In the DAMs, each motor is directly connected to drum using coupling without through any gearbox. The motors in figure 6.4 (a) are controlled by the servo-amplifiers put in the Servo-Amp cabinet shown in figure 6.4 (b).

When the two motors in one DAM rotate in the same direction, the pulling force will move the top plate. In the other hand, when the two motors rotate in different directions, the pulling force will not be produced; instead, the motion of wire will make the internal pulley on the top plate to rotate, the movement will be transmitted to the finger through gearing system. Hence, the fingers are rotated by the different rotation directions of motors on each DAM. Table 6.1 describes detail of the mechanical parameters of the 1D RDWM prototype.

6.2.2 Kinematics relation

Kinematics relation between wire velocity and actuator velocity:

$$\dot{\boldsymbol{l}} = \boldsymbol{J}_m \dot{\boldsymbol{q}}_m, \tag{6.1}$$

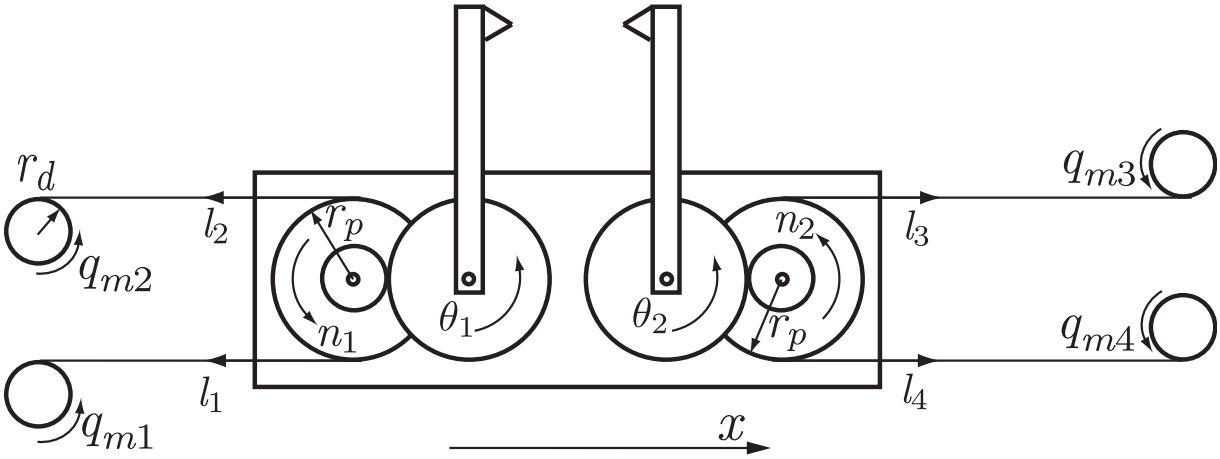

Figure. 6.1: Overview of the 1D RDWM experimental prototype.

Table 6.1 Mechanical parameters.

No.	Parameter	Notation	Value	Unit
1.	Drum radius	r_d	0.03	[m]
2.	Internal pulley radius	r_p	0.02	[m]
3.	Gear ratio	n_g	-72/32	
4.	Top plate mass	m	0.18	[kg]
5.	Motor inertia	J_m	0.164×10^{-4}	[kgm^2]
6.	Coupling inertia	J_c	0.0073×10^{-4}	[kgm^2]
7.	Drum inertia	J_{dr}	1.144×10^{-4}	[kgm^2]
8.	Motor-drum unit inertia	J_{mdr}	1.3153×10^{-4}	[kgm^2]

Kinematics relation between wire velocity and output velocity:

$$\dot{\boldsymbol{l}} = \boldsymbol{J}_t \dot{\boldsymbol{X}}, \tag{6.2}$$

Kinematics relation between actuator velocity and output velocity:

$$\dot{\boldsymbol{q}}_m = \boldsymbol{J} \dot{\boldsymbol{X}}, \tag{6.3}$$

$\dot{\boldsymbol{l}} = [\,\dot{l}_1\,\dot{l}_2\,\dot{l}_3\,\dot{l}_4\,]^{\mathrm{T}} \in \boldsymbol{R}^4$ is the wire velocity vector, where $\dot{l}_i$ is each wire velocity; $\dot{\boldsymbol{q}}_m = [\,\dot{q}_{m1}\,\dot{q}_{m2}\,\dot{q}_{m3}\,\dot{q}_{m4}\,]^{\mathrm{T}} \in \boldsymbol{R}^4$ is the actuator velocity vector, where $\dot{q}_{mi}$ is each actuator velocity; $\dot{\boldsymbol{X}} = [\,\dot{x}\dot{\theta}_1\,\dot{\theta}_2\,]^{\mathrm{T}} \in \boldsymbol{R}^3$ is the output velocity vector, where $\dot{x}$ is the top plate's velocity in the X direction, $\dot{\theta}_1$ and $\dot{\theta}_2$ are the finger's angular velocities, respectively.

Here,

$$\boldsymbol{J} = \boldsymbol{J}_m^{-1} \boldsymbol{J}_t, \tag{6.4}$$

$$\boldsymbol{J}_m = r_d \boldsymbol{E}_{4\times 4}, \tag{6.5}$$

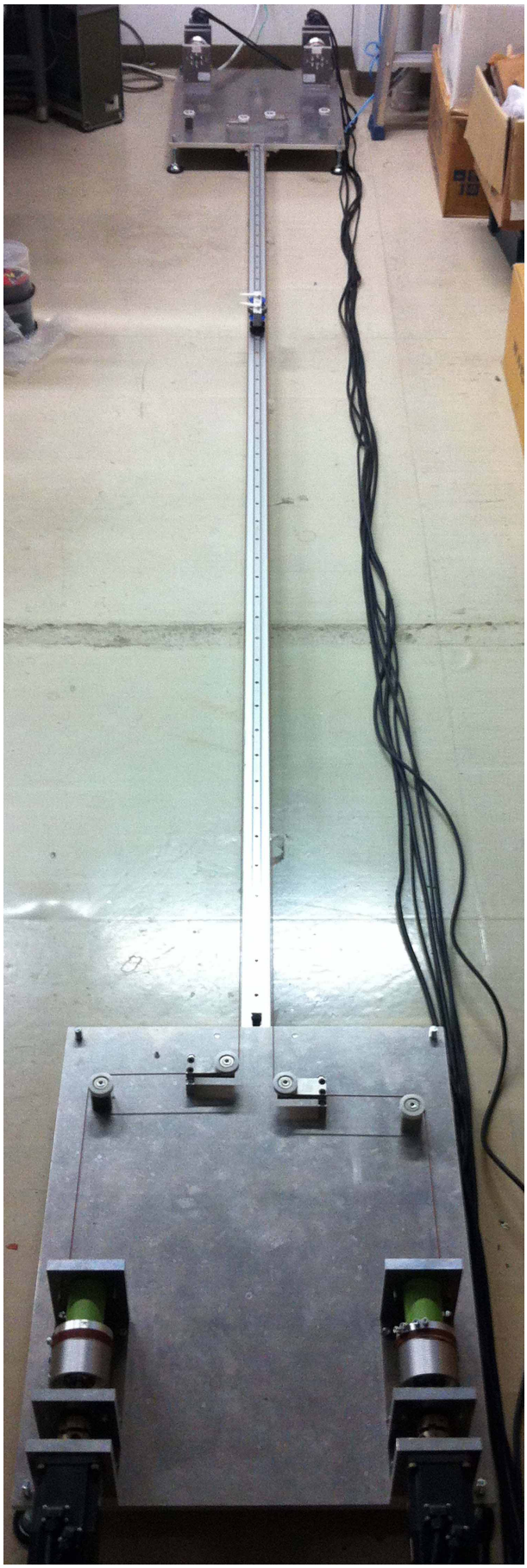

Figure. 6.2: 1D RDWM experimental prototype frame.

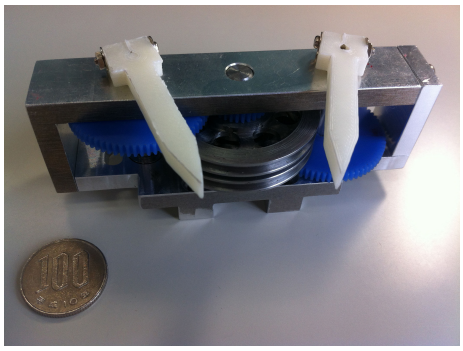

Figure. 6.3: Top plate.

(a) DAM.

(b) Servo-Amp cabinet.

Figure. 6.4: DAM and Servo-Amp cabinet.

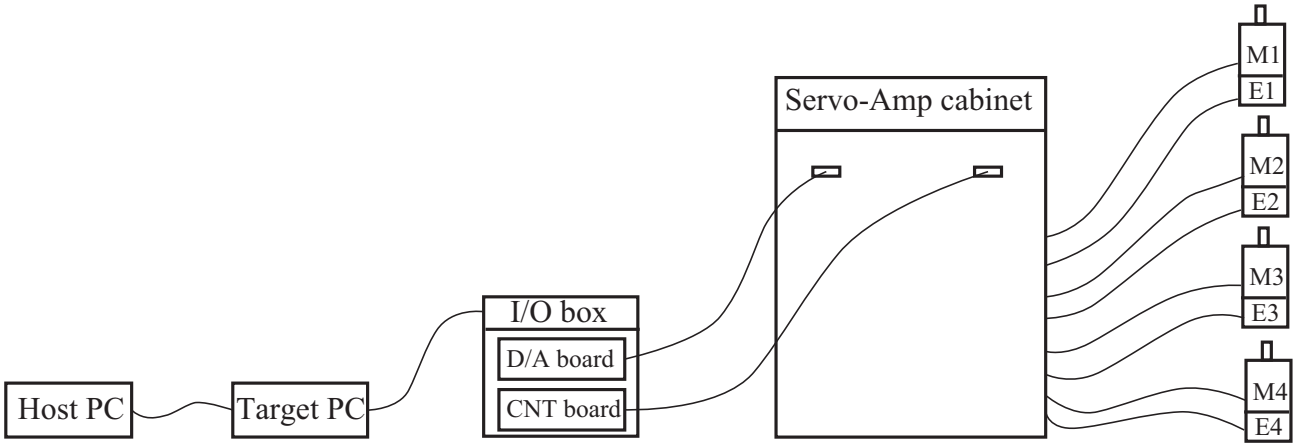

Figure. 6.5: Electronic interface diagram.

$$\boldsymbol{J}_t = \begin{bmatrix} 1 & r_p n_g & 0 \\ -1 & r_p n_g & 0 \\ 1 & 0 & r_p n_g \\ -1 & 0 & r_p n_g \end{bmatrix} \in \boldsymbol{R}^{4\times 3}. \tag{6.6}$$

Inverse kinematic relation:

$$\dot{\boldsymbol{X}} = \boldsymbol{J}^{+}\dot{\boldsymbol{q}}_m, \tag{6.7}$$

Here, $\boldsymbol{J}^{+}$ is the Pseudo-Inverse matrix of $\boldsymbol{J}$.

6.2.3 Specification of the control system

Table 6.2 shows all the components and their specification of the 1D RDWM prototype control system. The electronic interface diagram shown in figure 6.5 describes the connection of those components.

Table 6.2 Specification of the control system

No.	Component	Specification
1.	Host PC	Sony VAIO, core-i7, 2.1 Ghz, Ram 8GB
2.	Target PC	Dell, pentium 4, dual core, 2.4 Ghz, Ram 1GB
3.	DA board	Contec 12-24(PCI)
4.	CNT board	Contec 32-8M(PCI)
5.	Servo-Amplifier	Mitsubishi MR-J4-40A
6.	Servo motor	HG-MR-43BK
7.	Software	MATLAB Simulink xPC target 2012b

6.2.4 Control Diagram of the 1D RDWM

[64–67] described the basic control methods which are used in actuators and robotics. More suitable control methods had been discussed for wire driven mechanism [9, 13]. PID control method was used for the cable driven parallel robot with the internal force concept to ensure all cables are in tension [68]. In the effort to control this 1D RDWM prototype, a torque

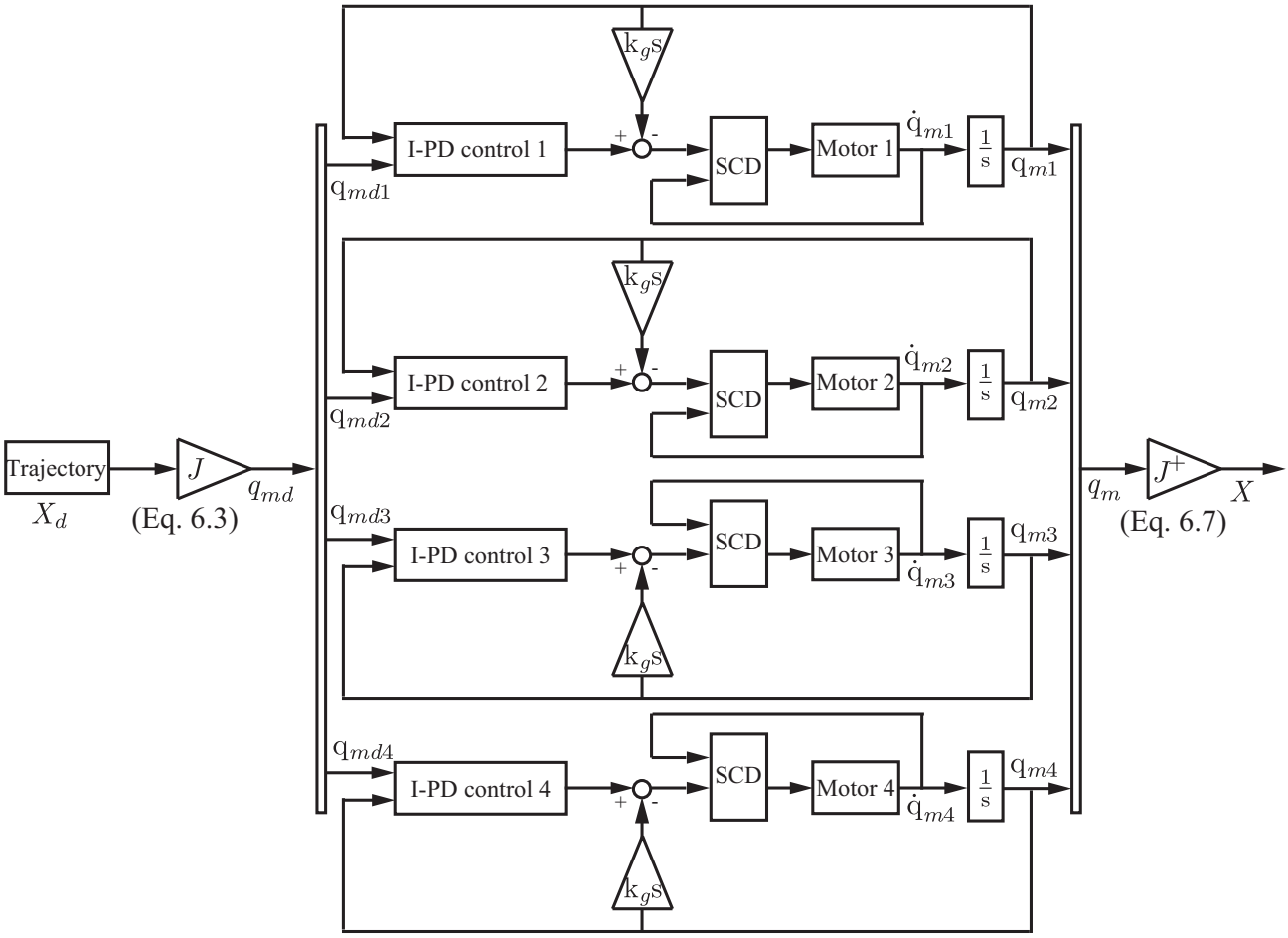

Figure. 6.6: 1D RDWM control system.

control driver with PD control method was used, however vibration from motors cannot be removed. Therefore, a control method based on I-PD control combining with speed control driver (SCD) will be presented. The experimental result discussed in the later part (subsection 6.3) shows that vibration of the top plate and fingers could be reduced a lot. Figure 6.6 shows the control system of the 1D RDWM using speed control driver and a control method based on I-PD control. By the input variable is the trajectory $\boldsymbol{X}_d$, it's easily to get rotation of each motor $\boldsymbol{q}_{mdi}$ to realize the desired trajectory by using the kinematics relation shown in Eq. 6.3. The desired motor rotations $\boldsymbol{q}_{mdi}$ will be sent to the I-PD control to calculate the desired voltage signal $\boldsymbol{v}_{mdi}$. The difference between this desired voltage signal with the feedback voltage from encoder will be the command signal that sent to the speed control driver to rotate the motor with the proper value for realizing the desired trajectory. The rotation of each motor will contribute to the motions of the top plate and fingers. The real motions of the top plate and fingers can be checked and compared with the desired trajectory by detecting the encoder signals and using the inverse kinematics relation in Eq. 6.7. Then, the problem of control the motions of top plate and fingers become the problem to control the motion of four motor-drum units.

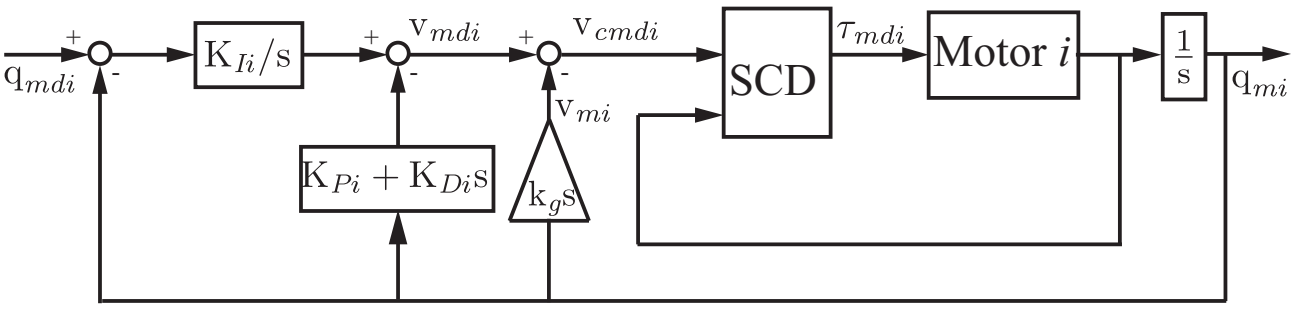

Figure. 6.7: Motor-drum unit control system.

6.2.5 Controlling of Motor-Drum Unit Using Speed Control Driver and a Control Method Based on I-PD Control

Figure 6.7 shows the control diagram for each motor-drum unit using speed control driver and a control method based on I-PD control. The command signal of this control method is shown as follows:

$$v_{cmdi} = \frac{K_{Ii}}{s}(q_{mdi(s)} - q_{mi(s)}) - (K_{Pi} + K_{Di}s)q_{mi(s)} - k_g s q_{mi(s)}, \tag{6.8}$$

where, the encoder feedback constant is derived by equation $\mathrm{K}_g = \frac{10}{\mathrm{n}_m \frac{2\pi}{60}}$ [Vs/rad], here n_m is the max motor speed. Normally, the dynamics information of a mechanism including motor units are unknown. Therefore they should be experimentally identified [69], then the way to derive the proper feedback gains of the control method should be considered using those identified dynamics information so that the mechanism can perform accuracy motions. In this stage of the research, the aim does not deeply focus on identifying dynamics information or deriving proper feedback gains but simply verifies how global motion and local motions can be produced by using DAMs. For the purpose to demonstrate how the mechanism works, the feedback gains of the control method are selected to be K_{Ii}= 2.5 [V/rads], K_{Pi}= 0.9 [V/rad], K_{Di}= 0.0045 [Vs/rad], $(i = 1, \ldots, 4)$. Then they will be used in the Matlab control diagram shown in figure 6.8. The experiment is proceeded under some conditions as follows:

Table 6.3 Experiment conditions

No.	Item	Condition
1.	Wire	ideal stiffness, without elasticity, mass
2.	Load on fingers	very small (≈ 0)
3.	Sampling time t_s	0.001 (s)

6.3. Result and Discussion

The experiment results in figure 6.9 and figure 6.10 show us how global motion and local motions can be produced although the motions are slow and imprecise.

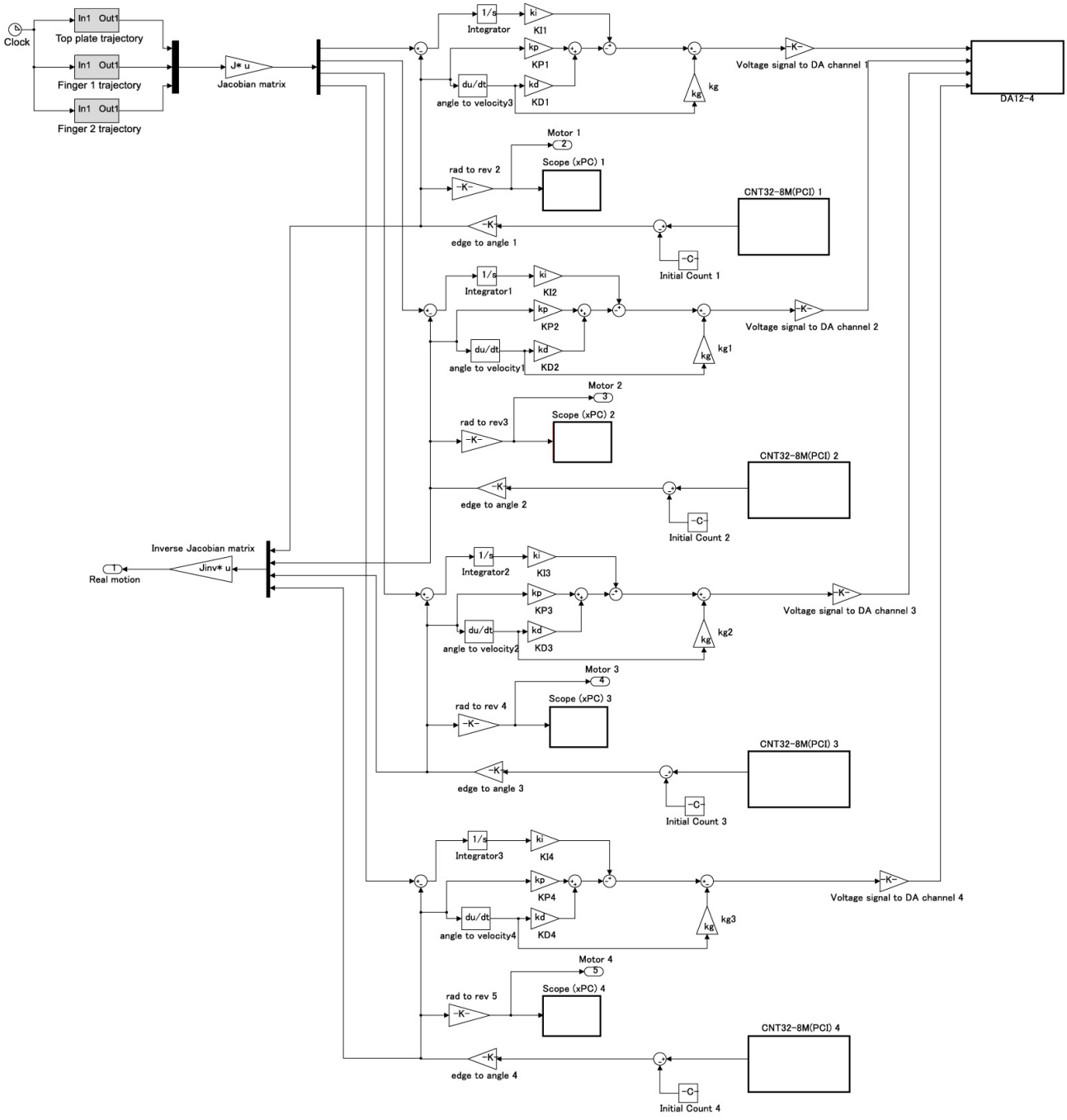

Figure. 6.8: Control Diagram in Matlab.

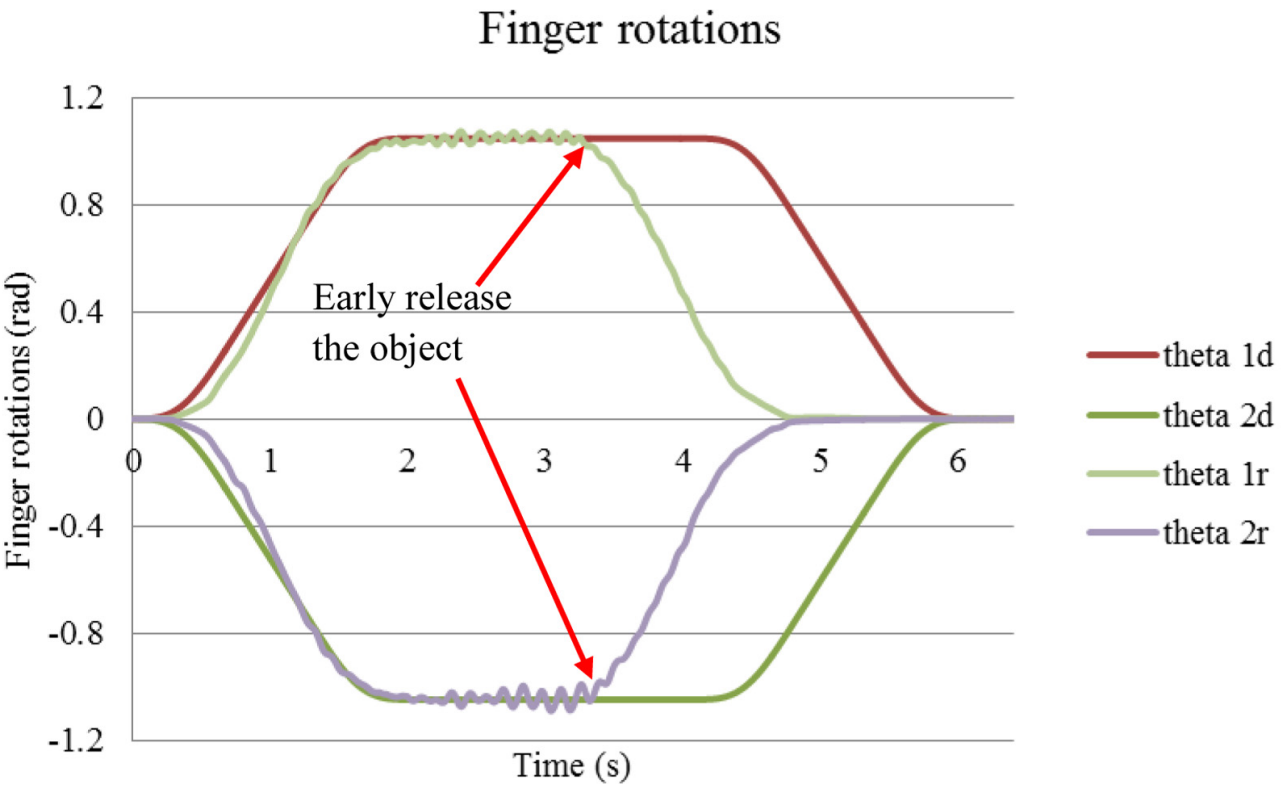

Figure. 6.9: Finger rotations.

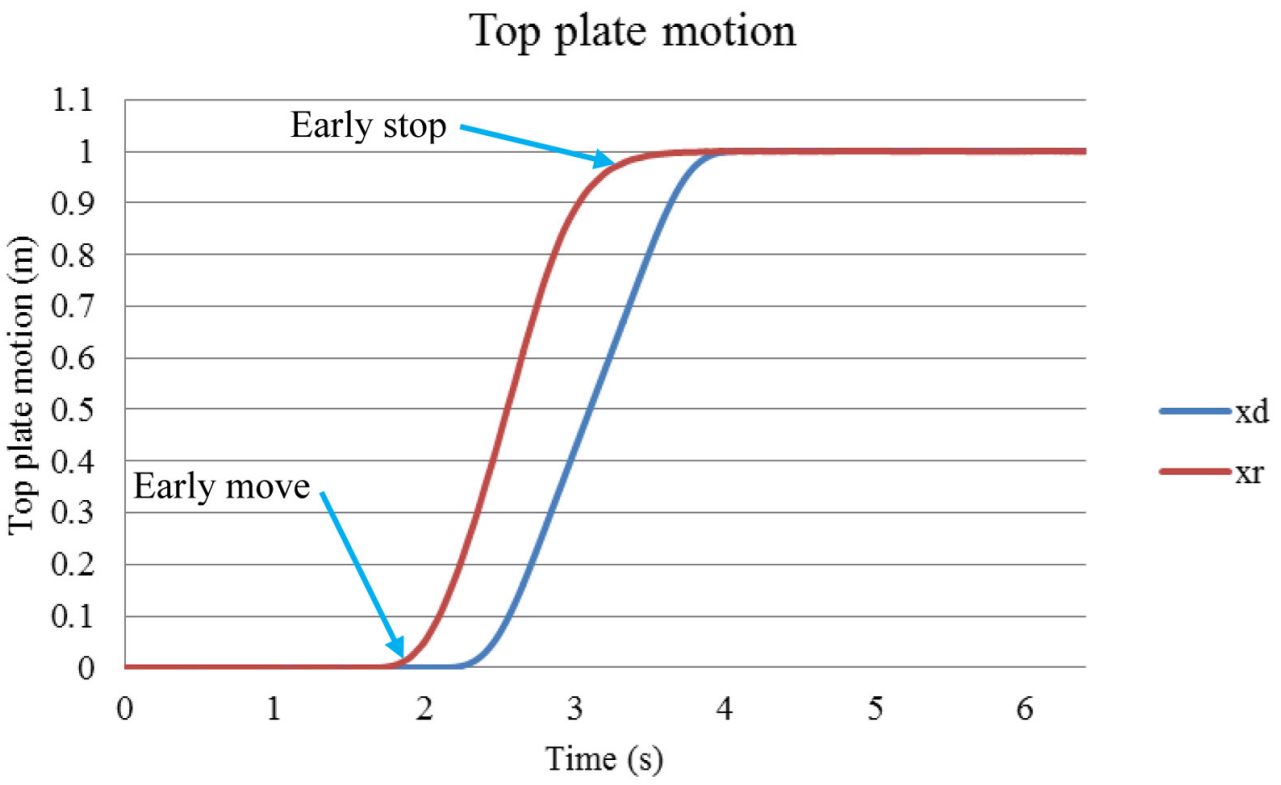

Figure. 6.10: Top plate motion.

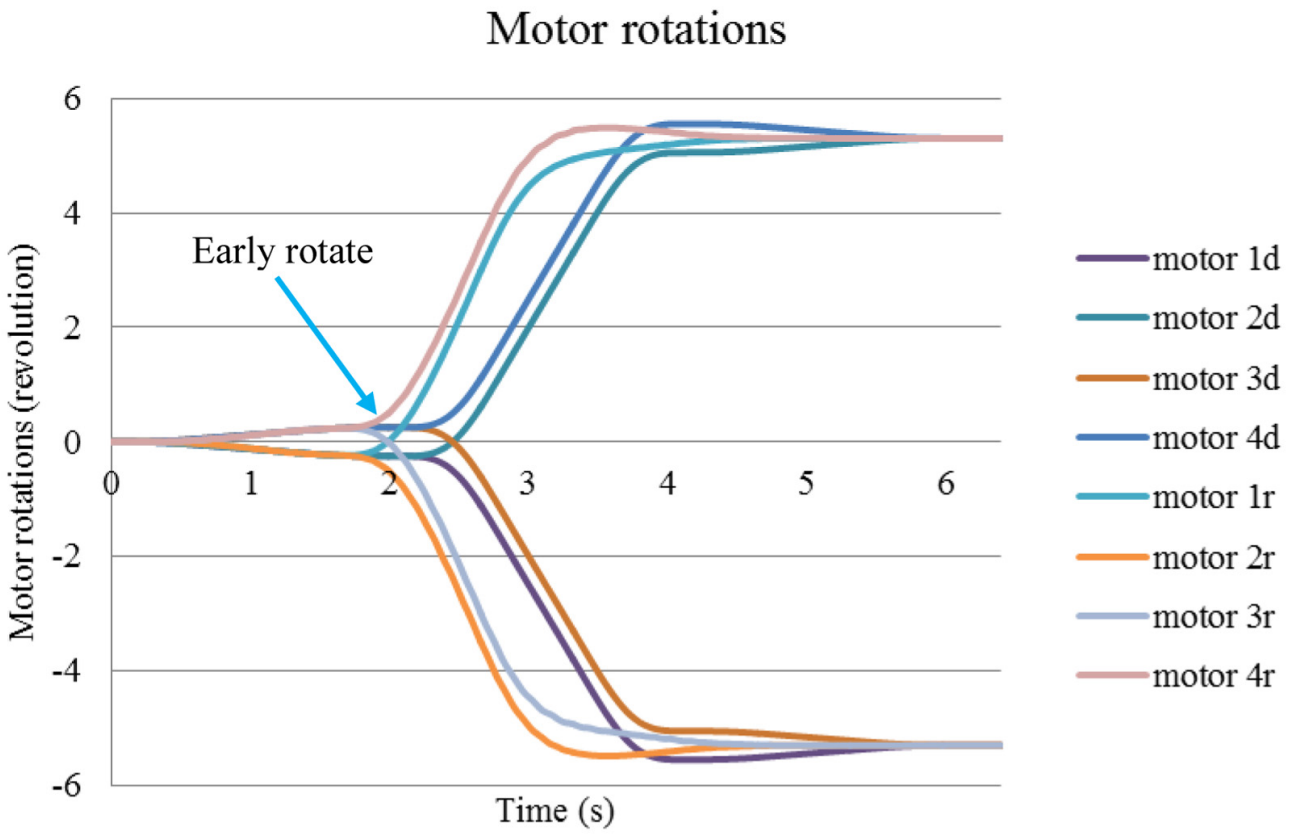

Figure. 6.11: Motor rotations.

The result of the finger motions is shown in figure 6.9. It's easy to see that the fingers begin to rotate for picking the object quite well; there are some vibrations of fingers which come from the motor sources in the grasping stage. However, the fingers rotate to release the object earlier than the trajectory.

The result of the motion of the top plate is shown in figure 6.10. It's easy to see that the top plate begins to move and approaches the desired position earlier than the trajectory.

Figure 6.11 shows the motor rotations to realize the global motion of the top plate and local motion of the fingers. In the picking stage (from beginning to second 2^{nd})and dropping stage (from second 4^{th} to second 6^{th}), only local motions of fingers are produced so just small rotation of motors are required. In the other hand, to realize the global motion the top plate in the moving stage (from second 2^{nd} to second 4^{th}), large rotation of motors are required.

The imprecise performances of the mechanism may come from two reasons. First of all, the dynamics information of the mechanism including the motor-drum units are not yet identified. Second, the feedback gains are selected as example values, without any proper method to derive them.

Therefore, for the mechanism to produce precise motions, first, the dynamics information should be identified. Second, a suitable method to derive proper values of feedback control gains should be used.

Chapter 7

Conclusion

7.1. Conclusion

This PhD thesis studied the design of redundant drive wire mechanism(RDWM) with velocity constraint modules(VCMs) to reduce the number of actuator for producing fast and precise motions. A DAM can contribute to fast motions of the top plate of an RDWM by providing large resultant forces on it, and can produce precise motions of the local mechanisms mounted on the top plate by providing moments to them. However, using DAMs will increase the number of actuators; meanwhile, to change the orientation of the top plate for performing tasks is unnecessary. Therefore, the orientation of the top plate should be fixed; then the local motions of fingers on the top plate will be used for tasks. To realize the RDWM with those ideas, some technical issues are investigated for designing of RDWM as follows.

In chapter 3, the issue of dealing with large size wire matrix was discussed. As presented in this chapter, designing an RDWM is challenging because DAMs require a large wire matrix to relate the resultant forces and wire tensions, which is used in the vector closure condition. Therefore, this chapter discussed ways of dealing with the vector closure condition of RDWM candidates for investigating the validity of the structure of the candidates. The main results reported in this chapter are summarized as follows:

1. The ability of a candidate RDWM to produce resultant forces in any direction can be judged by checking whether the vector closure condition holds for the part of the wire matrix that relates the resultant forces and the combination of the sums of the sets of two wire tensions of the DAMs. This method shows its effect when dealing with multi-dimension RDWM which contains many wires. By using just the essential part and ignoring the whole big size wire matrix, the judgment process becomes very simple, fast and convenient for designers.

2. It is found out that an RDWM has the same structure as a conventional wire mechanism with single actuator modules, where each wire is equivalent to a set of two wires for each DAM in the RDWM, when judging the vector closure condition.

In chapter 4, a method to reduce the required number of actuators for RDWM by introducing VCMs into its configuration was addressed. The concept of the research is producing the top plate with fast-translational motion for moving through large working space while fixing its orientations by using VCMs. Instead of changing the orientation of the whole top plate, the orientation of the end point of top plate can be changed largely to produce precise motion by local mechanism. This chapter also proposed a procedure that judges whether an RDWM configuration is appropriate for generating the target motions. The main results are summarized below:

1. A procedure for judging candidate RDWMs was introduced. Similar to a conventional wire mechanism, an RDWM must generate a resultant force in any direction over the whole motion space. The VCMs must then constrain the orientation of the top plate by judging the producible velocity space of the top plate. Because the top plate moves in a restricted region of the space, it must produce a resultant force in any direction within this space. Each of these requirements is tested in one step of the proposed three-steps judgment procedure.

2. The essential component of the new form of wire matrix which described in chapter 3 is used for step 1 of the judgment procedure which makes the procedure to be much more simple even when dealing with RDWM with many wires.

In chapter 5, the validity of utilizing just the essential component of the new form of wire matrix in the judgment procedure for RDWM candidates presented in chapter 4 was confirmed in numerical examples of 1D, 2D and 3D configurations. The examples clarified that using the essential component of the new form of wire matrix will reduce the burden of mathematical computation for the judgment method. They also verified that VCMs effectively reduce the number of actuators while maintaining the orientation of the top plate. Moreover, in the 3D RDWM configured using four sets of DAMs with VCMs, the sets of tensions in the four directions generate translational forces in any direction on the top plate, enabling global translational motions in 3D space.

In chapter 6, an experiment prototype of the 1D RDWM is set up and the experiment result was shown. The result verified the RDWM's concept on utilizing DAMs for producing global and local motions although those motions are not fast and imprecise.

7.2. Future works:

The research on RDWM is just at its initial stage with the investigations on the theory and designing methodology. There are many of works could be done for the future:

Firstly, in the current state of the research, wire is considered to possess ideal stiffness,

without the elasticity. Therefore the vibration behavior of the top plate which comes from the real wire with elasticity will not occurred. However, because wire has elasticity, vibration of the top plate can occur and makes bad affect to the operation of the mechanism in producing accuracy motions. An investigation on vibration from the wire elasticity and some methods for vibration suppression could be one of the future work.

Secondly, the proposed theory and methodology should be applied to set up the 2D and 3D experiment prototypes to verify the validity of using DAMs and VCMs in the structure of RDWM for producing high acceleration and high precise motions with the reduction number of actuators.

Thirdly, all the dynamics information of the 1D RDWM mechanism needs to be precisely identified, then an appropriate controller with the method to derive proper feedback gains should be developed to control the wire tension. Force sensors or strain gauge could be used to detect wire tension as the feedback signal. Then, some other kinds of sensors like acceleration sensor, laser sensor, vision sensor could be introduced into the prototype to improve the accuracy of the performance. After that those investigations could be applied for the 2D or 3D RDWM prototypes.

Appendix A

List of notations and symbols

Table A.1 List of notations and symbols

Notations or symbols	Description	Locations
${}^{B}\boldsymbol{p}_{Bij}$, ${}^{B}\dot{\boldsymbol{p}}_{Bij}$	position/ velocity of wire end points on the top plate w.r.t the base coordinate.	Eq. (3.1)
${}^{B}\dot{\boldsymbol{p}}_{T}$	velocity of the center of the top plate w.r.t the base coordinate.	Eq. (3.1)
${}^{B}\boldsymbol{\omega}$	angular velocity of the top plate	Eq. (3.1)
${}^{B}\boldsymbol{e}_{ij}$	wire vectors with unit length	Eqs. (3.3, 3.7, 3.11)
$\dot{l}_{ij}$	wire velocity	Eq. (3.3)
R_i	radius of local pulley	Eq. (3.3)
$\dot{\theta}_i$	angular velocity of local pulley	Eq. (3.3)
$\boldsymbol{F}$	resultant force vector	Eq. (3.5)
$\boldsymbol{T}$	wire tension vector	Eq. (3.5)
$\boldsymbol{W}$	wire matrix	Eqs. (3.5, 3.6)
N_D	number of DAMs	Eq. (3.6)
n	number of global motion DoFs of the top plate	Eqs. (3.6, 4.13, 4.18)
$\boldsymbol{W}_G$	matrix of resultant force on the top plate	Eqs. (3.7, 4.23)
$\boldsymbol{W}_L$	matrix of local moments on the local pulleys	Eq. (3.8)
$\boldsymbol{A}_{ij}$	wire end point on the frame	Chapters 3, 4.
$\boldsymbol{B}_{ij}$	wire end point on the top plate	Chapters 3, 4.
$\boldsymbol{C}_i$	center of $\boldsymbol{A}_{ij}\boldsymbol{B}_{ij}$	Chapters 3, 4.
$\boldsymbol{W}'$	new form of wire matrix	Eqs. (3.15, 3.16)
$\boldsymbol{T}'$	new form of wire tension vector	Eq. (3.15)
$\boldsymbol{W}'_G$	the essential part of new form of wire matrix	Eqs. (3.16, 3.17)
$\boldsymbol{W}'_L$	new form of local moment matrix	Eqs. (3.16, 3.17)
$\boldsymbol{W}_C$	contribution to produce resultant force on top plate	Eqs. (3.16, 3.19)
$\boldsymbol{T}_S$	vector of sums of wire tension in DAM	Sections 3.2.2, 3.2.3.
$\boldsymbol{T}_D$	vector of differences of wire tension in DAM	Sections 3.2.2, 3.2.3.
$\boldsymbol{W}'_{Gf}$	part of $\boldsymbol{W}'_G$ that related to resultant force	Eqs. (3.21, 3.22)
$\boldsymbol{W}'_{Gm}$	part of $\boldsymbol{W}'_G$ that related to resultant moment	Eqs. (3.21, 3.23)
$\boldsymbol{W}_{Cnz}$	non-zero part of matrix $\boldsymbol{W}_C$	Eqs. (3.21, 3.25)
n_f	number of DoFs under resultant force	Eq. (3.22)
n_m	number of DoFs under resultant moment	Eqs. (3.23, 3.25)
$\boldsymbol{n}$	resultant moment on the top plate	Eq. (3.26)
$\boldsymbol{n_S}$	moment from sums of wire tensions on DAMs	Eq. (3.26)
$\boldsymbol{n_D}$	moment from differences of wire tensions on DAMs	Eq. (3.26)

$\times$	The cross product of two vectors in R^3. For two vectors in R^2, the result of this product is a scalar as follows: give $\boldsymbol{a} = [a_1 \;\; a_2]^{\mathrm{T}}$, $\boldsymbol{b} = [b_1 \;\; b_2]^{\mathrm{T}}$; then: $\boldsymbol{a} \times \boldsymbol{b} = \begin{vmatrix} a_1 & a_2 \\ b_1 & b_2 \end{vmatrix} = a_1 b_2 - a_2 b_1$.	Eqs. (3.3, 3.7, 4.13, 4.18)
$\dot{\boldsymbol{q}}$, $\dot{\boldsymbol{q}}_m$	actuator velocity vector	Eqs. (4.3, 4.7, 6.1)
$\dot{\boldsymbol{l}}$	wire velocity vector	Eqs. (4.2, 4.3, 4.5, 6.1, 6.2)
$\boldsymbol{v}$	output velocity vector	Eqs. (4.2, 4.7, 4.8)
τ	motor torque vector	Eq. (4.4)
$\boldsymbol{J}$	Jacobian matrix of mechanism without VCM	Eqs. (4.3, 4.4, 4.7)
$\boldsymbol{J}_{vc}$	Jacobian matrix of mechanism with VCM	Eqs. (4.5, 4.6, 4.8)
$\dot{\boldsymbol{q}}_{vc}$	actuator velocity vector	Eqs. (4.5, 4.8)
τ_{vc}	motor torque vector of mechanism with VCMs	Eq. (4.6)
Subscripts:		
$_{Ld}$	denote component belongs to DAM.	Eqs. (4.21, 4.22, 4.23)
$_{Lv}$	denote component belongs to VCM.	Eqs. (4.21, 4.22, 4.23)
$_{N_D}$	number of DAM without VCM.	Eqs. (4.21, 4.22, 4.23)
$_{N_V}$	number of DAM with VCM.	Eqs. (4.21, 4.22, 4.23)
k	ordering number of DAM without VCM contains in DAM with VCM.	Eq. (4.18)
$\boldsymbol{W}_{Gi}$	matrix of global motion from DAM without VCM.	Eq. (4.23)
$\boldsymbol{W}_{GV_m}$	matrix of global motion from DAM with VCM.	Eq. (4.23)
$\boldsymbol{S}_{AC}$, $\boldsymbol{S}_{PC}$	active and passive constraint space.	Eq. (4.26)
$\boldsymbol{C}_P$	producible global velocity matrix.	Eqs. (4.33, 4.44, 4.48)
$\boldsymbol{W}_{CVC}$	Matrix of resultant force on the top plate in the constraint space.	Eqs. (4.37, 4.48)
$\boldsymbol{f}$	resultant force in the velocity producible space	Eqs. (4.34, 4.36, 4.46)
$\dot{\boldsymbol{X}}$	output velocity vector	Eqs. (6.2, 6.3)
$\boldsymbol{J}_m$	actuator Jacobian matrix	Eqs. (6.1, 6.4, 6.5)
$\boldsymbol{J}_t$	top plate Jacobian matrix	Eqs. (6.2, 6.4, 6.6)
$\boldsymbol{J}$	whole Jacobian matrix	Eqs. (6.3, 6.4)
$\boldsymbol{J}^+$	Pseudo-Inverse matrix of $\boldsymbol{J}$	Eq. (6.7)
r_p	internal pulley radius	Eq. (6.6)
r_d	drum radius	Eq. (6.5)
n_g	gear ratio	Eq. (6.6)
k_g	encoder constant	Eq. (6.8)
v_{mdi}	voltage command signal	Eq. (6.8)
K_{Ii}	integral feedback gain	Eq. (6.8)
K_{Pi}	proportional feedback gain	Eq. (6.8)
K_{Di}	derivative feedback gain	Eq. (6.8)

Appendix B

Derivation of the Normal Form and New Form Wire Matrix for RDWM based on DAMs with and without VCM

The method to derive the normal form and new form wire matrix for RDWM based on DAMs with VCMs is similar to the method that was applied for RDWM based on DAMs without VCM when considering DAMs with VCMs contain two DAMs without VCM. The results of those matrices are presented as follows:

B.1. Normal Form of Wire Matrix of RDWM contains DAMs with and without VCMs

The whole wire matrix of the RDWM contains DAMs with and without VCMs is defined as

$$\boldsymbol{W} = \begin{bmatrix} \boldsymbol{W}_G \\ \boldsymbol{W}_L \end{bmatrix} \in \boldsymbol{R}^{(n+N_D+2N_V)\times 2(N_D+2N_V)}, \tag{B.1}$$

where, the matrix $\boldsymbol{W}$ contains the matrix $\boldsymbol{W}_G$ of contributions to the resultant force on the top plate. $\boldsymbol{W}_G$ is given by:

$$\boldsymbol{W}_G = [\ \boldsymbol{W}_{G1}\ \ldots\ \boldsymbol{W}_{GN_D}\ \boldsymbol{W}_{GV1}\ \ldots\ \boldsymbol{W}_{GVN_V}]^{\mathrm{T}} \in \boldsymbol{R}^{n\times 2(N_D+2N_V)}, \tag{B.2}$$

here $\boldsymbol{W}_{Gi}$ and $\boldsymbol{W}_{GVm}$ are obtained from Eqs. (4.13) and (4.18); and the matrix $\boldsymbol{W}_L$ of contributions to the local moments of the local pulleys is given by:

$$\boldsymbol{W}_L = \begin{bmatrix} R_1 & -R_1 & 0 & 0 & \ldots & 0 & 0 \\ 0 & 0 & R_2 & -R_2 & \ldots & 0 & 0 \\ \vdots & \vdots & \vdots & \vdots & \vdots & \vdots & \vdots \\ 0 & 0 & 0 & 0 & \ldots & R_N & -R_N \end{bmatrix} \in \boldsymbol{R}^{(N_D+2N_V)\times 2(N_D+2N_V)} \tag{B.3}$$

B.2. New Form of Wire Matrix of RDWM contains DAMs with VCMs

The new expression of wire matrix $\boldsymbol{W}^{'}$ is given by

$$\boldsymbol{W}^{'} = \begin{bmatrix} \boldsymbol{W}^{'}_{G} & \boldsymbol{W}_{C} \\ \boldsymbol{O} & \boldsymbol{W}^{'}_{L} \end{bmatrix} \in \boldsymbol{R}^{(n+N_D+2N_V)\times 2(N_D+2N_V)}, \tag{B.4}$$

Inside the matrix $\boldsymbol{W}^{'}$, the matrix $\boldsymbol{W}^{'}_{L}$ contributes to producing local moments of pulleys on the top plate while the set of matrices $\boldsymbol{W}^{'}_{G}$ and $\boldsymbol{W}_{C}$ contributes to producing the resultant force and resultant moment on the top plate. The contents of $\boldsymbol{W}^{'}_{G}$, $\boldsymbol{W}^{'}_{L}$, and $\boldsymbol{W}_{C}$ are shown below:

$$\begin{aligned} \boldsymbol{W}^{'}_{G} = \Bigg[& {}^{B}\boldsymbol{e}_{1} & {}^{B}\boldsymbol{e}_{2} & \dots & {}^{B}\boldsymbol{e}_{N_D} & {}^{B}\boldsymbol{e}_{1} & {}^{B}\boldsymbol{e}_{1} \\ & {}^{B}\boldsymbol{p}_{TC1}\times{}^{B}\boldsymbol{e}_{1} & {}^{B}\boldsymbol{p}_{TC2}\times{}^{B}\boldsymbol{e}_{2} & \dots & {}^{B}\boldsymbol{p}_{TCN_D}\times{}^{B}\boldsymbol{e}_{N_D} & {}^{B}\boldsymbol{p}_{TC1}\times{}^{B}\boldsymbol{e}_{1} & {}^{B}\boldsymbol{p}_{TC1}\times{}^{B}\boldsymbol{e}_{1} \\ & \dots & {}^{B}\boldsymbol{e}_{N_V} & {}^{B}\boldsymbol{e}_{N_V} \\ & \dots & {}^{B}\boldsymbol{p}_{TC(2N_V-1)}\times{}^{B}\boldsymbol{e}_{N_V} & {}^{B}\boldsymbol{p}_{TC2N_V}\times{}^{B}\boldsymbol{e}_{N_V} \Bigg] \in \boldsymbol{R}^{n\times(N_D+2N_V)}, \end{aligned} \tag{B.5}$$

$$\boldsymbol{W}^{'}_{L} = \begin{bmatrix} R_1 & 0 & \dots & 0 \\ 0 & R_2 & \dots & 0 \\ \vdots & \vdots & \vdots & \vdots \\ 0 & 0 & \dots & R_{N_D+2N_V} \end{bmatrix} \in \boldsymbol{R}^{(N_D+2N_V)\times(N_D+2N_V)}, \tag{B.6}$$

$$\begin{aligned} \boldsymbol{W}_{C} = \Bigg[& \boldsymbol{O} \\ & \boldsymbol{p}_{TD1}\times{}^{B}\boldsymbol{e}_{1} & \boldsymbol{p}_{TD2}\times{}^{B}\boldsymbol{e}_{2} & \dots & \boldsymbol{p}_{TDN_D}\times{}^{B}\boldsymbol{e}_{N_D} & {}^{B}\boldsymbol{p}_{TD1}\times{}^{B}\boldsymbol{e}_{1} & {}^{B}\boldsymbol{p}_{TD1}\times{}^{B}\boldsymbol{e}_{1} \\ & \dots & {}^{B}\boldsymbol{p}_{TD(2N_V-1)}\times{}^{B}\boldsymbol{e}_{N_V} & {}^{B}\boldsymbol{p}_{TD2N_V}\times{}^{B}\boldsymbol{e}_{N_V} \Bigg] \in \boldsymbol{R}^{n\times(N_D+2N_V)}, \end{aligned} \tag{B.7}$$

$$\boldsymbol{O} = [\boldsymbol{0}]_{(N_D+2N_V)\times(N_D+2N_V)}\,. \tag{B.8}$$

Appendix C

Normal Form and New Form Wire Matrix of Each Mechanism

The normal form of wire matrix $\boldsymbol{W}$ is derived from Eq. (3.6) in the case of RDWM contains DAMs without VCM or from Eq. (B.1) in the case of RDWM contains DAMs with VCM; then the new form of wire matrix $\boldsymbol{W}^{'}$ is derived from Eq. (3.16) in the case of RDWM contains DAMs without VCM or from Eq. (B.4) in the case of RDWM contains DAMs with VCM. The results of those matrices for each mechanism discussed in chapter 5 are shown as follows:

C.1. Proper Configuration of the Planar RDWM with Fixed Orientation Around the Z-axis while Maintaining Translational Motion in the X and Y Directions

C.1.1 First configuration: The Mechanism Does Not Satisfy the 1^{st} Point of Step 1

The normal form of wire matrix

$$\boldsymbol{W}_2 = \begin{bmatrix} \boldsymbol{W}_{G2} \\ \boldsymbol{W}_{L2} \end{bmatrix} \in \boldsymbol{R}^{7\times 8}, \tag{C.1}$$

where:

$$\boldsymbol{W}_{G2} = \begin{bmatrix} 0 & 0 & 0 & 0 & 0 & 0 & 0 & 0 \\ -1 & -1 & -1 & -1 & 1 & 1 & 1 & 1 \\ 8 & 4 & -4 & -8 & 8 & 4 & -4 & -8 \end{bmatrix} \in \boldsymbol{R}^{3\times 8}, \tag{C.2}$$

$$\boldsymbol{W}_{L2} = \begin{bmatrix} 2 & -2 & 0 & 0 & 0 & 0 & 0 & 0 \\ 0 & 0 & 2 & -2 & 0 & 0 & 0 & 0 \\ 0 & 0 & 0 & 0 & 2 & -2 & 0 & 0 \\ 0 & 0 & 0 & 0 & 0 & 0 & 2 & -2 \end{bmatrix} \in \boldsymbol{R}^{4\times 8}. \tag{C.3}$$

The new form of wire matrix

$$\boldsymbol{W}_2^{'} = \begin{bmatrix} \boldsymbol{W}_{G2}^{'} & \boldsymbol{W}_{C2} \\ \boldsymbol{O} & \boldsymbol{W}_{L2}^{'} \end{bmatrix} \in \boldsymbol{R}^{7\times 8}, \tag{C.4}$$

where:

$$\boldsymbol{W}^{'}_{G2} = \begin{bmatrix} 0 & 0 & 0 & 0 \\ -1 & -1 & 1 & 1 \\ 6 & -6 & 6 & -6 \end{bmatrix}_{3\times 4}, \tag{C.5}$$

$$\boldsymbol{W}_{C2} = \begin{bmatrix} 0 & 0 & 0 & 0 \\ 0 & 0 & 0 & 0 \\ 2 & 2 & 2 & 2 \end{bmatrix}_{3\times 4}, \tag{C.6}$$

$$\boldsymbol{W}^{'}_{L2} = 2\boldsymbol{E}_{4\times 4}, \tag{C.7}$$

$$\boldsymbol{O} = [\boldsymbol{0}]_{4\times 4}, \tag{C.8}$$

C.1.2 Second configuration: The Mechanism does not satisfy the 2^{nd} point of Step 1

The normal form of wire matrix

$$\boldsymbol{W}_2 = \begin{bmatrix} \boldsymbol{W}_{G2} \\ \boldsymbol{W}_{L2} \end{bmatrix} \in \boldsymbol{R}^{7\times 8}, \tag{C.9}$$

where:

$$\boldsymbol{W}_{G2} = \frac{1}{5}\begin{bmatrix} 0 & 0 & 4 & 4 & 0 & 0 & 0 & 0 \\ -5 & -5 & -3 & -3 & 5 & 5 & 5 & 5 \\ -70 & -90 & -12 & -28 & -10 & -30 & -70 & -90 \end{bmatrix} \in \boldsymbol{R}^{3\times 8}. \tag{C.10}$$

$$\boldsymbol{W}_{L2} = \begin{bmatrix} 2 & -2 & 0 & 0 & 0 & 0 & 0 & 0 \\ 0 & 0 & 2 & -2 & 0 & 0 & 0 & 0 \\ 0 & 0 & 0 & 0 & 2 & -2 & 0 & 0 \\ 0 & 0 & 0 & 0 & 0 & 0 & 2 & -2 \end{bmatrix} \in \boldsymbol{R}^{4\times 8}. \tag{C.11}$$

The new form of wire matrix

$$\boldsymbol{W}^{'}_2 = \begin{bmatrix} \boldsymbol{W}^{'}_{G2} & \boldsymbol{W}_{C2} \\ \boldsymbol{O} & \boldsymbol{W}^{'}_{L2} \end{bmatrix} \in \boldsymbol{R}^{7\times 8}, \tag{C.12}$$

where:

$$\boldsymbol{W}^{'}_{G2} = \frac{1}{5}\begin{bmatrix} 0 & 4 & 0 & 0 \\ -5 & -3 & 5 & 5 \\ -80 & -20 & -20 & -80 \end{bmatrix} \in \boldsymbol{R}^{3\times 4}, \tag{C.13}$$

$$\boldsymbol{W}_{C2} = \frac{1}{5}\begin{bmatrix} 0 & 0 & 0 & 0 \\ 0 & 0 & 0 & 0 \\ 10 & 8 & 10 & 10 \end{bmatrix} \in \boldsymbol{R}^{3\times 4}, \tag{C.14}$$

$$\boldsymbol{W}_{L2}^{'} = 2\boldsymbol{E}_{4\times 4}, \tag{C.15}$$

$$\boldsymbol{O} = [\boldsymbol{0}]_{4\times 4}\,. \tag{C.16}$$

C.1.3 Third configuration: planar RDWM with four DAMs

The normal form of wire matrix

$$\boldsymbol{W}_2 = \begin{bmatrix} \boldsymbol{W}_{G2} \\ \boldsymbol{W}_{L2} \end{bmatrix} \in \boldsymbol{R}^{7\times 8}, \tag{C.17}$$

where

$$\boldsymbol{W}_{G2} = \frac{1}{5}\begin{bmatrix} -4 & -4 & 4 & 4 & 0 & 0 & 0 & 0 \\ -3 & -3 & -3 & -3 & 5 & 5 & 5 & 5 \\ 14 & -2 & 2 & -14 & 40 & 20 & -20 & -40 \end{bmatrix} \in \boldsymbol{R}^{3\times 8}. \tag{C.18}$$

$$\boldsymbol{W}_{L2} = \begin{bmatrix} 2 & -2 & 0 & 0 & 0 & 0 & 0 & 0 \\ 0 & 0 & 2 & -2 & 0 & 0 & 0 & 0 \\ 0 & 0 & 0 & 0 & 2 & -2 & 0 & 0 \\ 0 & 0 & 0 & 0 & 0 & 0 & 2 & -2 \end{bmatrix} \in \boldsymbol{R}^{4\times 8}. \tag{C.19}$$

The new form of wire matrix

$$\boldsymbol{W}_2^{'} = \begin{bmatrix} \boldsymbol{W}_{G2}^{'} & \boldsymbol{W}_{C2} \\ \boldsymbol{O} & \boldsymbol{W}_{L2}^{'} \end{bmatrix} \in \boldsymbol{R}^{7\times 8}, \tag{C.20}$$

where:

$$\boldsymbol{W}_{G2}^{'} = \frac{1}{5}\begin{bmatrix} -4 & 4 & 0 & 0 \\ -3 & -3 & 5 & 5 \\ -6 & -6 & 30 & -30 \end{bmatrix} \in \boldsymbol{R}^{3\times 4}, \tag{C.21}$$

$$\boldsymbol{W}_{C2} = \frac{1}{5}\begin{bmatrix} 0 & 0 & 0 & 0 \\ 0 & 0 & 0 & 0 \\ 8 & 8 & 10 & 10 \end{bmatrix} \in \boldsymbol{R}^{3\times 4}, \tag{C.22}$$

$$\boldsymbol{W}_{L2}^{'} = 2\boldsymbol{E}_{4\times 4}, \tag{C.23}$$

$$\boldsymbol{O} = [\boldsymbol{0}]_{4\times 4}\,. \tag{C.24}$$

C.1.4 Fourth configuration: planar RDWM with two DAMs and one DAM with a VCM

The normal form of wire matrix

$$\boldsymbol{W}_2 = \begin{bmatrix} \boldsymbol{W}_{G2} \\ \boldsymbol{W}_{L2} \end{bmatrix} \in \boldsymbol{R}^{7\times 8}, \tag{C.25}$$

where:

$$\boldsymbol{W}_{G2} = \frac{1}{5}\begin{bmatrix} -4 & -4 & 4 & 4 & 0 & 0 & 0 & 0 \\ -3 & -3 & -3 & -3 & 5 & 5 & 5 & 5 \\ 14 & -2 & 2 & -14 & 40 & 20 & -20 & -40 \end{bmatrix} \in \boldsymbol{R}^{3\times 8}. \tag{C.26}$$

$$\boldsymbol{W}_{L2} = \begin{bmatrix} 2 & -2 & 0 & 0 & 0 & 0 & 0 & 0 \\ 0 & 0 & 2 & -2 & 0 & 0 & 0 & 0 \\ 0 & 0 & 0 & 0 & 2 & -2 & 0 & 0 \\ 0 & 0 & 0 & 0 & 0 & 0 & 2 & -2 \end{bmatrix} \in \boldsymbol{R}^{4\times 8}. \tag{C.27}$$

The new form of wire matrix

$$\boldsymbol{W}_2^{'} = \begin{bmatrix} \boldsymbol{W}_{G2}^{'} & \boldsymbol{W}_{C2} \\ \boldsymbol{O} & \boldsymbol{W}_{L2}^{'} \end{bmatrix} \in \boldsymbol{R}^{7\times 8}, \tag{C.28}$$

where:

$$\boldsymbol{W}_{G2}^{'} = \frac{1}{5}\begin{bmatrix} -4 & 4 & 0 & 0 \\ -3 & -3 & 5 & 5 \\ -6 & -6 & 30 & -30 \end{bmatrix} \in \boldsymbol{R}^{3\times 4}, \tag{C.29}$$

$$\boldsymbol{W}_{C2} = \frac{1}{5}\begin{bmatrix} 0 & 0 & 0 & 0 \\ 0 & 0 & 0 & 0 \\ 8 & 8 & 10 & 10 \end{bmatrix} \in \boldsymbol{R}^{3\times 4}, \tag{C.30}$$

$$\boldsymbol{W}_{L2}^{'} = 2\boldsymbol{E}_{4\times 4}, \tag{C.31}$$

$$\boldsymbol{O} = [\boldsymbol{0}]_{4\times 4}\,. \tag{C.32}$$

C.1.5 Fifth configuration: improper planar RDWM with two DAMs and one DAM with a VCM

The normal form of wire matrix

$$\boldsymbol{W}_2 = \begin{bmatrix} \boldsymbol{W}_{G2} \\ \boldsymbol{W}_{L2} \end{bmatrix} \in \boldsymbol{R}^{7\times 8}, \tag{C.33}$$

where:

$$\boldsymbol{W}_{G2} = \frac{1}{5}\begin{bmatrix} 0 & 0 & 4 & 4 & 0 & 0 & 0 & 0 \\ -5 & -5 & -3 & -3 & 5 & 5 & 5 & 5 \\ -70 & -90 & -12 & -28 & -10 & -30 & -70 & -90 \end{bmatrix} \in \boldsymbol{R}^{3\times 8}. \tag{C.34}$$

$$\boldsymbol{W}_{L2} = \begin{bmatrix} 2 & -2 & 0 & 0 & 0 & 0 & 0 & 0 \\ 0 & 0 & 2 & -2 & 0 & 0 & 0 & 0 \\ 0 & 0 & 0 & 0 & 2 & -2 & 0 & 0 \\ 0 & 0 & 0 & 0 & 0 & 0 & 2 & -2 \end{bmatrix} \in \boldsymbol{R}^{4\times 8}. \tag{C.35}$$

The new form of wire matrix

$$\boldsymbol{W}_2^{'} = \begin{bmatrix} \boldsymbol{W}_{G2}^{'} & \boldsymbol{W}_{C2} \\ \boldsymbol{O} & \boldsymbol{W}_{L2}^{'} \end{bmatrix} \in \boldsymbol{R}^{7\times 8}, \tag{C.36}$$

where:

$$\boldsymbol{W}_{G2}^{'} = \frac{1}{5}\begin{bmatrix} 0 & 4 & 0 & 0 \\ -5 & -3 & 5 & 5 \\ -80 & -20 & -20 & -80 \end{bmatrix} \in \boldsymbol{R}^{3\times 4}, \tag{C.37}$$

$$\boldsymbol{W}_{C2} = \frac{1}{5}\begin{bmatrix} 0 & 0 & 0 & 0 \\ 0 & 0 & 0 & 0 \\ 10 & 8 & 10 & 10 \end{bmatrix} \in \boldsymbol{R}^{3\times 4}, \tag{C.38}$$

$$\boldsymbol{W}_{L2}^{'} = 2\boldsymbol{E}_{4\times 4}, \tag{C.39}$$

$$\boldsymbol{O} = [\boldsymbol{0}]_{4\times 4}. \tag{C.40}$$

C.2. Proper Configuration of 3D RDWM with Fixed Orientations Around X-, Y-, and Z-axes while Maintaining Translational Motions in the X, Y and Z Directions

C.2.1 First configuration: 3D RDWM with seven DAMs

The normal form of wire matrix

$$\boldsymbol{W}_3 = \begin{bmatrix} \boldsymbol{W}_{G3} \\ \boldsymbol{W}_{L3} \end{bmatrix} \in \boldsymbol{R}^{13\times 14}, \tag{C.41}$$

where:

$$\boldsymbol{W}_{G3} = \frac{1}{5}\begin{bmatrix} -3 & -3 & 3 & 3 & 0 & 0 & 0 & 0 & -3 & -3 & 0 & 0 & 3 & 3 \\ 0 & 0 & 0 & 0 & 3 & 3 & 3 & 3 & 0 & 0 & -3 & -3 & 0 & 0 \\ 4 & 4 & 4 & 4 & 4 & 4 & 4 & 4 & -4 & -4 & -4 & -4 & -4 & -4 \\ -16 & -32 & -32 & -16 & 10 & 10 & 10 & 10 & -32 & -16 & 10 & 10 & -16 & -32 \\ 10 & 10 & -10 & -10 & -32 & -16 & 16 & 32 & -10 & -10 & -8 & 8 & 10 & 10 \\ -12 & -24 & 24 & 12 & 24 & 12 & -12 & -24 & 24 & 12 & 6 & -6 & -12 & -24 \end{bmatrix} \in \boldsymbol{R}^{6\times 14}. \tag{C.42}$$

$$\boldsymbol{W}_{L3} = \begin{bmatrix} 2 & -2 & 0 & 0 & 0 & 0 & 0 & 0 & 0 & 0 & 0 & 0 & 0 & 0 \\ 0 & 0 & 2 & -2 & 0 & 0 & 0 & 0 & 0 & 0 & 0 & 0 & 0 & 0 \\ 0 & 0 & 0 & 0 & 2 & -2 & 0 & 0 & 0 & 0 & 0 & 0 & 0 & 0 \\ 0 & 0 & 0 & 0 & 0 & 0 & 2 & -2 & 0 & 0 & 0 & 0 & 0 & 0 \\ 0 & 0 & 0 & 0 & 0 & 0 & 0 & 0 & 2 & -2 & 0 & 0 & 0 & 0 \\ 0 & 0 & 0 & 0 & 0 & 0 & 0 & 0 & 0 & 0 & 2 & -2 & 0 & 0 \\ 0 & 0 & 0 & 0 & 0 & 0 & 0 & 0 & 0 & 0 & 0 & 0 & 2 & -2 \end{bmatrix} \in \boldsymbol{R}^{7\times 14}. \tag{C.43}$$

The new form of wire matrix

$$\boldsymbol{W}_{3}^{'} = \begin{bmatrix} \boldsymbol{W}_{G3}^{'} & \boldsymbol{W}_{C3} \\ \boldsymbol{O} & \boldsymbol{W}_{L3}^{'} \end{bmatrix} \in \boldsymbol{R}^{13\times 14}, \tag{C.44}$$

where:

$$\boldsymbol{W}_{G3}^{'} = \frac{1}{5}\begin{bmatrix} -3 & 3 & 0 & 0 & -3 & 0 & 3 \\ 0 & 0 & 3 & 3 & 0 & -3 & 0 \\ 4 & 4 & 4 & 4 & -4 & -4 & -4 \\ -24 & -24 & 10 & 10 & -24 & 10 & -24 \\ 10 & -10 & -24 & 24 & -10 & 0 & 10 \\ -18 & 18 & 18 & -18 & 18 & 0 & -18 \end{bmatrix} \in \boldsymbol{R}^{6\times 7}, \tag{C.45}$$

$$\boldsymbol{W}_{C2} = \frac{1}{5}\begin{bmatrix} 0 & 0 & 0 & 0 & 0 & 0 & 0 \\ 0 & 0 & 0 & 0 & 0 & 0 & 0 \\ 0 & 0 & 0 & 0 & 0 & 0 & 0 \\ 8 & -8 & 0 & 0 & -8 & 0 & 8 \\ 0 & 0 & -8 & -8 & 0 & -8 & 0 \\ 6 & 6 & 6 & 6 & 6 & 6 & 6 \end{bmatrix}_{\in} \boldsymbol{R}^{6\times 7}, \tag{C.46}$$

$$\boldsymbol{W}_{L3}^{'} = 2\boldsymbol{E}_{7\times 7}, \tag{C.47}$$

$$\boldsymbol{O} = [\boldsymbol{0}]_{7\times 7}\,. \tag{C.48}$$

C.2.2 Second configuration: 3D RDWM with four sets of DAMs with VCMs

The normal form of wire matrix

$$\boldsymbol{W}_3 = \begin{bmatrix} \boldsymbol{W}_{G3} \\ \boldsymbol{W}_{L3} \end{bmatrix} \in \boldsymbol{R}^{14\times 16}, \tag{C.49}$$

where:

$$\boldsymbol{W}_{G3} = \frac{1}{3}\begin{bmatrix} -1 & -1 & -1 & -1 & 2 & 2 & 2 & 2 & 1 & 1 & 1 & 1 & -2 & -2 \\ -2 & -2 & -2 & -2 & 2 & 2 & 2 & 2 & 2 & 2 & 2 & 2 & -2 & -2 \\ -2 & -2 & -2 & -2 & 1 & 1 & 1 & 1 & -2 & -2 & -2 & -2 & 1 & 1 \\ 34 & 26 & 10 & 2 & -24 & -12 & 12 & 24 & -34 & -26 & -10 & -2 & 24 & 12 \\ -24 & -12 & 12 & 24 & 7 & -1 & -17 & -25 & 24 & 12 & -12 & -24 & -7 & 1 \\ 7 & -1 & -17 & -25 & 34 & 26 & 10 & 2 & 7 & -1 & -17 & -25 & 34 & 26 \end{bmatrix}$$

$$\begin{bmatrix} -2 & -2 \\ -2 & -2 \\ 1 & 1 \\ -12 & -24 \\ 17 & 25 \\ 10 & 2 \end{bmatrix} \in \boldsymbol{R}^{6\times 16}. \tag{C.50}$$

$$\boldsymbol{W}_{L3} = 2\sqrt{2}\begin{bmatrix} 1 & -1 & 0 & 0 & 0 & 0 & 0 & 0 & 0 & 0 & 0 & 0 & 0 & 0 & 0 & 0 \\ 0 & 0 & 1 & -1 & 0 & 0 & 0 & 0 & 0 & 0 & 0 & 0 & 0 & 0 & 0 & 0 \\ 0 & 0 & 0 & 0 & 1 & -1 & 0 & 0 & 0 & 0 & 0 & 0 & 0 & 0 & 0 & 0 \\ 0 & 0 & 0 & 0 & 0 & 0 & 1 & -1 & 0 & 0 & 0 & 0 & 0 & 0 & 0 & 0 \\ 0 & 0 & 0 & 0 & 0 & 0 & 0 & 0 & 1 & -1 & 0 & 0 & 0 & 0 & 0 & 0 \\ 0 & 0 & 0 & 0 & 0 & 0 & 0 & 0 & 0 & 0 & 1 & -1 & 0 & 0 & 0 & 0 \\ 0 & 0 & 0 & 0 & 0 & 0 & 0 & 0 & 0 & 0 & 0 & 0 & 1 & -1 & 0 & 0 \\ 0 & 0 & 0 & 0 & 0 & 0 & 0 & 0 & 0 & 0 & 0 & 0 & 0 & 0 & 1 & -1 \end{bmatrix} \in \boldsymbol{R}^{8\times 16}. \tag{C.51}$$

The new form of wire matrix

$$\boldsymbol{W}_3^{'} = \begin{bmatrix} \boldsymbol{W}_{G3}^{'} & \boldsymbol{W}_{C3} \\ \boldsymbol{O} & \boldsymbol{W}_{L3}^{'} \end{bmatrix} \in \boldsymbol{R}^{14\times 16}, \tag{C.52}$$

where:

$$\boldsymbol{W}_{G3}^{'} = \frac{1}{3}\begin{bmatrix} -1 & -1 & 2 & 2 & 1 & 1 & -2 & -2 \\ -2 & -2 & 2 & 2 & 2 & 2 & -2 & -2 \\ -2 & -2 & 1 & 1 & -2 & -2 & 1 & 1 \\ 30 & 6 & -18 & 18 & -30 & -6 & 18 & -18 \\ -18 & -18 & 3 & -21 & 18 & -18 & -3 & 21 \\ 3 & -21 & 30 & 6 & 3 & -21 & 30 & 6 \end{bmatrix} \in \boldsymbol{R}^{6\times 8}. \tag{C.53}$$

$$\boldsymbol{W}_{C3} = \frac{2}{3}\begin{bmatrix} 0 & 0 & 0 & 0 & 0 & 0 & 0 & 0 \\ 0 & 0 & 0 & 0 & 0 & 0 & 0 & 0 \\ 0 & 0 & 0 & 0 & 0 & 0 & 0 & 0 \\ 2 & 2 & -3 & -3 & -2 & -2 & 3 & 3 \\ -3 & -3 & 2 & 2 & 3 & 3 & -2 & -2 \\ 2 & 2 & 2 & 2 & 2 & 2 & 2 & 2 \end{bmatrix} \in \boldsymbol{R}^{6\times 8}, \tag{C.54}$$

$$\boldsymbol{W}'_{L3} = 2\sqrt{2}\boldsymbol{E}_{8\times 8}, \tag{C.55}$$

$$\boldsymbol{O} = [\mathbf{0}]_{8\times 8}\,. \tag{C.56}$$

Appendix D

Conversion from face form to span form

The face form is converted to span form as shown below:

$$\boldsymbol{V} = \{\boldsymbol{v} | \boldsymbol{A}_V \boldsymbol{v} \leq \boldsymbol{b}_V\}, \tag{D.1}$$

$$= \left\{ \sum_{t=1}^{\beta} \lambda_t \boldsymbol{v}_t | \sum_{t=1}^{\beta} \lambda_t \leq 1, \lambda_t \geq 0, t \in [1, \beta] \right\}, \tag{D.2}$$

Equations (D.1) and (D.2) express the face form with linear inequality sets and the span form with the vertex sets, respectively. The face and span forms are conceptualized in panels (a) and (b) respectively in Fig. D.1, and the conversion is performed by the method proposed in [61].

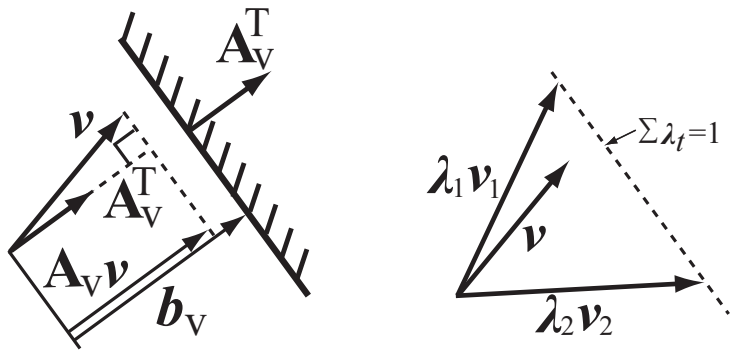

(a) Face form. (b) Span form.

Figure. D.1: Conversion from face form to span form.

Bibliography

[1] A. Ghaffar and M. Hassan: "Study on Cable Based Parallel Manipulator Systems for Subsea Applications", Proceedings of the 3^{rd} International Conference on Mechanical Engineering and Mechatronics, No. 154, pp. 1-8, 2014.

[2] R. Bostelman, W. Shackleford, F. Proctor and J. Albus: "The Flying Carpet: a Tool to Improve Ship Repair Efficiency", American Society of Naval Engineers Symposium, Manufacturing Technology for Ship Construction and Repair-Sep, 10-12, 2002, pp. 1-9, 2002.

[3] L. L. Cone: "Skycam: An Aerial Robotic Camera System", BYTE magazine-The Small Systems Journal, Vol. 10, No. 10, pp. 122 -124, 1985.

[4] S. Bouchard and C. M. Gosselin: "Kinematic Sensitivity of a Very Large Cable - Driven Parallel Mechanism", ASME-International Design Engineering Technical Conferences and Computers and Information in Engineering Conference, Vol. 2, pp. 851 -858, 2006.

[5] G. Meunier, B. Boulet and M. Nahon: "Control of an Overactuated Cable-Driven Parallel Mechanism for a Radio Telescope Application", IEEE Transactions on Control Systems Technology, Vol. 17, No. 5, pp. 1043-1054, 2009.

[6] Z. Rahmati and S. Behzadipour: "Analysis and Design of a Cable-Driven Mechanism for a Spherical Surgery Robot", 22^{nd} Iranian conference on Biomedical Engineering, pp. 221-226, 2015.

[7] C. Gosselin, R. Poulin and D. Laurendeau: "A planar Parallel 3-Dof Cable-Driven Haptic Interface", Systemics, Cybernetics and Informatics, Vol. 7, No. 3, pp. 66-71, 2009.

[8] A. Tzemanaki, L. Fracczak, D. Gillatt, A. Koupparis, C. Melhuish, R. Persad, E. Rowe, A. G. Pipe and S. Dogramadzi: "Design of a Multi-Dof Cable-Driven Mechanism of a Miniature Serial Manipulator for Robot-Assisted Minimally Invasive Surgery", IEEE International Conference on Biomedical Robotics and Biomechatronics, pp. 55-60, 2016.

[9] R. Ozawa, K. Hashirii, Y. Yoshimura, M. Moriya and H. Kobayashi: “Design and Control of a Three-Fingered Tendon-Driven Robotic Hand with Active and Passive Tendons”, Autonomous Robotics, Vol. 36, iss. 1-2, pp. 67-78, 2014.

[10] G. Palli and C. Melchiorri: “Friction Compensation Techniques for Tendon-Driven Robotic Hands”, Mechatronics, Vol. 24, pp. 108-117, 2014.

[11] J. M. Inouye and F. J. Valero-Cuevas: “Anthropomorphic Tendon-Driven Robotic Hands can Exceed Human Grasping Capabilities Following Optimization”, The International Journal of Robotics Research, pp. 1-12, 2013.

[12] E. M. Ficanha, M. Rastgaar and K. R. Kaufman: “A Two-Axis Cable-Driven Ankle-Foot Mechanism”, Robotics and Biomimetics, pp. 1-17, 2014.

[13] S. Kawamura, H. Kino and C. Won: “High-speed Manipulation by Using Parallel Wire-Driven Robots”, Journal Robotica, Vol. 18, pp. 13-21, 2000.

[14] K. Nagai, M. Matsumoto, K. Kimura and B. Masuhara: “Development of Parallel Manipulator ‘NINJA’ with Ultra-High-Acceleration”, IEEE - International Conference on Robotics and Automation, Vol. 3, pp. 3678-3685, 2003.

[15] P. Vischer and R. Clavel: “Kinematic Calibration of The Parallel Delta Robot”, Robotica, Vol. 16, pp. 207-218, 1998.

[16] F. Pierrot, P. Dauchez and A. Fournier: “HEXA: a Fast Six-DOF Fully-Parallel Robot”, Advanced Robotics, Vol. 2, pp. 1158-1163, 1991.

[17] K. Nagai, Y. Nishibu, K. Dake and A. Yamanaka: “Design of a High Speed Parallel Mechanism Based on Virtual Force Redundancy Concept”, IEEE - International Conference on Industrial Technology, Vol. 1, pp. 1-6, 2009.

[18] M. Higashimori, M. Kaneko, A. Namiki and M. Ishikawa: “Design of 100G Capturing Robot Based on Dynamic Preshaping”, IEEE - International conference on Intelligent Robots and System, Vol. 24, No. 9, pp. 743-753, 2005.

[19] Y. Koseki, T. Arai, K. Sugimoto, T. Takatuji and M. Goto: “Design and Accuracy Evaluation of High-Speed and High Precision Parallel Mechanism”, Proc. 1998 IEEE, Vol. 3, pp. 1340-1345, 1998.

[20] H. Kozuka, J. Arata, K.Okuda, A. Onaga, M. Ohno, A. Sano and H. Fujimoto: “Compliant-Parallel Mechanism for High Precision Machine with a Wide Range of Working Area”, IEEE/RSJ International Conference on Intelligent Robots and Systems, Vol. 3, pp. 2519-2524, 2012.

[21] G. Piras, W.L. Cleghorn and J.K. Mills: "Dynamic Finite-Element Analysis of A Planar High-Speed, High-Precision Parallel Manipulator with Flexible Links", Mechanism and Machine Theory, Vol. 40, pp. 849-862, 2005.

[22] Stephan Algermissen, Michael Rose, Ralf Keimer and Elmar Breitbach: "High-speed parallel robots with integrated vibration suppression for handling and assembly", IOP Publishing - Smart Structures and Materials, pp. 798-812, 1999.

[23] K. Bialas: "Application of mechanical and electrical elements in reduction of vibration", Journal of Achievements in Materials and manufacturing Engineering, Vol. 52, iss. 1, pp. 31-38, 2012.

[24] Y. B. Bedoustani, P. Bigras, H. D. Taghirad and I. A. Bonev: "Lagrangian Dynamics of Cable-Driven Parallel Manipulators: a Variable Mass Formulation", Transactions of the Canadian Society for Mechanical Engineering, Vol. 35, No. 4, pp. 529-542, 2011.

[25] M. A. Khosravi and H. D. Taghirad: "Dynamic Analysis and Control of Cable Driven Robots with Elastic Cables", Transactions of the Canadian Society for Mechanical Engineering, Vol. 35, No. 4, pp. 543-557, 2011.

[26] S. H. Yeo, G. Yang and W. B. Lim: "Design and Analysis of Cable-Driven Manipulators with Variable Stiffness", Mechanism and Machine Theory, Vol. 69, pp. 230-244, 2013.

[27] T. Le Nhat, H. Dobashi, K. Ito and K. Nagai: "Design of Vibration Suppression Mechanism in Two Wires Drive Mechanism for Producing High Acceleration and High Precision motions", Robot Society of Japan, 2014.

[28] H. Osumi, Y, Utsugi and M. Koshikawa: "Development of a Manipulator Suspended by Parallel Wire Structure", Proc. 2000 IEEE/RSJ, Vol. 1, pp. 498-503, 2000.

[29] H. Osumi and M. Saitoh: "Control of a Redundant Manipulator Mounted on a Base Plate Suspended by Six Wires", Proc. 2006 IEEE/RSJ International Conference on Intelligent Robots and System, Vol. 1, pp. 73-78, 2000.

[30] R. Lampariello, J Heindl, R Koeppe and G. Hirzinger: "Reactionless Control for Two Manipulators Mounted on a Cable-Suspended Platform", IEEE - International conference on Intelligent Robots and System, Vol. 1, pp. 91-97, 2006.

[31] B. Cong Pham, S. H. Yeo, G. Yang, M. S Kurbanhusen and I. Chen: "Force- Closure Workspace Analysis of Cable-Driven Parallel Mechanisms", Mechanism and Machine Theory, pp. 53-69, 2006.

[32] B. Cong Pham, S. H. Yeo, G. Yang and I. Chen: "Workspace Analysis of Fully Restrained Cable-Driven Manipulators", Robotics and Autonomous Systems, pp. 901-912, 2009.

[33] D. Van Nguyen: "Constructing Force Closure Grasps", The International Journal of Robotics Research, Vol. 7, No. 3, pp.3-16, 1988.

[34] G. Marc, J. P. Merlet and D. Daney: "Wrench- Feasible Workspace of Parallel Cable Driven Mechanisms", IEEE - International conference on Robotics and Automation, pp. 1492-1497, 2007.

[35] G. Marc, D. Daney and J. P. Merlet: "Interval Analysis Based Determination of the Wrench-Feasible Workspace of Parallel Cable Driven Robots", IEEE Transaction on Robotics, Vol. 27, No. 1,pp. 1-13, 2011.

[36] Mohammad M. Aref and Hamid D. Taghirad: "Geometrical Workspace Analysis of A Cable Driven Redundant Parallel Manipulator: KNTU CDRPM", IEEE International Conference on Intelligent Robots and Systems, pp. 1958-1963, 2011.

[37] A. Alikhani, S. Behzadipour, S. A. S. Vanini and A. Alasty: "Workspace Analysis of a Three DoF Cable-Driven Mechanism", Journal of Mechanisms and Robotics, Vol. 1, No. 041005, pp. 1-7, 2009.

[38] S. Lahouar, E. Ottaviano, S. Zeghoul, L. Romdhane and M. Ceccarelli: "Collision Free Path-Planning for Cable-Driven Parallel Robots", Robotics and Autonomous Systems, Vol. 57, pp. 1083-1093, 2009.

[39] Y. Wischnitzer, N. Shvalb and M. Shoham: "Wire-driven Parallel Robot: Permitting Collisions Between Wires", The International Journal of Robotics Research, Vol. 27, No. 9, pp. 1007-1026, 2008.

[40] B. Khoshnevis: "Automated Construction by Contour Crafting-Related Robotics and Information Technologies", Automation in Construction, Vol. 13, pp. 5-19, 2004.

[41] G. Fernandes and L. Feitosa: "Impact of Contour Crafting on Civil Engineering", International Journal on Engineer Research and Technology, Vol. 4, iss. 08, pp. 628-632, 2015.

[42] P. Bosscher, R L. Williams II, L. Sebastian Bryson and Daniel Castro-Lacouture: "Cable-Suspended Robotic Contour Crafting System", Automation in Construction, Vol. 17, iss. 1, pp. 45-55, 2007.

[43] R L. Williams II, M. Xin and P. Bosscher: "Contour-Crafting-Cartesian-Cable Robot System: Dynamics and Controller Design", 32nd Mechanisms and Robotics Conference-ASME, Vol. 2, pp. 1-7, 2008.

[44] A. Alikhani, S. Behzadipour, A. Alasty and S. Ali Sadough Vanini: "Design of a Large-Scale Cable-Driven Robot with Translational Motion", Robotics and Computer-Integrated Manufacturing, Vol. 27, iss. 2, pp. 357-366, 2011.

[45] S. Behzadipour and A. Khajepour: "A New Cable- Based Parallel Robot with Three Degrees of Freedom", Springer, Multi-body System Dynamics, Vol. 13, iss. 4, pp. 371-383, 2005.

[46] K. Nagai, H. Hanafusa, Y. Takahashi, H. Bunki, I. Nakanishi, T. Yoshinaga and T. Ehara: "Development of a Power Assistive Device for Self-Supported Transfer Motion", IEEE/RSJ-International Conference on Intelligent Robots and System, Vol. 2, pp. 1433-1438, 2002.

[47] K. Nagai, K. Ito, Y. Hayashi and T. Le Nhat: "ワイヤ駆動機構", Patent Number: 5974416, 2016. (in Japanese)

[48] K. Nagai, T. Le Nhat, Y. Hayashi, K. Ito: "Proposal of Redundant Drive Wire Mechanism for Producing Motions with High Acceleration and High Precision", IEEE/SICE-International Symposium on System Intergration, pp. 1049-1054, 2011.

[49] T. Le Nhat, H. Dobashi and K. Nagai: "Configuration of Redundant Drive Wire Mechanism Using Double Actuator Modules", ROBOMECH Journal, Vol. 3, iss. 25, pp. 1-16, 2016.

[50] K. Nagai, T. Le Nhat, Y. Hayashi, K. Ito: "Kinematical Analysis of Redundant Drive Wire Mechanisms with Velocity Constraint", IEEE/International conference on Mechatronics and Automation, pp. 1496-1501. 2012.

[51] T. Le Nhat, H. Dobashi and K. Nagai: "Kinematical and Static Force Analysis on Redundant Drive Wire Mechanism with Velocity Constraint Modules to Reduce the Number of Actuators", ROBOMECH Journal, Vol. 3, iss. 22, pp. 1-22, 2016.

[52] T. Le Nhat, H. Dobashi and K. Nagai: "Erratum to: Kinematical and Static Force Analysis on Redundant Drive Wire Mechanism with Velocity Constraint Modules to Reduce the Number of Actuators", ROBOMECH Journal, Vol. 3, iss. 24, pp. 1, 2016.

[53] K. Nagai, H. Yoshida, T. Le Nhat: “Consideration of Construction of Wire Mechanism Based on Multi-Wire Driven Method”, Proceedings of 17th Robotics Symposia, pp. 98-103, 2012. (in Japanese)

[54] K. Nagai, H. Yoshida, D. Yoshimori: “Kinematical Analysis of Parallel Mechanism Using Multi-Wire Driven Method”, Journal of Robotics Society of Japan, Vol. 29, No. 9, pp. 65-72, 2011. (in Japanese)

[55] H. Kino, S. Yabe and S. Kawamura: “A force display system using a serial-link structure driven by a parallel-wire mechanism”, Advanced Robotics, Vol. 19, No. 1, pp. 21-37, 2005.

[56] K. Nagai, I. Nakanishi: “Analysis of Exoskeletal Robotic Orthoses Concerning Possibility of Assistance and User’s Safety”, IEEE-International Workshop on Robot and Human Interactive Communication, pp. 73-78, 2003.

[57] V. Chvatal: “Linear Programming”, W. H. Freeman and Company, 1983.

[58] S. Hirai: “Analysis and Planning of Manipulation Using the Theory of Polyhedral Convex Cones”, PhD thesis, 1991.

[59] S. Hirai: “Kinematics and Statics of Manipulation Using the Theory of Polyhedral Convex Cones and Their Application to the Planning of Manipulative Operations”, Journal of Robotics Society of Japan, Vol. 17, No. 1, pp. 68-83, 1999. (in Japanese)

[60] S. Hirai: “Kinematics of Manipulation Using the Theory of Polyhedral Convex Cones and Its Application to Grasping and Assembly Operations”, Trans. of the Society of Instrument and Control Engineers, Vol. E2, No. 1, pp. 10-17, 2002.

[61] H. Hirukawa, T. Matsui and K. Takase: “A Fast Algorithm for the Analysis of the Constraint for Motion of Polyhedra in Contact and Its Application to Departure Motion Planning”, Journal of Robotics Society of Japan, Vol. 9, No. 7, pp. 841-848, 1999. (in Japanese)

[62] T. Yoshikawa: “Passive and Active Closures by Constraining Mechanisms”, Transactions of the ASME, Vol. 121, pp. 418-424, 1999.

[63] A. Afshari and A. Meghdari: “New Jacobian Matrix and Equations of Motion for a 6 Dof Cable-Driven Robot”, International Journal of Advanced Robotic Systems, Vol. 4, No. 1, pp. 63-68, 2007.

[64] T. Yoshikawa: “Foundations of Robotics: Analysis and Control”, The MIT Press Cambridge, Massachusetts, London, England, pp. 263-267, 1990.

[65] Y. Kanamiya: “Introduction to Robotics in English- Kinematics, Dynamics and Control”, Corona Publishing Co., Ltd, 2008.

[66] Y. Shirai: “ロボット工学”, Ohmsha Publishing Company, pp. 31-51, 2008. (in Japanese)

[67] B C. Kuo and J. Tal: “Incremental Motion Control-DC Motors and Control Systems”, SRL Publishing Company, pp. 201-212, 1979.

[68] M. A. Khosravi and H. D. Taghirad: “Robust PID Control of Fully-Constrained Cable Driven Parallel Robots”, Mechatronics, Vol. 24, pp. 87-97, 2014.

[69] K. Nagai, H. Dobashi, T. Sashinaka and K. Yamaguchi: “Introducing Kinematical Redundant Degree of Freedom into High Speed Parallel Mechanism with Driving Force Redundancy for Producing Precise Motions”, Journal of Robotics Society of Japan, Vol. 33, No. 5, pp. 379-386, 2015. (in Japanese)